The shape of brain structures, cortical thickness, and resting state fMRI as tools for prediction of Alzheimer's disease progression

Thesis (cumulative thesis)

Presented to the Faculty of Arts and Social Science
of the University of Zurich
for the Degree of Doctor of Philosophy

by Clemens Schroeder

Accepted in the fall semester 2017

on the Recommendation of the Doctoral Committee:
Prof. Dr. Mike Martin, University of Zurich (main advisor)
Prof. Dr. med. Christoph Hock
PD Dr. Lars Michels

Zurich, 2017

“We demand rigidly defined areas of doubt and uncertainty!”

- Douglas Adams, The Hitchhiker's Guide to the Galaxy -

Acknowledgements

I thank my main advisor Prof. Dr. Mike Martin for enabling me to write this thesis at his chair and for providing critical support whenever I needed it, and for his valuable advice regarding organization and planning of my project.

* * *

I thank my second supervisor Prof. Dr. med. Christoph Hock for his support and for providing the infrastructure and financing necessary to pursue my project at the former Division of Psychiatry Research, today named Institute for Regenerative Medicine, of the Faculty of Medicine of the University of Zurich.

* * *

I thank my third supervisor PD Dr. Lars Michels for providing critical infrastructure at the University Hospital Zurich and for his close cooperation and involvement in multiple studies I have worked on.

* * *

I thank Dr. Sandra Leh-Seal for her guidance and advice regarding many projects at the Gerontopsychiatric Centre Hegibach and for involving me in studies on a variety of topics.

* * *

I thank Dr. Andrea Kälin for being a fantastic role model during our joint time at the Gerontopsychiatric Centre Hegibach, with her remarkable discipline and seemingly limitless drive leaving a lasting impression. I also thank her for our pleasant cooperation afterwards.

* * *

I thank Dr. med. Anton Gietl for his pivotal role in securing the financing of my doctoral program, for his careful examination of - and excellent, thoughtful suggestions regarding - multiple ethics proposals and manuscripts I prepared, and for the valuable time he invested in me this way.

* * *

I thank Daniel Summermatter for being an awesome co-worker with his naturally humorous, open and helping attitude and his intricate knowledge of clinical neuropsychology in the elderly. I also thank him for being an important source of emotional support.

* * *

I thank Jiri van Bergen for his positive and supportive attitude towards me and for being my friend, especially as a companion during conferences and retreats and for his invaluable hints regarding software- and programming-related issues.

* * *

I thank PD Dr. Valerie Treyer for her invaluable support with regard to data processing in PMOD, repeatedly saving the day with her great expertise.

* * *

I thank my sister Sara Schroeder for her strong emotional support and for being a reliable, permanent, stable and consistently positive influence on my life. I thank her for caring and being there for me.

* * *

I thank Madeleine Fritschi, my partner in life, for all her support and understanding and for being a well of happiness, energy and well-being. I thank her for being the start and the end of most of my days, enfolding each of them into a wrapping that is in itself a great gift.

Abstract

A very large and growing number of individuals worldwide suffer from Alzheimer's disease (AD). Early diagnosis is paramount to achieving optimal effectiveness for disease-modifying treatments.

To date, the predictive value of cortical thickness and the shapes of hippocampus and thalamus has been underinvestigated. Therefore, the aim of the first study was to investigate these measures as potential indicators of AD progression in cognitively healthy elderly subjects.

The second study features a design with two time points and investigated the predictive value of striatal and thalamic shape as well as cortical thickness for conversion from mild cognitive impairment (MCI) to dementia due to AD.

Resting state functional MRI (rsfMRI) studies have shown differences in functional connectivity between individuals with AD and healthy control subjects. However, relatively subtle aspects of study design have a significant impact on connectivity measures, hampering reproducibility of results across research groups. Hence, the third study investigated whether participant information influenced subsequently measured functional connectivity within and between networks.

The present rsfMRI study contributes to reproducibility and comparability of results across research groups. The other two studies yielded promising results for hippocampal and thalamic shape as early predictors of AD progression.

Zusammenfassung

Eine sehr grosse und zunehmende Zahl von Personen weltweit leidet an der Alzheimerkrankheit. Daher ist eine frühe Diagnose unverzichtbar, um ein optimales Behandlungsergebnis zu erreichen.

Bisher wurde der Vorhersagewert von kortikaler Dicke und Formen von Gehirnstrukturen zu wenig untersucht. Deshalb war das Ziel der ersten Studie, diese Masse als potenzielle Indikatoren des Fortschreitens der Alzheimerkrankheit in kognitiv gesunden älteren Personen zu untersuchen.

Die zweite Studie weist ein Design mit zwei Zeitpunkten auf und untersuchte die Vorhersagekraft striataler und thalamischer Form sowie kortikaler Dicke für die Konversion von leichter kognitiver Beeinträchtigung zu Alzheimerdemenz.

Studien zu fMRT im Ruhezustand zeigten Unterschiede in funktioneller Konnektivität zwischen Personen mit Alzheimerdemenz und gesunden Kontrollprobanden. Jedoch beeinflussen bereits subtile Aspekte des Studiendesigns Masse von Konnektivität signifikant, was die Reproduzierbarkeit durch andere Forschungsgruppen einschränkt. Daher wurde mit der dritten Studie untersucht, ob Information der Teilnehmenden die nachfolgend gemessene Konnektivität innerhalb und zwischen Netzwerken beeinflusste.

Die vorliegende fMRI-Studie trägt zur Reproduzierbarkeit und Vergleichbarkeit von Resultaten bei. Die anderen zwei Studien brachten vielversprechende Resultate für hippokampale und thalamische Form als frühe Prädiktoren des Fortschreitens der Alzheimerkrankheit hervor.

Contents

1 Introduction

Globally, the number of individuals with dementia was estimated to be 47 million in 2016. According to the World Alzheimer Report of said year, this number is expected to increase to over 131 million by 2050 due to population aging. Dementia also has a huge economic impact. The total estimated worldwide cost of dementia is US$ 818 billion, and it will become a trillion dollar disease by 2018 (Prince, Comas-Herrera, Knapp, Guerchet, & Karagiannidou, 2016). The most common cause of dementia is Alzheimer's disease (AD), which accounts for 60 to 80 percent of cases (Alzheimer's Association, 2017). AD is characterized by gradual onset of cognitive decline, usually involving impairments in learning and recall of recently learned information, and progression from mild cognitive impairment (MCI) to dementia, involving cognitive or behavioral impairment in two or more domains and interfering with activities of daily living or work (McKhann et al., 2011). In addition to its gruesome effect on the lives of individuals with the disease, AD takes a heavy toll on the social surroundings of patients, with an estimated 18.2 billion unpaid hours of care given to people with dementia in 2016 in the United States alone (Alzheimer's Association, 2017).

Despite its large burden on society, there is no cure for AD. Currently, the approved treatments are the cholinesterase inhibitors rivastigmine, galantamine, and donezepil for mild to moderate AD (Birks, 2006) and the N-methyl-D-aspartate receptor antagonist memantine (McShane, Areosa Sastre, & Minakaran, 2006). However, these treatments target cognitive symptoms rather than the underlying pathophysiological process. Clinical research has therefore shifted to disease-modifying treatments that interfere with specific steps of the pathogenic cascade (Galimberti & Scarpini, 2011), such as the antibody aducanumab triggering the clearance of Aβ plaques (Sevigny, Chiao, Bussiere, et al., 2016; Sevigny et al., 2017). Such disease-modifying treatments are thought to be most effective when applied in preclinical stages of AD (Counts, Ikonomovic, Mercado, Vega, & Mufson, 2017; Laske et al., 2015; Masdeu, Kreisl, & Berman, 2012; Villemagne et al., 2013), and Aβ-modifying therapies are thought to profit particularly from initiation before the

onset of neuronal degeneration (Sperling, Aisen, et al., 2011). Because the AD pathophysiological process is thought to begin many years before the onset of cognitive symptoms, with abnormal Aβ levels in the brain more than 15 years before the onset of dementia (Villemagne et al., 2013), the search for biomarkers that reliably predict AD progression before the onset of cognitive symptoms is of great importance.

In this chapter, the most important pathological features of AD as well as criteria for diagnosis of MCI and dementia due to AD will be described. Additionally, the current state of preclinical biomarker research will be summarized and the current role of structural and functional MRI for prediction of AD progression will be outlined. Chapter 2 includes information about the methods applied and the measures analyzed in the three studies comprising this thesis, followed by Chapter 3 outlining the aims and hypotheses of each study. Chapter 4 presents the empirical studies, whose results will be discussed in chapter 5, which includes elaborations on their implications for the field of AD biomarker research as well as limitations and possible avenues of future investigations.

1.1 The two key neuropathological features of AD

AD is characterized by the presence of a number of pathological features including astrogliosis, microglial cell activation, granulovacuolar degeneration and Hirano bodies (Serrano-Pozo, Frosch, Masliah, & Hyman, 2011). Yet, the two most prominent AD hallmarks are the extracellular deposition of insoluble Aβ aggregates and the intracellular accumulation of neuritic plaques, neurofibrillary tangles (NFT), and neuropil threads (H. Braak & Braak, 1991b), both of which must be observed in post-mortem pathology for a definitive diagnosis (Hyman et al., 2012; Hyman & Trojanowski, 1997). Aβ plaques form as a consequence of the misfolding of Aβ peptides, whereas tau aggregates form as a result of the misfolding of microtubule-associated protein tau (Nussbaum, Seward, & Bloom, 2013). It is unclear whether amyloid or tau pathology occurs first in the neuropathological cascade of AD, but both processes start long before symptom onset (H. Braak, Zetterberg, Del Tredici, & Blennow, 2013; Jack et al., 2013; Villemagne et al., 2013).

Parameters of amyloid and tau pathology can be measured in vivo in the cerebrospinal fluid (CSF) after lumbar puncture, or in the brain by PET, using a suitable radioligand.

1.2 Preclinical AD, MCI, and dementia due to AD

In their 2011 revision of the 1984 criteria for the clinical diagnosis of AD, the National Institute on Aging (NIA) and the Alzheimer's Association (AA) provided recommendations on AD diagnosis for three distinct phases of the disease course: the preclinical asymptomatic phase, the pre-dementia symptomatic phase, and the dementia phase (Jack et al., 2011). One working group developed a research framework for the preclinical, or presymptomatic, phase of AD (Sperling, Aisen, et al., 2011), one working group developed criteria for the symptomatic pre-dementia phase, MCI (Albert et al., 2011), while another working group developed criteria for the dementia phase (McKhann et al., 2011).

Preclinical AD

The proposed research framework proposed for preclinical AD by the responsible NIA-AA working group includes three stages. The first stage is characterized by amyloid positivity, established by PET neuroimaging evidence of Aβ accumulation or low CSF $A\beta_{42}$ levels, in the absence of biomarkers of neurodegeneration and cognitive or behavioral symptoms. During the second stage, amyloid positivity is accompanied by such measures of neuronal injury, including elevated CSF total tau or phospho-tau, AD-typical hypometabolism observed by ^{18}fluorodeoxyglucose (FDG) PET, gray matter loss in an AD-typical spatial pattern or hippocampal atrophy observed by MRI, and possibly fMRI connectivity measures of the default mode network. The third stage, in addition to amyloid positivity and early neuronal injury, includes subtle cognitive decline in relation to a previously established baseline with performance still in the normal range.

MCI

The clinical syndrome constituting MCI due to AD described by the working group is highly similar to that described in earlier publications (Petersen, 2004; Winblad et al., 2004). Core clinical criteria for the diagnosis of MCI due to AD are (i) concern by the patient, a close informant, or a skilled clinician regarding a change in cognition, (ii) impairment in at least one cognitive domain (memory, executive function, attention, language, visuospatial skills), (iii) maintained independence in daily life with only minimal aids or assistance, and (iv) no significant impairment in social or occupational functioning (Albert et al., 2011). Episodic memory is the most commonly affected in individuals with MCI who progress to dementia due to AD. In a neuropsychological assessment, cognitive impairment typically implies a deviation from age and education matched norms of at least 1 to 1.5 standard deviations.

In the second study of the present work, diagnosis of MCI was made on the basis of the highly similar criteria published by Winblad et al. (2004), requiring (i) classification as not normal, not demented, (ii) largely preserved activities of daily living, and (iii) evidence of cognitive decline measured in one of two ways, the first being report by self or informant and deficits on objective cognitive tasks, the second being decline over time in objective neuropsychological tasks.

Dementia due to AD

Core clinical criteria for dementia, irrespective of its cause, are cognitive or behavioral symptoms that interfere with everyday functioning, constitute a decline from previous levels of functioning, and are not explained by delirium or major psychiatric disorder (McKhann et al., 2011). In addition, cognitive impairment is diagnosed by combining information about patient history from the patient and a knowledgeable informant with an objective cognitive assessment. The neuropsychiatric symptoms involve two or more domains out of the following: acquiring and remembering new information; reasoning, handling of complex tasks, judgment; visuospatial abilities;

language, including speaking, reading, and writing; and personality, behavior, or comportment.

To assume that dementia diagnosed in a specific individual is caused by AD, additional criteria have to be met in order to assign a diagnosis of probable AD dementia, possible AD dementia, or probable or possible AD dementia with evidence of the AD pathophysiologial process. The first and second term are intended for all clinical settings, while the third is intended for research settings.

The additional criteria for a diagnosis of probable AD dementia outlined by the NIA-AA working group are (i) gradual onset over months or years, (ii) clear history of cognitive decline established by report or observation, (iii) deficits in at least two cognitive domains evident on history and examination, and (iv) absence of substantial cerebrovascular disease, core features of dementia with Lewy bodies other than dementia, prominent features of behavioral variant frontotemporal dementia, semantic variant primary progressive aphasia or nonfluent/agrammatic variant primary progressive aphasia, and any other active neurological disease or non-neurological comorbidity as well as use of medication substantially affecting cognition. The level of certainty for this diagnosis is increased by documented cognitive decline based on cognitive testing and information from informants, and by evidence of a causative genetic mutation in APP, PSEN1, or PSEN2.

Criteria for possible AD dementia are an atypical course, with sudden onset of cognitive decline or insufficient documentation of decline progression, or mixed etiology, with concomitant (i) cerebrovascular disease, (ii) additional features of Lewy body dementia, (iii) medical comorbidity or medication use with a potentially substantial effect on cognition.

The diagnosis of probable AD dementia with evidence of the AD pathophysiological process is characterized by increased certainty about the postulated underlying cause of the clinical diagnosis of dementia syndrome. This increase in certainty stems from the use of biomarkers of Aβ deposition in the brain, measured by PET amyloid imaging, and cerebrospinal fluid (CSF) $A\beta_{42}$, as well as elevated total and phosphorylated tau levels in the CSF, low tracer uptake during FDG PET in temporo-parietal cortex, and high atrophy on structural MRI in medial parietal cortex and medial, lateral, and basal temporal

lobe.

The diagnosis of possible AD dementia with evidence of the AD pathophysiological process is based on the presence of non-AD dementia and biomarker evidence of AD pathophysiological process or fulfilled neuropathological criteria for AD.

1.3 Early predictors of AD progression

PET, MRI, and CSF biomarkers can increase the certainty in the attribution of a dementia syndrome to AD, but they also have predictive value for AD progression in nondemented individuals (Jack et al., 2013). In a model proposed by an NIA-AA international workgroup (Sperling, Aisen, et al., 2011), these biomarkers become abnormal in an ordered sequence: First, biomarkers of Aβ accumulation, including amyloid PET imaging and CSF $A\beta_{42}$, become abnormal. Second, biomarkers of synaptic dysfunction, including FDG PET and fMRI, become abnormal. Third, structural MRI becomes abnormal.

Levels of CSF $A\beta_{42}$ have been shown to correspond to those of brain amyloid imaging by Pittsburgh compound B (PiB) PET and their relation to CSF tau levels predicted conversion from a Clinical Dementia Rating (CDR) (Morris, 1993) of 0 to a greater score (Fagan et al., 2007). This ratio of CSF tau, which is thought to be a marker of neurodegeneration and synaptic dysfunction together with FDG PET and MRI (Counts et al., 2017; Trojanowski et al., 2010), to CSF $A\beta_{42}$ has also been shown to predict progression from MCI to AD (Trojanowski et al., 2010). At the MCI stage, CSF $A\beta_{42}$, total tau, and threonine 181 phospho-tau each achieved good accuracy at identifying incipient AD (Mattsson et al., 2009). The ability of FDG PET (Drzezga et al., 2005; Mosconi et al., 2004) and hippocampal volume measured by structural MRI (Devanand et al., 2007; Grundman et al., 2002) to discriminate between subjects with MCI and AD dementia and predict conversion from MCI to AD has also been demonstrated.

However, the NIA-AA workgroup acknowledged that AD etiology is still uncertain and several researchers emphasized how amyloid-independent factors can lead to dementia in AD and may play an earlier or more central

role in its pathogenesis than Aβ (Herrup, 2010; Pimplikar, Nixon, Robakis, Shen, & Tsai, 2010). They also acknowledge that some individuals display all AD neuropathological features at autopsy but never showed dementia in their lifetime, and that it is unclear whether a best combination of biomarkers for prediction of clinical symptoms exists. Hence, research on preclinical AD biomarkers using different imaging modalities, novel analysis methods and refined measures is warranted in the search for optimal prediction of AD progression.

1.4 The role of structural MRI for prediction of AD progression

As a consequence of the need to initiate treatment in the presymptomatic phase of AD, preventive screening of a large number of cognitively normal elderly individuals would be necessary. Thus, the instruments necessary for diagnostic measurement of suitable biomarkers would optimally be widely available and non-invasive. MRI measures identifying presymptomatic brain changes indicative of Aβ pathology would be a viable option in this regard. Structural MRI for volumetric and morphometric analysis of the hippocampus is routinely used in AD research and has been repeatedly shown to predict progression from MCI to AD dementia (G. Chételat et al., 2005; Tapiola et al., 2008) with greater atrophy in cognitively unimpaired subjects with future cognitive symptoms than subjects who remained cognitively healthy (Tondelli et al., 2012a). Hippocampal atrophy has been proposed as a possible marker of incipient AD in MCI (Dubois et al., 2007; Frisoni, Fox, Jack, Scheltens, & Thompson, 2010). Although hippocampal atrophy is closely related to cognitive impairment, this established biomarker becomes abnormal relatively late according to current models of AD progression biomarkers (Counts et al., 2017; Jack et al., 2013). Hence, several investigations have focused on more localized measures of hippocampal atrophy, examining hippocampal subfields separately (Kerchner et al., 2010a) or detecting spatially confined changes with 3D maps (Apostolova et al., 2010). These localized structural MRI measures are potential presymptomatic AD biomarkers: Cognitively normal individuals who later developed aMCI and AD showed greater CA1 and subiculum atrophy

than stable cognitively normal individuals (Apostolova et al., 2010), and localized inward changes in left hippocampal surface predicted progression of non-demented elderly individuals to dementia due to AD (Csernansky et al., 2005).

1.5 The role of functional MRI for prediction of AD progression

Investigations of the potential of resting-state functional MRI (rsfMRI) for early detection of AD have shown promising results and rsfMRI is discussed as a biomarker preceding Aβ biomarkers (Jack et al., 2013). In autosomal dominant AD, default-mode network (DMN) functional connectivity has been found to decrease with increasing CDR and to be lower in asymptomatic mutation carriers that noncarriers with prominent involvement of the posterior cingulate cortex (PCC) (Chhatwal et al., 2013), suggesting alterations in this functional network already at the preclinical stage. An earlier study using task-related fMRI showed that PCC activity during a sensory-motor processing task was decreased in individuals with mild AD compared to age-matched elderly controls (Greicius, Srivastava, Reiss, & Menon, 2004), suggesting that DMN functional connectivity may also be an early AD biomarker in late-onset AD. Connectivity changes in multiple resting state networks were similar in autosomal dominant and late-onset AD in a longitudinal rsfMRI study, and functional connectivity decreased with increasing CDR in both groups (Thomas et al., 2014). Using the PCC as seed region, a multi-center study revealed decreased functional connectivity with other DMN regions in each of the four dementia centers and in the pooled sample for individuals with MCI or AD compared to healthy controls (Wohlert et al., 2016).

Whereas these results are promising, research into functional connectivity of resting state networks as early AD biomarkers to date has been relatively scarce. Hence, replication of the published results is a crucial future step for this line of research. Methodological considerations play a pivotal role in the search for a stable, reliable biomarker derived from rsfMRI. In a recent evaluation of a previous multi-center study by their group (Wohlert et al., 2016), a team of researchers concluded that rsfMRI acquisition at

multiple centers limits its use in the diagnosis of MCI and AD (Teipel et al., 2017), concluding that multiscanner variability is an important confound of group differences. There are also confounds of connectivity measured by rsfMRI at the individual study level, related to study design. Participants are instructed to lie still and keep their eyes closed, open, or fixated on a cross in front of them during scanning, depending on the study site. This slight variation in study design has been shown to influence reliability and consistency of connectivity patterns (R. Patriat, Molloy EK, et al., 2013) and to lead to differences in DMN connectivity (Yan et al., 2009). Hence, resting state network connectivity is a promising candidate in the search for presymptomatic AD biomarkers, but determining which aspects of study design have a notable influence on rsfMRI measures will play a crucial role in future research.

2 Methods

2.1 PET acquisition

PiB, the tracer used for amyloid imaging in the first study of the present work, was synthesized in an on-site cyclotron (16.5 MeV, GE). A detailed describtion of the sequence of reactions for [^{11}C]-methyl triflate production is available elsewhere (Gietl et al., 2015). Tracer preparation was conducted based on the published procedure for radiolabeling (Solbach, Uebele, Reischl, & Machulla, 2005). Each participant received an antecubital venous injection of approximately 350 MBq of PiB. Data acquisition was performed during 70 minutes (4 × 15, 8 × 30, 9 × 60, 2 × 180 and 10 × 300 s).

2.2 MRI acquisition

MRI was acquired on a 3T Philips Achieva scanner for the first study and on a 1.5T Philips Achieva scanner for the other two studies.

T1-weighted data in the first study were acquired with the following parameters: repetition time 8.2 ms, echo time 3.7 ms and 8° flip angle, field of view 240 mm (AP) × 220 mm (FH) × 188 mm (RL), 220 axial slices with 1-mm

single-slice thickness (voxel dimensions: 0.94 × 0.94 × 1 mm). T1-weighted data in the second study were acquired with the following parameters: 166 slices, repetition time: 6.9 ms, echo time: 3.2 ms, flip angle: 8°, field of view: 240 × 240 × 166 mm (anterior-posterior, foot-head, right-left), slice thickness: 1 mm, total scan time: 15 min. T1-weighted data in the third study were acquired using an inversion recovery turbo field echo sequence with the following parameters: time of repetition = 6.9 ms, time of echo = 3.1 ms, flip angle = 8°, field of view = 240 mm, 400 x 400 scan matrix, slice thickness 1.2 mm, 166 slices, voxel size 0.6 x 0.6 mm)

In the third study, fMRI was done using echo-planar imaging and SENSE (sensitivity encoding for fast MRI (Pruessmann, Weiger, Scheidegger, & Boesiger, 1999)) with the following parameters: time of repetition = 3s, time of echo = 50 ms, flip angle = 90°, field of view = 220 mm, 128 x 128 scan matrix, slice thickness 3 mm, 34 slices, voxel size 1.72 x 1.72 mm. was acquired after the rs-fMRI scan.

2.3 Automated segmentation of brain structures

Whereas manual delineation is sometimes described as the gold standard for image segmentation, this approach requires a prohibitive amount of time in large datasets (Pipitone et al., 2014) and is vulnerable to variability within and between expert human raters (Chakravarty et al., 2009; Shattuck et al., 2008). Hence, segmentation of the hippocampus and subcortical structures in the first and second study was performed by using the Multiple Automatically Generated Templates (MAGeT Brain) algorithm, which performs registration of multiple input atlases to a template library consisting of a representative sample of all target images, which in turn is used as the basis of target image labelling (Chakravarty et al., 2013). This results in a large number of labels for the segmented voxels in each target image, requiring a method to fuse them into one final label per segmented voxel. The value of MAGet Brain segmentation of the hippocampus and hippocampal subfields has been assessed in a series of experiments by the Computational Brain Anatomy Laboratory (CoBrA Lab) at the Douglas Mental Health University Institute (Verdun, QC, Canada; affiliated with McGill University)

(Pipitone et al., 2014). In an experimental evaluation of three different fusion methods: voxel-wise majority vote (Collins & Pruessner, 2010), cross-correlation weighted majority vote (Aljabar, Heckemann, Hammers, Hajnal, & Rueckert, 2009), and normalized mutual information weighted majority vote (Studholme, Hill, & Hawkes, 1999), their performance did not significantly differ and the voxel-wise majority voting procedure was used in the remainder of the experiments (Pipitone et al., 2014) as well as in subsequent research (Amaral, Park, Devenyi, Lynn, Pipitone, Winterburn, Chavez, Schira, Lobaugh, Voineskos, et al., 2016; Chakravarty et al., 2015; Raznahan et al., 2014). The five input atlases used for hippocampal subfield segmentation were produced on the basis of high-resolution T1 and T2 images acquired on a 3T scanner and had final super-sampled isotropic voxel dimensions of 0.3mm (Winterburn et al., 2013). The input atlas used for thalamus and striatum segmentation was produced on the basis of histological data (Chakravarty, Bertrand, Hodge, Sadikot, & Collins, 2006).

2.4 Shape and surface area calculation

Calculation of shape and surface area measures required 3D meshes of the structures of interest, which were constructed using the Marching Cubes algorithm (Lerch, Carroll, et al., 2008), and used the multiple nonlinear subject-to-atlas deformation fields. For better precision and accuracy and to limit the influence of noise and error, the nonlinear portions of the transformations from each subject to all templates were concatenated and averaged across the template library (Borghammer et al., 2010; Dorr, Lerch, Spring, Kabani, & Henkelman, 2008; Frey et al., 2011). Displacement in millimeters was then established at each vertex of the 3D mesh by calculating the dot product of the surface normal and the nonlinear deformation vector. Surface area was calculated by assigning to each vertex a third of the area of each triangle it was a part of. Blurring was performed using a 5 mm duffusion smoothing kernel.

2.5 Cortical thickness calculation

Like measures of shape and surface area, cortical thickness is a vertex-wise parameter allowing for the detection of localized changes. In the present work, CT was calculated with the CIVET pipeline (version 1.1.10, Montreal Neurological Institute at McGill University, Montreal, Quebec, Canada) (Ad-Dab'bagh et al., 2006). In this pipeline, data are analyzed in a common space. Hence, individual T1 data were linearly registered to the symmetric ICBM 152 template (Collins, Neelin, Peters, & Evans, 1994; Mazziotta, Toga, Evans, Fox, & Lancaster, 1995) before skull stripping (Smith, 2002) and tissue segmentation into gray and white matter and CSF (Tohka, Zijdenbos, & Evans, 2004; Zijdenbos, Forghani, & Evans, 1998). After these initial steps, the pipeline used deformable models that make use of a partial volume classification (Kim et al., 2005) for reconstruction of the inner and outer surfaces of the cortex before applying a method described in detail elsewhere (Lerch & Evans, 2005) to measure the distance in millimeters between corresponding vertices. To increase statistical power and signal-to-noise ratio, blurring was performed on the cortical thickness maps with a 20 mm diffusion smoothing kernel (Chung & Taylor, 2004).

2.6 Resting state fMRI

Resting state data were analyzed using the functional connectivity toolbox CONN (version 14h; http://www.nitrc.org/projects/conn/) and the Group ICA of fMRI Toolbox (GIFT; version 3.0a; http://mialab.mrn.org/software/gift/). In CONN, Pre-processing steps included realignment, temporal filtering (0.01 – 0.1 Hz, Biswal, Yetkin, Haughton, and Hyde (1995)), detrending, slice-timing correction, coregistration, segmentation, normalisation, spatial smoothing (8 mm) and anatomical component-based noise correction (aCompCor) method (Behzadi, Restom, Liau, & Liu, 2007) to correct for physiological noise, which outperforms global signal correction (Chai, Castanon, Ongur, & Whitfield-Gabrieli, 2012) and increases the validity of ensuing analyses (Whitfield-Gabrieli & Nieto-Castanon, 2012). In the present work, analysis was applied on spherical regions of interest (ROI) predefined by CONN using Talairach Daemon

(http://www.talairach.org/daemon.html) labels. In GIFT, principal component analysis was run on the dataset of each subject before group ICA, which resulted in 20 independent components estimated by the infomax algorithm (Bell & Sejnowski, 1995). Group ICA was run both using the entire sample, for significance testing of group differences in non-artefact (neuronal) components, and separately for the experimental and control groups in order to assess correspondence of components between the two groups. MRIcron (http://www.nitrc.org/projects/mricron) was used to discern artefactual from neuronal components and to identify RSNs. The ICASSO toolbox (research.ics.aalto.fi/ica/icasso) was used to run the infomax algorithm 20 times for reliability assessment, starting with different initial values and using a bootstrap technique (minimal cluster size 16, maximal cluster size 20).

3 Aims, research questions, and hypotheses

The main aims of the present work were to examine the potential of hippocampal, thalamic, and striatal shape and cortical thickness as biomarkers in preclinical AD and to investigate the influence of participant information on a promising candidate for prediction of AD progression in cognitively unimpaired elderly individuals: functional connectivity within and between RSNs measured using rsfMRI.

3.1 Study 1

The research question of the first study was whether AD biomarker reserach using structural MRI data would profit from using localized measures of shape, surface area, subfield volumes and cortical thickness rather than volumes of entire structures. Different hippocampal (H. Braak & Braak, 1991b), thalamic (Aggleton, Pralus, Nelson, & Hornberger, 2016; H. Braak & Braak, 1991a), and cortical (Dickerson et al., 2008; Dickerson et al., 2011) regions are affected sequentially by AD pathology and thus, our hypothesis was that already in cognitively unimpaired individuals, these localized measures would correlate with AD pathology. This hypothesis was tested in

cognitively unimpaired individuals by correlating hippocampal, thalamic, and striatal shape, SA, and volume with amyloid load of the respective region and of the neocortex measured by PiB PET. We also correlated hippocampal subfield volumes with hippocampal and neocortical amyloid load, and cortical tickness with neocortical amyloid load.

3.2 Study 2

The research question of the second study was whether localized structural MRI measures differentiate between healthy elderly and MCI subgroups of individuals who later converted to AD dementia or remained stable. In this study, we measured volumes of the hippocampus and its subfields, the thalamus and its nuclei, the striatum, and the globus pallidus in addition to thalamic and striatal shape as well as cortical thickness. We compared converters at baseline and time of conversion and non-converters at baseline to their respective age and sex matched control group. We hypothesized that all three MCI groups would differ from matched controls, with more pronounced differences in converters. In addition, we conducted a receiver operating characteristic curve analysis to test the hypothesis that localized measures improve classification based solely on volume information.

3.3 Study 3

The research question of the third study was whether RSN functional connectivity is affected by participant information. Several studies have found that this is the case for variation of participant instruction (R. Patriat, Molloy EK, et al., 2013; K. Van Dijk et al., 2010; Yan et al., 2009), hampering the comparison of findings across study sites and impeding generalizability and reproducibility of results from rsfMRI analyses. We hypothesized that participant information would also affect rsfMRI measures and investigated connectivity between individual regions of interest as well as within and between functional networks. To test this hypothesis, we compared two groups of elderly subjects and experimentally manipulated their information status during scanning.

4 Empirical evidence

4.1 Hippocampal shape alterations are associated with regional Aβ load in cognitively normal elderly individuals

Schroeder, Clemens[a], Park, Min Tae M[b,c], Germann, Jürgen[c], Chakravarty, M. Mallar[c,d], Michels, Lars[e], Kollias, Spyros[e], Kroll, Sara[f], Buck, Alfred[g], Treyer, Valerie[g], Savaskan, E[a], Unschuld, Paul G[a], Nitsch, Roger M[a], Kälin, Andrea M[a], Hock, Christoph[a], Gietl, Anton F[a]*, Leh, Sandra E[a]*

a Institute for Regenerative Medicine, University of Zurich

b Schulich School of Medicine and Dentistry, Western University, London, Canada

c Cerebral Imaging Centre, Douglas Mental Health University Institute, McGill University, Montréal, Canada

d Departments of Psychiatry and Biomedical Engineering, McGill University, Montreal, Canada

e Institute of Neuroradiology, University of Zurich

f Department of Psychiatry, Psychotherapy and Psychosomatics, University of Zurich

g Department of Nuclear Medicine, University Hospital Zurich

* These authors contributed equally to this work.

Corresponding authors:
Sandra Leh, Klinik für Alterspsychiatrie, Minervastrasse 145, CH-8032 Zürich
Phone: +41 44 389 1558, Fax: +41 44 389 1414, E-mail: sandra.leh-seal@bli.uzh.ch

Clemens Schroeder, Klinik für Alterspsychiatrie, Minervastrasse 145, CH-8032 Zürich
Phone: +41 44 389 1677, Fax: +41 44 389 1414, E-mail: clemens.schroeder@uzh.ch

The authors have no conflict of interest.

Abstract

Aβ deposition is a driving force of Alzheimer's disease pathology and can be detected early by amyloid positron emission tomography. Identifying presymptomatic structural brain changes associated with Aβ deposition might lead to a better understanding of its consequences and provide early diagnostic information. In this respect we analyzed measures of cortical thickness and subcortical volumes along with hippocampal, thalamic and striatal shape and surface area by applying novel analysis strategies for structural magnetic resonance imaging. We included 69 cognitively normal elderly subjects after careful clinical and neuropsychological workup. Standardized uptake value ratios (cerebellar reference) for uptake of 11-C-Pittsburgh Compound B (PiB) were calculated from positron emission tomographic data for a cortical measurement and for bilateral hippocampus, thalamus and striatum. Associations to shape, surface area, volume and cortical thickness were tested using regression models that included significant predictors as covariates. Left anterior hippocampal shape was associated with regional PiB uptake ($p < 0.05$, FDR-corrected), whereas volumes of the hippocampi and their subregions were not associated with the cortical measurement or uptake in the other regions (all $p > 0.05$, FDR-corrected). Within the entorhinal cortical region of both hemispheres, thickness was negatively associated with cortical uptake ($p < 0.05$, FDR-corrected). Hence, localized shape measures and cortical thickness may be potential biomarkers of presymptomatic Alzheimer's disease.

Keywords

beta-amyloid; hippocampal shape; Alzheimer's disease; Magnetic resonance imaging; positron emission tomography

Introduction

Sporadic Alzheimer's disease (AD) is a major global health burden with no cure available at the moment. It has become evident that the pathological process may start decades before the onset of clinical symptoms (Villemagne et al., 2013). Therefore, diagnostic criteria have been developed to identify the preclinical stages of Alzheimer's disease (Sperling, Aisen, et al., 2011) with the ultimate goal of facilitating studies on early intervention. Currently, the A-4 trial examines if the antibody solanezumab may be beneficial in cognitively asymptomatic subjects selected on the basis of a positive amyloid-pet (Laske, 2014). It is hypothesized that intervention at presymptomatic stages is most effective treatment when cognitive functioning can be stabilized at the highest possible level (Masdeu et al., 2012). Furthermore, substances directed at Abeta-reduction are believed to be more effective if given early in the disease process. A scenario of early detection would require a high number of cognitively normal elderly individuals to undergo preventive screening. Hence, it is desirable to obtain diagnostic measures non-invasively and at comparatively low cost. In this respect, magnetic resonance imaging (MRI) measurements capable of identifying early brain changes associated with amyloid deposition would pose an attractive option.

Highly localized structural MRI measures such as cortical thickness (CT) and subcortical shape and surface area (SA) of brain structures are necessary to detect highly spatially confined presymptomatic changes. Using CT analysis, a recent study presented results that are consistent with cortical thinning during progression from preclinical AD to dementia due to AD (Dickerson et al., 2011). In addition, evidence for early thalamic abnormalities in Alzheimer's disease is growing (Aggleton et al., 2016). Previous studies have reported thalamic differences between normal-aging subjects and individuals with amnestic MCI using texture analysis (de Oliveira et al., 2011)

and smaller thalamic volume in MCI compared to controls with normal cognition (Yi et al., 2015). In a recent study from our group, we found thalamic and striatal shape differences between individuals with MCI and individuals with normal cognition in the absence of volumetric differences (Leh et al., 2016). These findings suggest that thalamic shape changes occur early in AD and underline the importance of thalamic shape information in the search for presymptomatic AD biomarkers and point to an important role of the anterior thalamic nuclei in AD research which play an important role in episodic memory. In contrast to thalamic shape, hippocampal morphology has already been studied repeatedly in AD (de Flores, La Joie, & Chetelat, 2015) and studies comparing patients with AD to healthy control subjects have shown inward deformation of cornu ammonis (CA) 1 (Frisoni et al., 2008; Wang et al., 2003). In one previous study, localized inward changes in left hippocampal surface significantly predicted progression of non-demented elderly individuals to dementia due to AD (Csernansky et al., 2005).

In this study, we therefore used structural MRI measures of CT and hippocampal, thalamic and striatal volume, shape and SA to identify brain changes associated with amyloid deposition measured by Pittsburgh compound B (PiB) positron emission tomography (PET) in cognitively normal elderly individuals.

Materials and methods

Participants

A total of 69 cognitively healthy elderly participants (32 women, age 55–80 years) from a longitudinal cohort study were included. Seventeen of these participants have already been included in a previous publication from our group focusing on structural differences between individuals with amnestic MCI and cognitively normal subjects (Leh et al., 2016). Inclusion and exclusion criteria have been published previously (Gietl et al., 2015; Schreiner et al., 2014; Steininger et al., 2014). Cognitive health was confirmed by clinical examination consisting of clinical workup and neuropsychological assessment and a Mini-Mental State Examination (MMSE) score of ≥27.

Participants were excluded if one or more of the following conditions were met: contraindication against MRI or venipuncture, substance abuse with a possible effect on cognition, change in red blood cell count of clinical significance, allergy to PiB or one of its constituents, history of severe allergic reactions to drugs or allergens, critical or medically unstable illness, pregnancy or lactation and significant exposure to radiation.

Descriptive data for all metric control, volume and standardized uptake value ratio (SUVR) variables can be found in Table 1.

Table 1. Descriptive data for all control, volume and SUVR variables

Variable	M	SD
Age (years)	68.087	6.029
Education (years)	15.101	2.739
ICV (cubic centimeters)	1326.871	205.983
Volume of left hippocampus*	17.446	2.467
Volume of right hippocampus*	17.242	2.405
Volume of left CA1*	5.471	0.733
Volume of right CA1*	5.560	0.749
Volume of left subiculum*	2.459	0.371
Volume of right subiculum*	2.684	0.407
Volume of left CA4/DG*	4.269	0.683
Volume of right CA4/DG*	4.254	0.643
Volume of left CA2/CA3*	1.162	0.211
Volume of right CA2/CA3*	1.074	0.236
Volume of left SRLM*	4.086	0.649
Volume of right SRLM*	3.669	0.603
Cortical SUVR	1.245	0.275
SUVR of left hippocampus	1.238	0.106
SUVR of right hippocampus	1.235	0.098
SUVR of left thalamus	1.425	0.193
SUVR of right thalamus	1.404	0.176
SUVR of left striatum	1.342	0.256
SUVR of right striatum	1.343	0.252

M, mean; SD, standard deviation; ICV, intracranial volume; CA, cornu ammonis; DG, dentate gyrus; SRLM, strata radiata/lacunosum-moleculare; SUVR, standardized uptake value ratio.

*Adjusted for ICV and multiplied by 104.

This study was conducted in compliance with the Helsinki Declaration and approved by the cantonal ethics committee of Zurich, Switzerland (E_64_2009). Written informed consent was obtained from each participant prior to study enrolment.

PET acquisition

The PET acquisition procedure has been previously published (Gietl et al., 2015; Schreiner et al., 2014; Steininger et al., 2014). Each participant received an antecubital venous injection of approximately 350 MBq of PiB (PiB synthesis has been described before in Gietl et al., 2015). A 70-min dynamic PET scan (4 × 15, 8 × 30, 9 × 60, 2 × 180 and 10 × 300 s) was performed. Voxel spacing was 2.34 × 2.34 × 3.27 mm.

MR acquisition

MR acquisition has been published previously (Gietl et al., 2015). T1-weighted data were acquired on a 3-T Phillips Achieva with the following parameters: repetition time 8.2 ms, echo time 3.7 ms and 8° flip angle, field of view 240 mm (AP) × 220 mm (FH) × 188 mm (RL), 220 axial slices with 1-mm single-slice thickness (voxel dimensions: 0.94 × 0.94 × 1 mm).

Subcortical segmentation and volume calculation

Segmentation of bilateral hippocampus, thalamus and striatum as well as hippocampal subfields was performed by using the Multiple Automatically Generated Templates (MAGeT Brain) algorithm (Chakravarty et al., 2013) using a voxel-wise majority vote (Collins & Pruessner, 2010). The input atlases used for hippocampal subfield segmentation were produced by Winterburn et al. (Winterburn et al., 2013) and have been validated for use with MAGeT brain (Pipitone et al., 2014). The five subfields delineated in these atlases are cornu ammonis (CA) 1, subiculum, CA 4 and dentate gyrus, CA 2 and 3 and stratum radiatum/lacunosum/moleculare (SRLM). We used five input atlases that were registered to a subset of 21 subjects, a number that had been shown to be optimal in previous research (Pipitone et al., 2014), to generate a template library. The input atlas used for thalamus and striatum segmentation was produced by Chakravarty, Bertrand, Hodge,

Sadikot, & Collins(Chakravarty et al., 2006). A visualization of the left-hemispheric part of these volumes of interest is displayed in Fig. 1.

Figure 1. Subcortical segmentation.

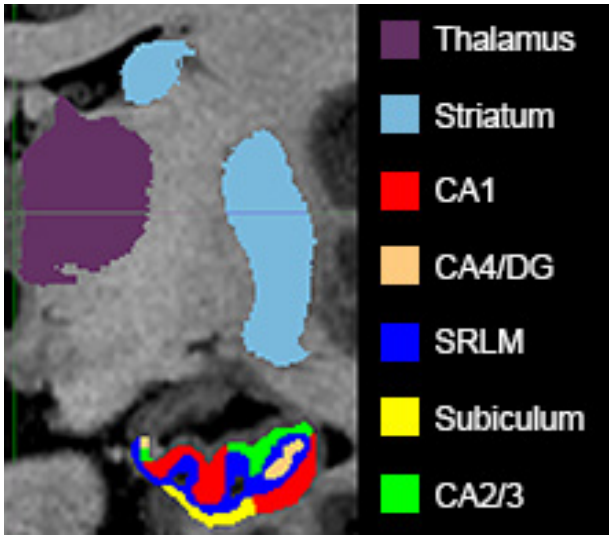

Figure 1. Segmentation of the thalamus, the striatum and the five hippocampal subfields. Left-hemispheric structures are depicted.

For each subject, volumes of total hippocampi and their subfields were derived from the number of voxels resulting from segmentation. These volumes were then divided by the total intracranial volume of the subject and the resulting value was used for analysis. Calculation of total intracranial volume has been described previously (Buckner et al., 2004).

Determination of cortical 11-C-PiB-SUVR (cortical SUVR from now on) as a measure of cortical plaque burden

Image processing was done automatically under visual control with PMOD PNEURO tool Version 3.4 (PMOD LTD, Zurich, Switzerland) and described in detail before (Gietl et al., 2015). The average of the first 13 frames of the dynamic scans was co-registered with the structural MR image using a normalized mutual-information–based registration. After normalization, a maximum probability atlas (Hammers N30R83) (Gousias et al., 2008; Hammers et al., 2003) was used to define 48 VOIs based on the

segmentation of GM and white matter. Segmentation was performed on the individual MRI (at least 50% GM probability). The combined transformation matrices (PET to MR and MR to Montreal Neurologic Institute [MNI] space) were applied to the dynamic PET images to perform all further analyses in MNI space. The average tracer uptake 50–70 min was then calculated for the segmented grey matter VOIs. For derivation of cortical SUVR, 24 bilateral cortical brain structures of the Hammers N30R83 atlas (http://doc.pmod.com/pneuro/7674.htm) – excluding occipital lobe, insula, primary motor and sensorimotor cortices – were merged using a volume-weighted averaging procedure, ascertaining that the uptake in larger regions contributes more to this average than the uptake in smaller regions. Bilateral cerebellar grey matter uptake, which was also derived from the Hammers N30R83 atlas, served as a reference for standardization between subjects because of the relatively late involvement of the cerebellar grey matter in plaque pathology, as done before (Johnson et al., 2016; Liu et al., 2015). The ratio of the cortical VOI's average uptake and the average cerebellar grey matter uptake is termed “cortical SUVR” and serves as a measure of cortical plaque burden.

Regional 11-C-PIB-SUVR (regional SUVR from now on) calculation

Image processing for regional SUVR calculation was done with PMOD FUSION tool Version 3.5 (PMOD LTD, Zurich, Switzerland). Also in this analysis the average of the first 13 frames was co-registered with the structural MR image using a normalized mutual-information–based registration. Registration success was determined by visual inspection performed by our group. The regions specifically studied for shape changes within this project for hippocampal, thalamic and striatal SUVR calculation were derived from automatic subcortical segmentation with the MAGeT Brain algorithm as described above. This algorithm has been demonstrated to outperform FreeSurfer and FSL FIRST (Pipitone et al., 2014). Segmentation was performed in subject space of the individual MR. The PET to MR transformation matrices from the registration process were applied to the dynamic PET images to be able to place the MR-derived regions on the PET image. Subsequent analyses were performed in subjects’ MR space. Again,

the average tracer uptake 50–70 min was then calculated for the segmented VOIs. The cerebellar reference region used for calculation of regional SUVR was segmented using the LONI probabilistic brain atlas (LPBA40) (Shattuck et al., 2008). The ratio of the specific uptake of a particular VOI and the cerebellar grey matter uptake is termed “regional SUVR”.

Shape and SA calculation

Delineation of bilateral hippocampus, thalamus and striatum was carried out using a method adapted from Lerch et al. (Lerch, Carroll, et al., 2008) to measure local inward and outward displacements. For a detailed description, see Lerch et al. (Lerch, Carroll, et al., 2008) and Raznahan et al. (Raznahan et al., 2014). SA calculation was performed as described previously (Raznahan et al., 2014).

Cortical thickness calculation

CT was calculated with the CIVET pipeline (version 1.1.10, Montreal Neurological Institute at McGill University, Montreal, Quebec, Canada) (Ad-Dab’bagh et al., 2006). First, the T1 image of each subject was linearly registered to the symmetric ICBM 152 template (Collins et al., 1994; Mazziotta et al., 1995). Then, skull stripping (Smith, 2002) and tissue segmentation into gray and white matter and cerebrospinal fluid (CSF) (Tohka et al., 2004; Zijdenbos et al., 1998) were carried out. Next, the interface between gray matter and CSF and the inner white matter surface were constructed for each hemisphere using deformable models (Kim et al., 2005). For each of the resulting 40 962 vertices per hemisphere, the distance in millimeters between the inner and the outer surface was measured using a previously described method (Lerch & Evans, 2005). To increase statistical power and signal-to-noise ratio, blurring was performed on the cortical thickness maps with a 20-mm diffusion smoothing kernel (Chung & Taylor, 2004).

Data analysis

For statistical analysis, the R software package (https://www.r-project.org/) (R Core Team, 2014) was used. In addition, the RMINC (R for Medical Imaging NetCDF) library

(https://wiki.mouseimaging.ca/display/MICePub/RMINC/) (Lerch & Nikelski, 2009) was used for statistical analysis of the associations between shape/SA/CT and cortical/regional SUVR.

To specify the most adequate model in each regression analysis, the following procedure was performed: First, the relevance of each of the following potential covariates was assessed by using the covariate and cortical or regional SUVR as regressors: age (in years), gender, education (in years), total intracranial volume and APOE genotype. Second, a regression model was specified retaining only the significant covariates as regressors. Models testing associations between volumes and SUVR did not include total intracranial volume as a covariate because these volumes were normalized by total intracranial volume. In this sample, education and APOE genotype did not significantly predict hippocampal volume, thalamic volume, striatal volume, shape or CT.

Associations between volumes and SUVR

All volumes were adjusted for total intracranial volume using a method described previously (Buckner et al., 2004). To investigate the associations between SUVR and hippocampal total and subfield volumes as well as thalamic and striatal volumes, regression models were specified with volume as regressand and cortical or regional SUVR as regressor. First, these 32 models were specified including age, gender, education and APOE genotype as covariates. In these 32 models, education was never a significant covariate, APOE genotype was significant three times, age 24 times and gender 28 times. Therefore, regression models using age and gender as covariates were specified to investigate the associations between SUVR and volumes. The resulting P-values were Benjamini-Hochberg FDR corrected for multiple comparisons with number of comparisons m set to 12, taking into consideration the high dependency of hippocampal subfield volumes from each other and total hippocampal volume.

Associations between shapes or SA and SUVR

To investigate the association between shapes and cortical or regional SUVR, a regression model was specified at each vertex with displacement as

regressand and cortical or regional SUVR as regressor. First, these 12 models were specified including age, gender, education, total intracranial volume and APOE genotype as covariates. In these 12 models, age, education and APOE genotype were never significant covariates, total intracranial volume was significant 8 times and gender 12 times. Therefore, regression models using gender and total intracranial volume as covariates were specified to investigate the associations between SUVR and shapes. In each of these cases, the resulting test statistics were FDR corrected for multiple comparisons (Benjamini-Hochberg). FDR-corrected values of $P < 0.05$ were considered significant.

To investigate the association between SA and cortical or regional SUVR, a regression model was specified at each vertex with SA as regressand and cortical or regional SUVR as regressor. First, these 12 models were specified including age, gender, education, total intracranial volume and APOE genotype as covariates. In these 12 models, APOE genotype was never a significant covariate, education was significant once, gender was significant 5 times, age 8 times and total intracranial volume 12 times. Therefore, regression models using gender, age and total intracranial volume as covariates were specified to investigate the associations between SUVR and SA. In each of these cases, the resulting test statistics were FDR corrected for multiple comparisons (Benjamini-Hochberg). FDR-corrected values of $P < 0.05$ were considered significant.

Associations between CT and cortical SUVR

To investigate the association between CT of each hemisphere and cortical SUVR, a regression model was specified at each vertex with CT as regressand and cortical SUVR as regressor. First, these two models were specified including age, gender, education, total intracranial volume and APOE genotype as covariates. In both models, age and total intracranial volume were significant covariates. Therefore, regression models using age and total intracranial volume as covariates were specified to investigate the associations between cortical SUVR and CT. Again, the resulting test statistics were FDR corrected for multiple comparisons (Benjamini-Hochberg). FDR-corrected values of $P < 0.05$ were considered significant. To determine

the cortical regions wherein significant associations occurred, two separate atlases were used (Amunts et al., 2005; Mai, Majtanik, & Paxinos, 2015).

Associations between cognitive performance and SUVR or volume

To confirm that cortical/regional SUVR and volume were not associated with cognitive performance in our sample of cognitively normal elderly subjects, regression models were specified for nine measures pertaining to memory and executive function (Table 2). For memory assessment, the German-language verbal learning and memory test “Verbaler Lern- und Merkfähigkeitstest” (VLMT) was used, providing learning, recall and recognition measures of verbal memory (Helmstaedter, Lendt, & Lux, 2001; Volz-Sidiropoulou, Poll, Forkmann, & Gauggel, 2010), as well as digit span forward from the Wechsler Memory Scale - Revised (Härting et al., 2000). For assessment of executive function, the following neuropsychological measures were obtained: Digit span backward from the Wechsler Memory Scale – Revised (Härting et al., 2000), verbal (semantic) fluency and letter (phonemic) fluency from the CERAD-plus test battery (Thalmann et al., 1997), the five-point test (5PT) (Kelemen & Fenton, 2010; Regard, Strauss, & Knapp, 1982) and a measure from the trail making test (TMT) (Reitan, 1958) calculated by dividing the result of its B version by the result of its A version, which represents executive function.

Table 2. Neuropsychological measures, descriptive data and covariates used in regression analyses

Neuropsychological measure	Cognitive domain	Significant covariates		M	SD
		SUVR	Volume		
VLMT	Verbal memory - acquisition [a]	Sex	Sex, ICV (left thalamus: sex)	55.014	8.13
	Verbal memory - recall [b]	None	None	1.957	1.851
	Verbal memory - recognition [c]	Age, Sex	Age, Sex (left striatum: sex)	12.681	2.648
Digit span forward	Working memory	None	None	7.072	1.621
Digit span backward	Executive function	Education	Education	6.565	1.736
Verbal (semantic) fluency (animals)	Executive function	Genotype	Genotype (left thalamus: none)	24.406	6.013
Letter (phonemic) fluency (S words)	Executive function	None	None	30.522	10.997
5PT	Executive function	None	None	28.116	7.565
TMT B/A	Executive function	None	None	2.537	0.96

VLMT, Verbaler Lern- und Merkfähigkeitstest; 5PT, five-point test; TMT, trail making test (versions A and B); ICV, intracranial volume.

[a] This measure is the sum of the immediate recall from five consecutive runs of learning 15 words.

[b] This measure is the delayed recall score.

[c] This measure is the difference between the number of correctly recognized and the number of falsely identified words out of a list of previously presented and new words.

Results

Associations between volumes and SUVR

Descriptive data for volumes and SUVR are shown in Table 1. Volumes of bilateral hippocampus and hippocampal subfields CA4/DG, CA2/CA3 and SRLM, left hippocampal subiculum and CA1 subfields as well as right thalamus were associated with cortical SUVR but not with regional SUVR (see Table 3).

Associations between shapes or SA and SUVR

Significant associations were found between left thalamic shape outward deformations and cortical SUVR in the region of its anterior nuclei (Fig. 2A), as well as between left thalamic SA and regional SUVR in the area of its pulvinar (Fig. 2B). In addition, significant associations were found between left anterior hippocampal shape and regional SUVR, predominantly in its CA1 and subiculum regions, with dorsal outward and ventral inward deformations, respectively (Fig. 2C).

Associations between CT and cortical SUVR

Significant negative associations between CT and SUVR were found for the left and right hemisphere. The areas of these associations corresponded highly between the hemispheres and occurred within the entorhinal cortex (EC) region (Fig. 3).

Associations between cognitive performance and SUVR or volumes

Descriptive data for measures of cognitive performance are shown in Table 2. No associations between cognitive performance and SUVR (Table 4) or volumes (Table 5) were significant after Bonferroni-Holm correction for multiple comparisons.

Table 3. Associations between SUVR and volumes

Volume of interest	cortical SUVR				regional SUVR			
	t value	p value	Rank	(i/m)Q	t value	p value	Rank	(i/m)Q
Thalamus	-1.138	0.259	12	0.050	0.046	0.963	29	0.121
	-1.371	0.175	10	0.042	-0.915	0.363	13	0.054
Striatum	-0.037	0.971	31	0.129	0.044	0.965	30	0.125
	0.351	0.727	21	0.088	0.224	0.824	26	0.108
Hippocampus	-1.827	0.072	4	0.017	0.239	0.812	25	0.104
	-1.265	0.210	11	0.046	0.690	0.493	18	0.075
CA1	-1.699	0.094	5	0.021	0.291	0.772	22	0.092
	-0.849	0.399	14	0.058	0.846	0.401	15	0.063
CA2/3	-2.020	0.047	2	0.008	0.265	0.792	23	0.096
	-2.298	0.025	1	0.004	0.721	0.473	16	0.067
CA4/DG	-1.401	0.166	8	0.033	0.562	0.576	20	0.083
	-1.388	0.170	9	0.038	0.223	0.824	27	0.113
Subiculum	-1.468	0.147	6	0.025	-0.167	0.868	28	0.117
	-0.605	0.548	19	0.079	0.252	0.802	24	0.100
Stratum	-1.864	0.067	3	0.013	-0.016	0.987	32	0.133
	-1.456	0.150	7	0.029	0.721	0.473	17	0.071

j = Rank, m = 12 (number of comparisons), Q = 0.05 (significance threshold)

SUVR = subjective uptake value ratio, CA = cornu ammonis, DG = dentate gyrus

Figure 2. Associations between shapes or SA and SUVR

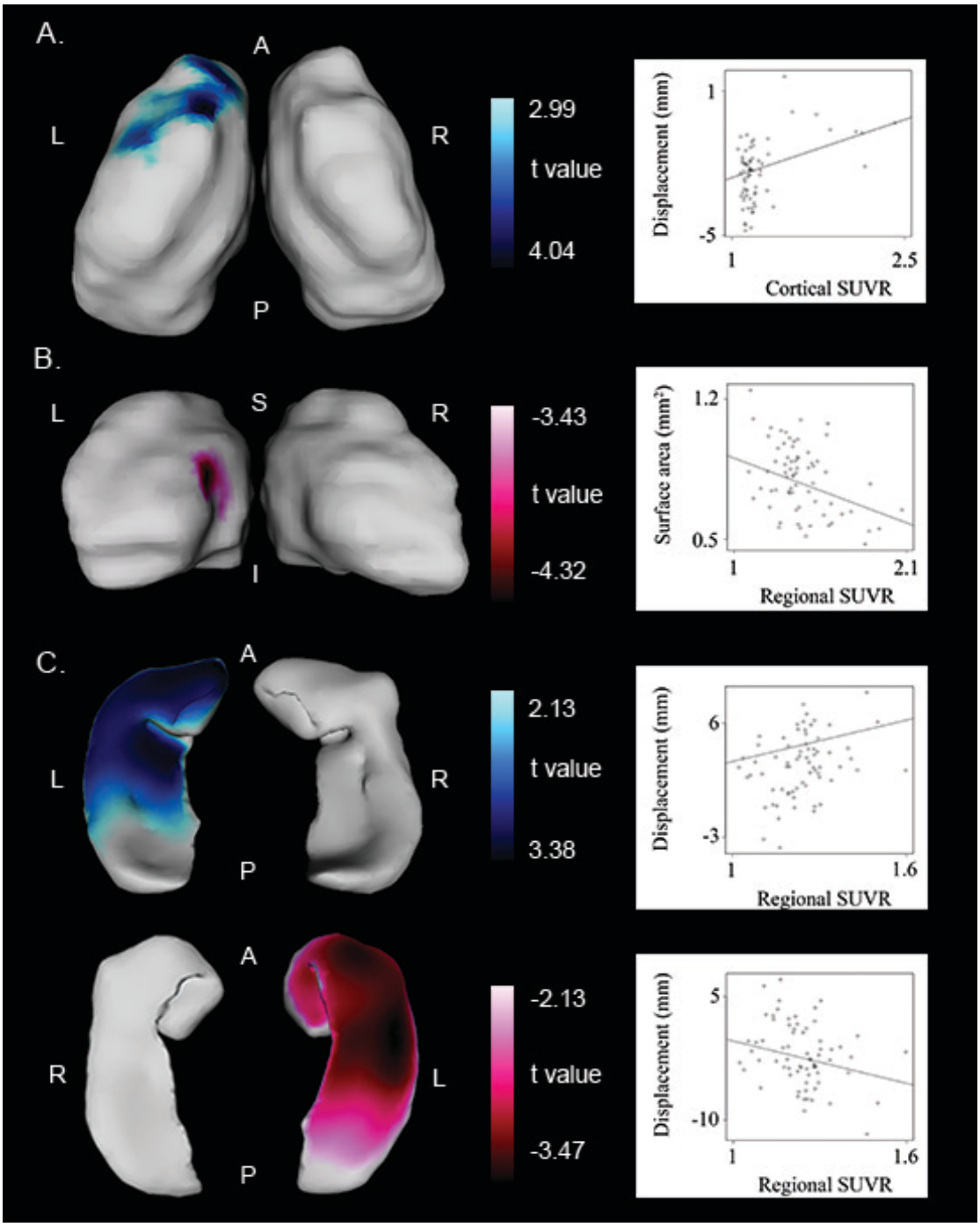

Figure 2. (A) Colored areas show significant associations between thalamic shape and cortical SUVR using a FDR-corrected P value of 0.05. Scatterplots on the right-hand side illustrate dispersion of values at peak vertices (minimal and maximal t value). Dorsal view of bilateral thalamus shows associations between outward deformations and cortical SUVR in the area of the left anterior dorsal nuclei. (B) Colored areas show significant associations between thalamic SA and regional SUVR using a FDR-corrected P value of

0.05. This posterior view of bilateral thalamus shows negative associations between SA and regional SUVR in the area of the left mediodorsal nucleus. Scatterplot on the right-hand side illustrates dispersion of values at the peak vertex (minimal t value). (C) Colored areas show significant associations between hippocampal shape and regional SUVR using a FDR-corrected P value of 0.05. Scatterplots on the right-hand side illustrate dispersion of values at peak vertices (minimal and maximal t value). Upper row: Dorsal view of bilateral hippocampus shows associations between outward deformations and regional SUVR in the area of the left anterior hippocampus. Lower row: Ventral view of bilateral hippocampus shows associations between inward deformations and regional SUVR. L, left; R, right; A, anterior; P, posterior; S, superior; I, inferior.

Figure 3. Associations between CT and cortical SUVR

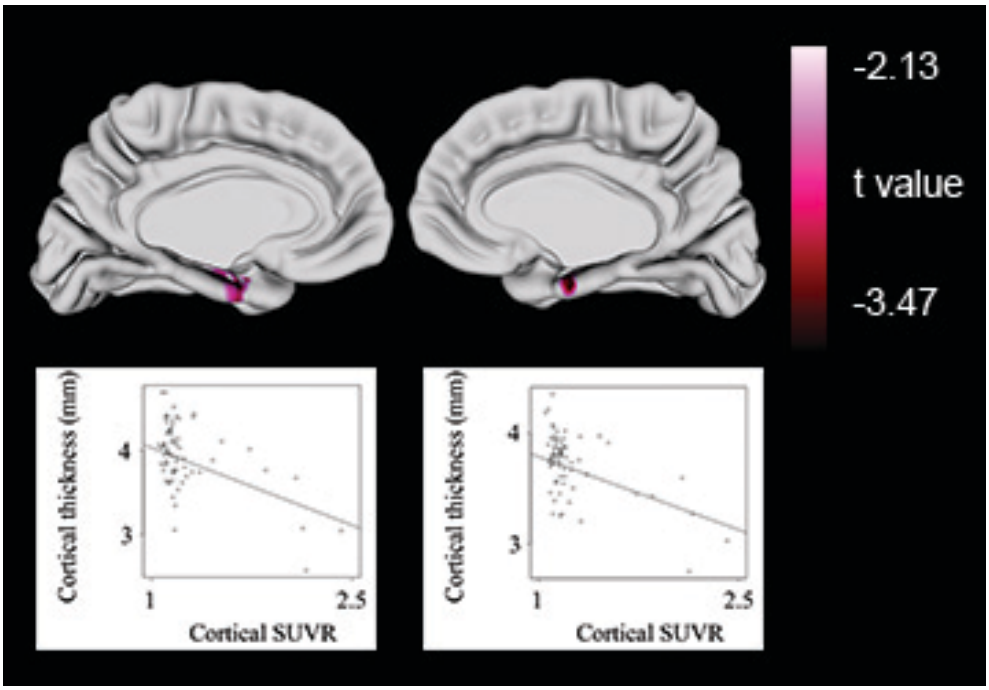

Figure 3. Upper row: Colored areas show significant associations between CT and cortical SUVR using a FDR-corrected P value of 0.05. This medial view of both hemispheres shows negative associations between CT and cortical SUVR in the area of bilateral EC. Lower row: Scatterplots illustrate dispersion of values at peak vertices (minimal t values).

Table 4. Associations between SUVR and cognitive performance

Neuropsychological measure		Tracer uptake region						
		Cortex	Thalamus		Striatum		Hippocampus	
			left	right	left	right	left	right
Verbal memory - acquisition (VLMT)	t value	0.384	0.253	1.452	-0.046	0.553	0.431	0.552
	p value	0.702	0.801	0.151	0.963	0.582	0.668	0.583
	Rank	45	56	8	62	37	44	38
	(i/m)Q	0.036	0.044	0.006	0.049	0.029	0.035	0.030
Verbal memory - recall (VLMT)	t value	-0.920	0.046	0.366	-0.100	-0.606	-0.312	0.518
	p value	0.361	0.963	0.716	0.920	0.546	0.756	0.606
	Rank	19	61	47	60	34	52	41
	(i/m)Q	0.015	0.048	0.037	0.048	0.027	0.041	0.033
Verbal memory - recognition (VLMT)	t value	1.076	-0.381	-0.120	0.504	0.856	0.927	1.137
	p value	0.286	0.705	0.905	0.616	0.395	0.358	0.260
	Rank	17	46	58	42	22	18	13
	(i/m)Q	0.013	0.037	0.046	0.033	0.017	0.014	0.010
Digit span forward	t value	0.314	-0.235	-0.566	0.106	-0.014	-1.563	-1.285
	p value	0.754	0.815	0.574	0.916	0.988	0.123	0.203
	Rank	51	57	36	59	63	6	11
	(i/m)Q	0.040	0.045	0.029	0.047	0.050	0.005	0.009
Digit span backward	t value	-1.567	-0.680	-0.468	-1.398	-1.481	-0.527	-1.116
	p value	0.122	0.499	0.642	0.167	0.143	0.600	0.269
	Rank	5	32	43	9	7	40	14

	(i/m)Q	0.004	0.025	0.034	0.007	0.006	0.032	0.011
Verbal (semantic) fluency (animals)	t value	0.848	0.579	0.916	1.096	0.773	0.808	0.356
	p value	0.400	0.565	0.363	0.277	0.442	0.422	0.723
	Rank	23	35	20	15	27	25	48
	(i/m)Q	0.018	0.028	0.016	0.012	0.021	0.020	0.038
Letter (phonemic) fluency (S words)	t value	-0.265	-0.760	-1.254	-0.281	-0.711	1.087	0.698
	p value	0.792	0.450	0.214	0.780	0.480	0.281	0.488
	Rank	55	28	12	53	30	16	31
	(i/m)Q	0.044	0.022	0.010	0.042	0.024	0.013	0.025
5PT	t value	1.596	-0.329	-0.266	0.814	0.673	-0.749	-0.904
	p value	0.115	0.743	0.791	0.418	0.503	0.456	0.369
	Rank	4	49	54	24	33	29	21
	(i/m)Q	0.003	0.039	0.043	0.019	0.026	0.023	0.017
TMT B/A	t value	1.866	0.328	2.027	1.364	2.337	0.546	0.773
	p value	0.066	0.744	0.047	0.177	0.022	0.587	0.442
	Rank	3	50	2	10	1	39	26
	(i/m)Q	0.002	0.040	0.002	0.008	0.001	0.031	0.021

i = Rank, m = 63 (number of comparisons), Q = 0.05 (significance threshold)

Table 5. Associations between volumes and cognitive performance

Neuropsychological measure		Region					
		Thalamus		Striatum		Hippocampus	
		left	right	left	right	left	right
Verbal memory - acquisition (VLMT)	t value	0.512	1.553	2.024	1.661	1.976	2.243
	p value	0.610	0.125	0.047	0.102	0.052	0.028
	Rank	41	16	4	14	6	1
	(i/m)Q	0.038	0.015	0.004	0.013	0.006	0.001
Verbal memory - recall (VLMT)	t value	1.269	1.111	1.053	1.205	0.919	0.844
	p value	0.209	0.271	0.296	0.232	0.361	0.402
	Rank	22	26	27	24	30	33
	(i/m)Q	0.020	0.024	0.025	0.022	0.028	0.031
Verbal memory - recognition (VLMT)	t value	0.384	0.225	1.387	0.527	0.847	0.981
	p value	0.702	0.823	0.170	0.600	0.400	0.330
	Rank	43	46	21	39	32	28
	(i/m)Q	0.040	0.043	0.019	0.036	0.030	0.026
Digit span forward	t value	-1.807	-1.718	-0.851	-0.969	-1.664	-1.484
	p value	0.075	0.091	0.398	0.336	0.101	0.143
	Rank	9	11	31	29	13	19
	(i/m)Q	0.008	0.010	0.029	0.027	0.012	0.018
Digit span backward	t value	-1.786	-1.603	-2.016	-1.426	-2.082	-1.126
	p value	0.079	0.114	0.048	0.159	0.041	0.264
	Rank	10	15	5	20	3	25

	(i/m)Q	0.009	0.014	0.005	0.019	0.003	0.023
Verbal (semantic) fluency (animals)	t value	2.165	1.689	0.757	0.519	0.043	0.774
	p value	0.034	0.096	0.452	0.605	0.966	0.442
	Rank	2	12	36	40	53	34
	(i/m)Q	0.002	0.011	0.033	0.037	0.049	0.031
Letter (phonemic) fluency (S words)	t value	0.227	0.177	-0.131	-0.157	-0.237	-0.761
	p value	0.821	0.860	0.896	0.876	0.813	0.449
	Rank	45	47	50	48	44	35
	(i/m)Q	0.042	0.044	0.046	0.044	0.041	0.032
5PT	t value	-1.857	-1.899	-0.399	-0.709	-1.526	-1.498
	p value	0.068	0.062	0.691	0.481	0.132	0.139
	Rank	8	7	42	37	17	18
	(i/m)Q	0.007	0.006	0.039	0.034	0.016	0.017
TMT B/A	t value	0.047	0.011	0.054	-0.139	0.681	1.215
	p value	0.963	0.991	0.957	0.890	0.498	0.229
	Rank	52	54	51	49	38	23
	(i/m)Q	0.048	0.050	0.047	0.045	0.035	0.021

i = Rank, m = 54 (number of comparisons), Q = 0.05 (significance threshold)

Discussion

The goal of this study was to investigate structural brain changes in cognitively healthy elderly subjects with various degrees of cerebral amyloid deposition. We showed that bilateral hippocampal volumes were not significantly associated with regional SUVR in healthy subjects, extending findings from a study of patients with mild AD (Y. T. Chang et al., 2015). In contrast to our findings, previous studies showed that hippocampal volumes were related to cortical PiB uptake in healthy elderly subjects (Hsu et al., 2015; Mormino et al., 2008), and a recent study using PiB PET and CSF tau and ptau to classify participants into stages of preclinical AD found smaller hippocampal volumes in later preclinical stages (Gordon et al., 2016). In addition, hippocampal atrophy in CA1 and the subiculum has been shown to predict progression to amnestic MCI in cognitively normal elderly individuals (Apostolova et al., 2010; Kerchner et al., 2010a). Here, our findings would be consistent with the assumption that Aβ deposition precedes hippocampal atrophy (Jack et al., 2013; Mormino et al., 2008). With respect to the staging model of preclinical Alzheimer's disease (Sperling, Aisen, et al., 2011), it could be that our population represents a very early stage with predominantly amyloid deposition without concomitant hippocampal atrophy. Left hippocampal shape was not significantly associated with cortical, but with regional SUVR. These findings suggest that early hippocampal shape changes may reflect a localized reaction to amyloid deposition. Hippocampal shape has been shown to be associated with Aβ measured in CSF in healthy elderly individuals in a previous study (Carmichael et al., 2012). This study derived shape measures from independent component analysis, where components defined a subregion of the three-dimensional hippocampus representation. In contrast, vertex-wise displacement values were used in this study. Whereas CSF Aβ allows a global estimation of cerebral amyloid deposition, by using amyloid-PET we were able to separately analyze cortical and regional SUVR in this study. Hence, the present results are more informative with regard to the localization of significant associations between hippocampal shape and SUVR and they extended the previous findings by

showing that hippocampal but not cortical Aβ load was associated with hippocampal shape.

The localization of these associations with left anterior CA 1 corroborates previous findings in MCI patients (de Flores et al., 2015) and is in line with a previous study on progression of non-demented elderly individuals to dementia due to AD (Csernansky et al., 2005). This finding should be interpreted in the context of our results revealing entorhinal cortical thickness associations with cortical SUVR. The EC is affected early by tau pathology in AD (H. Braak & Braak, 1991b) and projects to the hippocampus via the perforant pathway, which is not only the primary input to the hippocampal formation but also originates from cells that show neurofibrillary tangles in AD (Hyman, Van Hoesen, Kromer, & Damasio, 1986). Adding amyloid deposits to the perforant pathway terminal zone of neurons containing pathological tau has recently been shown to increase the extent of dystrophic axons and strongly alter the connectivity of these neurons in a transgenic mouse model (Pooler et al., 2013). Thus, shape changes associated with amyloid deposition may represent axonal damage due to amyloid toxicity in entorhinal neurons containing pathological tau. Hippocampal SUVR has been shown to correlate with fluid attenuated inversion recovery intensities, indicating tissue edema, in cognitively normal elderly subjects (Schreiner et al., 2014), supporting the view that a degenerative process underlies the association between hippocampal SUVR and shape found in this study.

Furthermore, our analyses revealed significant associations between shape and cortical SUVR in the region of the anterior dorsal nuclei of the left thalamus. The anterior thalamic nuclei contain numerous neurofibrillary tangles in AD (H. Braak & Braak, 1991a) and are implicated in memory (Jankowski et al., 2013). They have been shown to receive inputs from the subiculum in rat and monkey (Aggleton, Desimone, & Mishkin, 1986; Wright, Erichsen, Vann, O'mara, & Aggleton, 2010), a hippocampus region that has been shown to be affected early by histopathological events in AD in mice (Trujillo-Estrada et al., 2014). In light of these findings, our results indicate that localized variations in left thalamic shape may reflect early changes in memory circuits preceding cognitive symptoms. The fact that left but not right

thalamic shape was associated with cortical SUVR is consistent with findings of asymmetrical brain changes in AD with left-hemispheric predominance (Thompson et al., 2003).

EC thickness was bilaterally associated with cortical SUVR consistent with an early involvement of the EC in the AD continuum. The EC is a region affected early by NFT pathology in AD (H. Braak & Braak, 1991b), and localized EC atrophy may accelerate up to 10 years before clinical symptom onset (Younes, Albert, Miller, & BIOCARD Research Team, 2014). Because of the low number of individuals with high cortical SUVR, it may be argued that these outliers cause an overestimation of the true associations with CT. However, their localization is in striking correspondence with a previously reported AD cortical thinning signature in asymptomatic individuals (Dickerson et al., 2008; Dickerson et al., 2011).

We found no association between SUVR or volumes and a number of cognitive performance measures, which is consistent with the notion that the earliest pathological changes in AD may occur 10–20 years before symptom onset (Laske, 2014) and in line with a recent publication reporting no significant difference between amyloid-positive and amyloid-negative cognitively normal elderly individuals in verbal, visual and semantic memory, executive function and processing speed (Besson et al., 2015).

One limitation of our study is the resolution of PET images, which prohibits more localized quantification of tracer uptake such as calculation of a separate SUVR for each hippocampal subregion. Another limitation might be that we decided within this healthy group to not apply partial volume correction which could affect the accuracy of quantitative PET analysis (Rullmann et al., 2016). Considering that we found no effect of volume on regional SUVR, we assume that there is no bias introduced by not applying a partial volume correction. Furthermore, the regions of interest analyses were focused on individually segmented and grey matter delined regions reducing the general effect of atrophy on regional averages.

In addition, future studies should incorporate longitudinal data from cognitively normal elderly subjects progressing to MCI and cognitively stable elderly subjects to obtain quantitative estimates of the predictive value of local deformations of medial temporal lobe structures with regard to cognitive

decline. Our CT results suggest that in addition to the hippocampus, the EC should be characterized in terms of shape using our methodology to compare the predictive value of changes in EC thickness with that of changes in EC shape. In conclusion, the results of this study suggest that structural brain changes occur in association with amyloid deposition in presymptomatic AD and that these changes are detectable by measures of hippocampal shape and entorhinal cortical thickness. This positions these measurements as potential biomarkers of presymptomatic AD.

4.2 Subcortical shape changes, hippocampal atrophy, and cortical thinning in future Alzheimer's disease patients

Andrea M. Kälin[1*], Min Tae M. Park[2,3], M. Mallar Chakravarty[2,4], Jason P. Lerch[5], Lars Michels[6], Clemens Schroeder[1], Sarah D. Broicher[7], Spyros Kollias[6], Roger M. Nitsch[1], Anton F. Gietl[1], Paul G. Unschuld[1], Christoph Hock[1], Sandra E. Leh[1*]

[1]Institute for Regenerative Medicine, University of Zurich, Schlieren, Switzerland
[2]Cerebral Imaging Centre, Douglas Mental Health University Institute, Montreal, Canada
[3]Schulich School of Medicine and Dentistry, Western University, London, Canada
[4]Department of Psychiatry and Institute of Biomaterials and Biomedical Engineering, University of Toronto, Toronto, Canada
[5]The Hospital for Sick Children, University of Toronto, Toronto, Canada
[6]Institute of Neuroradiology, University of Zurich, Zurich, Switzerland
[7]Neuropsychology Unit, Department of Neurology, University Hospital Zurich, Zurich, Switzerland

*Correspondence: Sandra E. Leh sandra.leh-seal@irem.uzh.ch, Andrea M. Kälin andreakaelin@gmx.ch

Abstract

Efficacy of future treatments depends on biomarkers identifying patients with mild cognitive impairment at highest risk for transitioning to Alzheimer's disease. Here, we applied recently developed analysis techniques to investigate cross-sectional differences in subcortical shape and volume alterations in patients with stable mild cognitive impairment (MCI) (n = 23, age range 59–82, 47.8% female), future converters at baseline (n = 10, age range 66–84, 90% female) and at time of conversion (age range 68–87)

compared to group-wise age and gender matched healthy control subjects (n = 23, age range 61–81, 47.8% female; n = 10, age range 66–82, 80% female; n = 10, age range 68–82, 70% female). Additionally, we studied cortical thinning and global and local measures of hippocampal atrophy as known key imaging markers for Alzheimer's disease. Apart from bilateral striatal volume reductions, no morphometric alterations were found in cognitively stable patients. In contrast, we identified shape alterations in striatal and thalamic regions in future converters at baseline and at time of conversion. These shape alterations were paralleled by Alzheimer's disease like patterns of left hemispheric morphometric changes (cortical thinning in medial temporal regions, hippocampal total and subfield atrophy) in future converters at baseline with progression to similar right hemispheric alterations at time of conversion. Additionally, receiver operating characteristic curve analysis indicated that subcortical shape alterations may outperform hippocampal volume in identifying future converters at baseline. These results further confirm the key role of early cortical thinning and hippocampal atrophy in the early detection of Alzheimer's disease. But first and foremost, and by distinguishing future converters but not patients with stable cognitive abilities from cognitively normal subjects, our results support the value of early subcortical shape alterations and reduced hippocampal subfield volumes as potential markers for the early detection of Alzheimer's disease.

Introduction

Recent findings have demonstrated that beta-amyloid can be effectively removed from the brain, which may have a beneficial effect on cognitive function (Sevigny, Chiao, Bussière, et al., 2016). Following the concept of the amyloid-hypothesis, Alzheimer's disease (AD) treatment methods that are currently under investigation may be most efficacious in preclinical or early disease stages (Golde, Schneider, & Koo, 2011; Sevigny, Chiao, Bussière, et al., 2016; Sperling, Jack, & Aisen, 2011), referred to as mild cognitive impairment (MCI). Here, MCI is used as umbrella term covering subjects with stable cognitive impairment without progression to AD as well as

subjects with worsening of cognitive impairment and progression to AD. Considering that only the latter will benefit from potential treatment methods, the establishment and validation of biomarkers that accurately identify future converters to AD among individuals with MCI is crucial.

Structural magnetic resonance imaging (MRI) allows the quantification of brain atrophy and represents a key imaging marker for the early detection of AD. Specifically, reduced gray matter volume in medial temporal lobe regions including the hippocampal formation may precede the clinical onset of AD by 10 years (Tondelli et al., 2012b). Consequently, the applicability of hippocampal subfield segmentation in clinical populations has gained increasing attention, with different studies providing evidence for predominant cornu ammonis (CA)1 and subiculum atrophy in MCI (Atienza et al., 2011; Pluta, Yushkevich, Das, & Wolk, 2012; Yushkevich, Pluta, et al., 2015) and AD (Frisoni et al., 2008; Mueller & Weiner, 2009; Wisse, Biessels, Heringa, et al., 2014). Cortical thickness analysis constitutes another widely accepted approach to measure gray matter atrophy in AD, and cortical thinning has been found in MCI and AD (Lerch, Pruessner, et al., 2008; Liao et al., 2014), in late compared to early amnestic MCI (Ye et al., 2014), and in future converters (Bakkour, Morris, & Dickerson, 2009; Julkunen et al., 2010; Y. Li et al., 2012; Liao et al., 2014). Although gray matter alterations assessed by MRI represent valuable biomarkers for AD, the appropriate characterization of the progressing pattern of AD pathology across the brain (H. Braak & Braak, 1991a, 1991b) might require the consideration of multiple structures as well as standardized procedures/analysis methods. Additionally, as results from hippocampal subfield analyses have indicated, more local information about different structures might further contribute to the characterization of AD-typical patterns of morphometric alterations.

Despite evidence for subcortical amyloid and neurofibrillary tangle formation in AD (H. Braak & Braak, 1990, 1991b), MRI research has drawn its attention to AD related subcortical structure changes only recently. Advanced segmentation techniques now permit the quantification of subcortical volumes and provide the basis for subcortical shape analysis. Although volume loss and/or shape alterations in the thalamus (J. H. Roh et al., 2011; Stepan-Buksakowska et al., 2014; Zarei et al., 2010), putamen (Cho et al., 2014; de

Jong et al., 2011; J. H. Roh et al., 2011) and caudate nucleus (Cho et al., 2014; Madsen et al., 2010; J. H. Roh et al., 2011) have been identified in AD, little is known about subcortical volumetric and shape differences in MCI in general, and in future converters in particular. Given the connectivity of the thalamus and striatum to other AD-relevant structures, such as the hippocampus (Zarei et al., 2010), alterations in these structures may be of high value for the early detection of AD.

Here, we investigated subcortical volume and shape alterations as well as cortical thickness and volumes in the hippocampus and its subfields in MCI with stable cognitive abilities compared to healthy control subjects (HC) as well as in MCI with future conversion to AD at their baseline and conversion timepoints. In this manner we were able to elucidate the potential value of subcortical shape measures and their ability to improve the identification of future converters to AD. Further, we use cortical and hippocampal measures to demonstrate anatomical trajectories of the subjects under study, thereby confirming their role in the early detection of AD.

We expected stable MCI subjects to show no morphometric alterations typically related to AD, such as hippocampal atrophy or cortical thinning when compared with HC. In contrast, we expected morphometric alterations in accordance with known AD related histopathological processes in future converters at baseline and—more pronounced—at time of conversion. Specifically, and based on the pattern of AD related neurofibrillary tangle formation (H. Braak & Braak, 1990, 1991a, 1991b), we expected volume reductions in the hippocampus (CA1, subiculum), the thalamus (anterior subregions) and the striatum in future converters at baseline and at time of conversion. Further confirming AD related neurodegenerative patterns (Bakkour et al., 2009; Dickerson et al., 2008; Lerch, Pruessner, et al., 2008; Liao et al., 2014; Ye et al., 2014) in future converters at baseline and at time of conversion, we additionally expected cortical thinning in mediotemporal as well as lateral parietal and frontal regions and in the limbic system. Most importantly, and considering that subcortical volume reductions as well as possible secondary downstream effects may lead to thalamic and striatal shape alterations, we expected shape alterations in these structures to occur in both, future converters at basline and at time of conversion.

Materials and Methods

Participants

We selected participants from different pre-existing longitudinal cohorts at the Memory Clinic of the Division of Psychiatry Research and Psychogeriatric Medicine, University of Zurich. Briefly, participants were recruited from the outpatient population of the Memory Clinic or through advertisements in the local media. HC were retrospectively and additionally recruited through inquiries of caregivers or relatives of the patients. MCI was diagnosed according to Winblad et al. (Winblad et al., 2004), based on performance in multiple tests covering the following cognitive domains: episodic memory, executive function, attention/psychomotor processing speed, language and visual-constructive abilities. Impairment was defined if at least one score per domain was 1.5 SD below group means provided by test-specific normative data. Conversion to dementia was diagnosed when clinical work up indicated progression and significant impairment in activities of daily living. This was assessed by a multidisciplinary team under the supervision of an experienced psychiatrist.

For the present study, inclusion criteria for MCI subjects were: amnestic MCI (single or multiple domain) diagnosis and availability of MRI data at baseline and follow-up. Exclusion criteria were: left-handedness, significant medication or drug abuse as well as clinically significant neurological and psychiatric or internal disease that may affect cognition, MRI findings of infarction or other focal lesions, multiple lacunes or lacunes in critical memory structures. A total of 33 baselines from subjects with amnestic MCI were considered for the present study. The population was stratified into subjects with stable cognitive abilities during an approximately 2-year follow-up (MCI-S, n = 23), and subjects with future cognitive worsening and conversion to probable AD (MCI-CB, n = 10) within a 2-year time frame during follow-up. Additionally, data from the MCI-CB group at time of conversion was obtained (MCI-CC, n = 10). Inclusion criteria for HC were: stable cognitive health ascertained by clinical work up and neuropsychological testing during an approximately 2-year follow-up. Exclusion criteria were: MRI exclusion

criteria, left-handedness, evidence for abuse of alcohol and drugs, psychiatric, neurological or significant other system diseases. Three groups of HC were identified for group wise age and gender matching with MCI-S, MCI-CB, and MCI-CC, and MRI data was acquired following the description in section Magnetic Resonance Image Acquisition. The final demographic details are presented in Table 1. This study was approved by the cantonal ethics committee of canton Zurich, Switzerland, in accordance with the Helsinki Declaration. All participants provided written informed consent prior to study inclusion.

Table 1. Demographic information and cognitive measures for patient and control groups.

	Group 1			Group 2			Group 3		
	HC	MCI-S	*p*	HC	MCI-CB	*p*	HC	MCI-CC	*p*
N	23	23		10	10		10	10	
Age, years	70.96 5.78	71.22 6.54	.887	75.90 5.99	76.20 6.25	.914	77.40 5.34	78.00 6.24	.778
Education, years	14.35 2.69	14.17 3.01	.672	14.70 4.03	13.40 3.40	.376	13.30 2.41	13.40 3.41	.804
Gender, M/F	12/11	12/11	1.000	2/8	1/9	1.000	3/7	1/9	.582
FU time, months[a]	46.91 33.89	25.91 8.41	N/A	39.50 32.35	20.80 4.98	N/A	48.10 33.22	N/A	N/A
MMSE, /30	29.83 0.38	28.09 1.67	.000*	29.30 0.95	26.60 1.95	.000*	29.30 1.06	23.50 2.55	.000*
aMCI s/m	N/A	0 / 23	N/A	N/A	3 / 7	N/A	N/A	N/A	N/A
Episodic Memory									
VLMT learning	57.96 10.96	40.39 8.41	.000*	54.80 12.12	27.86 6.49	.000*	57.10 12.17	24.90 5.74	.000*
VLMT recall	12.39 2.25	6.19 3.47	.000*	11.50 2.50	1.71 1.49	.000*	11.20 2.86	0.79 1.69	.000*
Executive Functions									
Animal fluency	25.48 5.55	19.04 5.11	.000*	22.10 4.45	15.20 3.85	.002*	23.40 3.80	11.80 4.31	.000*
Letter fluency	33.09 11.33	22.78 11.00	.003*	29.90 7.76	25.20 10.01	.259	32.50 8.38	24.70 9.79	.072
DigitSpan bw	6.87 1.79	5.13 1.68	.001*	5.50 1.08	5.40 1.17	.976	5.70 1.89	5.30 1.49	.606
Psychomotor speed / Attention									
TMT A	36.65 8.20	50.87 23.57	.011*	44.50 7.05	43.90 10.82	.885	39.50 12.32	58.50 20.11	.020*
TMT B	87.52 25.80	156.39 60.8	.000*	111.60 36.7	162.50 75.8	.079	101.3 37.28	N/A[b]	N/A[b]
Language									
BNT	14.74 0.45	13.61 1.15	.000*	14.90 0.32	13.70 1.25	.015*	14.80 0.42	12.80 1.47	.000*

Values are means and standard deviations if not specified otherwise. HC, healthy control subjects; MCI-S, stable mild cognitive impairment at baseline; MCI-CB, mild cognitive impairment converters at baseline; MCI-CC, mild cognitive impairment converters at time of conversion; M/F, male/female; FU, follow-up; MMSE, Mini Mental State Examination; aMCI s/m, amnestic mild cognitive impairment single domain (s), multiple domain (d);

VLMT, Verbaler Lern- und Merkfähigkeitstest; bw, backward; TMT, Trail Making Test; BNT, Boston Naming Test; N/A, not applicable. * Significant p value test by ANOVA (normally distributed data), Mann U Whitney (not normally distributed data), and Pearson's X2 test (categorical variables). aTime from baseline MRI to the time of Alzheimer's disease diagnosis for MCI-CB; time from baseline MRI to the last available visit for MCI-S; time from the first HC diagnosis to the last available visit for HC, bhigh percentage of missing values due to the subjects' impairment did not allow statistical analyses.

Magnetic resonance image acquisition

All (MRI) were performed on the same 1.5 Tesla Phillips Achieva scanner using an 8-element head coil. Whole-brain high-resolution 3D T1-weighted structural data was obtained by using the following scanning parameters: 166 slices, repetition time: 6.9 ms, echo time: 3.2 ms, flip angle: 8°, field of view: 240 × 240 × 166 mm (anterior-posterior, foot-head, right-left), slice thickness: 1 mm, total scan time: 15 min.

Image processing: subcortical structures and hippocampus

Segmentation of the striatum, thalamus and thalamic nuclei was performed using a recently developed label-fusion-based segmentation method that had previously proven its high accuracy (Chakravarty et al., 2013). Briefly, the MAGeT-Brain algorithm applies multiple automatically generated templates from a single atlas derived from manually segmented serial histological data comprising 108 basal ganglia and thalamic structures as defined using three different references (Gloor, 1997; Hirai & Jones, 1989; Schaltenbrand & Wahren, 1977). We used two of the segmentations produced from the MAGeT-Brain pipeline, the first are the whole striatum (caudate and putamen) and thalamus, and the second are the thalamic subnuclei as per the Hirai and Jones definitions (1989). The thalamus was segmented into pulvinar-, anterior-, and central nuclei and lateral dorsal-, lateral posterior-, medial dorsal nuclei, ventral anterior nuclei (VA), ventral lateral nuclei (VL), ventral posterior nuclei (VP) and lateral geniculate nucleus (LGN) and medial geniculate nucleus (MGN) as per the Hirai and Jones (1989) nomenclature. Segmentation of the hippocampus and its subfields was performed using five high-resolution atlases developed and validated for use with MAGeT-Brain (Pipitone et al., 2014; Winterburn et al., 2013). The hippocampus was segmented into cornu ammonis (CA) 1, CA2-CA3, CA4/Dentate gyrus, strata radiatum/lacunosum/moleculare, and subiculum.

Surface-based shape analyses

Striatal and thalamic shape analysis was performed by using an adapted surface-based methodology (Magon et al., 2014; Raznahan et al., 2014; Shaw et al., 2015). Briefly, surface-based representations of the

striatum and thalamus were defined on the input atlas. The nonlinear portions of the transformations that map each subject to the input template were concatenated and then averaged to limit the effects of noise and error and to increase precision and accuracy. Next, the dot product between the nonlinear deformation vector (of the inverse of the averaged atlas-to-subject transformation) and the surface normal at each vertex (a unit vector describing the direction perpendicular to the surface) was estimated. This measure provides an estimate of the local measure of inward or outward displacement along the normal. Then, surface-area values were blurred using a 5 mm surface-based diffusion smoothing kernel (Chakravarty et al., 2015; Raznahan et al., 2014). Resulting inward and outward displacements (measured in millimeters) were estimated relative to a detailed subcortical atlas previously described (Chakravarty et al., 2015). An inward displacement (contraction) represents a surface that is deformed inwards relative to the model that we were using and vice-versa for the outward displacement (expansion).

Cortical thickness analysis

Cortical thickness was estimated by using the automated CIVET pipeline (version 1.1.10; Montreal Neurological Institute at McGill University, Montreal, Quebec, Canada). Briefly, the native images were linearly registered to the symmetric ICBM 152 template (Collins et al., 1994; Mazziotta et al., 2001). Intensity nonuniformities were corrected using the N3 algorithm (Sled, Zijdenbos, & Evans, 1998). The skull was removed (Smith, 2002), and brain tissue was segmented into white matter, gray matter, cerebrospinal fluid (CSF) using the Intensity—Normalized Stereotaxic Environment for Classification of Tissues (INSECT) algorithm (Tohka et al., 2004; Zijdenbos et al., 1998). Deformable models were used to construct the inner white matter surface and gray matter-CSF interface in both hemispheres (Kim et al., 2005) revealing 40,962 vertex points at each surface. Cortical thickness was then measured as the distance, in millimeters, between each vertex point at the inner and the corresponding point at the outer surface using the method proposed by Lerch and Evans (Lerch & Evans, 2005). The cortical thickness

maps were blurred using a 20 mm diffusion smoothing kernel to increase signal-to-noise ratio and statistical power.

Intracranial volume

The comparison of gray matter volumes across groups requires taking into account interindividual variability in brain morphology. Values of intracranial volume (ICV) indicate premorbid brain volume, and thus are often used to adjust volumes for subsequent volume analyses. When examining volume reductions in neurodegenerative disease, considering ICV allows for estimation of atrophy caused by neurodegenerative mechanisms rather than by interindividual differences in head size and brain morphology.

In the present work, the FreeSurfer pipeline (version 5.1.0) was used to calculate total intracranial volume (eTIV) representing an estimate for ICV as described in Buckner et al. (2004). Briefly, each individual is registered to an atlas template. The Atlas Scaling Factor obtained by this transformation represents the whole-brain volume adjustment that is required to match each individual to the atlas template and is thus used to automatically generate eTIV. This automated method has been shown to be equivalent to manual correction (Buckner et al., 2004) and has previously been used for normalization in several AD studies (Westman, Aguilar, Muehlboeck, & Simmons, 2013; Westman, Muehlboeck, & Simmons, 2012; Westman et al., 2011).

Statistical analyses

Group comparisons of demographic and conitive data were applied using analysis of variance (ANOVA) or Mann-Whitney U-Test. Pearson's chi-square test was used for categorical variables. Tests were performed with a significance level of $p < 0.05$. Between-group differences in volumetric raw data (MCI-S, MCI-CB and MCI-CC vs. matched HC) were examined by including age and gender as covariates in the multiple linear regression models. These analyses were repeated by using volumes relative to eTIV (volume/eTIV*100) in order to adjust volumes for differences in head size. P-values resulting from volume analyses were adjusted for multiple testing by using Bonferroni-Holm correction (level of significance for hippocampus,

striatum and thalamus starting with $p < 0.05/2$; level of significance for hippocampal subfields starting with $p < 0.05/10$). The same models were performed for investigating between-group shape and cortical thickness differences. Vertex-wise analyses results are reported on a q-value corrected for multiple testing, using a false discovery rate (FDR) of 10% as in previous publications in our group (Janes, Park, Farmer, & Chakravarty, 2015; Wheeler et al., 2013). Receiver operating characteristic (ROC) curves were computed to evaluate and compare the accuracy of striatal and thalamic shape alterations, and of hippocampus total volumes as established AD imaging marker for discriminating HC from MCI-CB. ROC curves are produced by plotting the true positive rate (sensitivity) against the false positive rate (1-specificity) for different thresholds. The area under the curve (AUC) is then calculated and provides information about the ability of the morphometric data to discriminate between patients and HC. AUC values of 1.0 indicate perfect discriminative abilities; values of < 0.6 indicate poor discriminative abilities. For these analyses, between group t statistics from comparison between HC and MCI-CB were used. More precisely, for all vertices whose t-values constituted a local minimum (or maximum), the average of the displacement values in mm was computed for each subject. This was done separately for each structure and hemisphere. Statistical analyses were performed with IBM SPSS statistics 21 and RMINC package (R for Medical Imaging NetCDF; https://github.com/Mouse-Imaging-Centre/RMINC), an image analysis software library developed for the R statistical environment (http://www.r-project.org).

Results

Descriptive statistics for demographic information and cognitive data is listed in Table 1.

Volumetric analyses in MCI-S

Apart from reduced bilateral striatal volumes, and when analyzing volumes relative to eTIV, there were no volume differences in any of the

investigated structures in MCI-S when compared with HC (see Table 2). Significance and p-values were similar when using raw volumes instead of volumes relative to eTIV (see Table 3). A segmentation map of the thalamus is shown in Figure 1, and of the hippocampus in Figure 2.

Table 2. Volume sizes relative to eTIV for patient and control groups.

	Group 1			Group 2			Group 3		
	HC	MCI-S	*p*	HC	MCI-CB	*p*	HC	MCI-CC	*p*
eTIV, cm^3	1586.33 177.35	1546.71 155.10	.424	1499.99 155.00	1498.05 133.58	.976	1487.72 132.59	1507.66 133.52	.741
Hippocampus total, left	.14206 .01670	.13915 .02510	.670	.14995 .01635	.11236 .013455	.000*	.14493 .00780	.10656 .01278	.000*
Subiculum	.02103 .00250	.01972 .00379	.162	.02210 .00243	.01650 .00230	.000*	.02060 .00222	.01579 .00260	.000*
CA1	.04545 .00509	.04568 .00773	.872	.04834 .00525	.03648 .00436	.000*	.04651 .00348	.03587 .00509	.000*
CA2-CA3	.00851 .00180	.00849 .00200	.966	.00882 .00184	.00752 .00154	.088	.00904 .00088	.00659 .00162	.001*
CA4/Dentate gyrus	.03399 .00460	.03264 .00611	.415	.03594 .00464	.02756 .00380	.000*	.03500 .00282	.02583 .00354	.000*
Strata	.03308 .00449	.03262 .00682	.821	.03475 .00417	.02428 .00335	.000*	.03377 .00247	.02249 .00255	.000*
Hippocampus total, right	.14140 .01557	.14454 .01796	.495	.14991 .01238	.12429 .02027	.001*	.14467 .00825	.11796 .01651	.000*
Subiculum	.01936 .00235	.01907 .00326	.753	.02079 .00254	.01677 .00321	.005*	.01998 .00258	.01590 .00277	.001*
CA1	.04698 .00538	.04862 .00607	.335	.05002 .00413	.04260 .00668	.005*	.04862 .00335	.04165 .00626	.005*
CA2-CA3	.00926 .00125	.00958 .00162	.449	.00961 .00135	.00848 .00195	.068	.00933 .00179	.00750 .00210	.044*
CA4/Dentate gyrus	.03396 .00414	.03464 .00396	.519	.03560 .00418	.02973 .00471	.002*	.03426 .00261	.02795 .00360	.000*
Strata	.03184 .00438	.03263 .00516	.534	.03377 .00266	.02671 .00517	.000*	.03249 .00237	.02497 .00398	.000*
Thalamus total, left	.32430 .02209	.32525 .02228	.882	.33248 .01846	.32428 .02484	.433	.32998 .02614	.31843 .02588	.431
LGN	.00705 .00084	.00701 .00066	.894	.00727 .00159	.00688 .00119	.475	.00713 .00085	.00658 .00115	.220

MGN	.01009	.00150	.10103	.00082	.898	.01017	.00133	.00965	.00126	.320	.01081	.00133	.00981	.00114	.106
Anterior nuclei	.00548	.00092	.00539	.00086	.665	.00531	.00057	.00555	.00087	.328	.00533	.00072	.00575	.00100	.257
Central nuclei	.01578	.00014	.01538	.00151	.447	.01597	.00137	.01500	.00143	.158	.01624	.00188	.01491	.00165	.177
Lateral dorsal nuclei	.00276	.00073	.00295	.00080	.418	.00283	.00074	.00324	.00054	.086	.00307	.00072	.00332	.00069	.252
Lateral posterior nuclei	.02229	.00299	.02363	.00275	.128	.02276	.00238	.02432	.00167	.108	.02363	.00197	.02401	.00233	.695
Medial dorsal nuclei	.05222	.00562	.05085	.00544	.415	.05292	.00427	.05046	.00626	.336	.05276	.00650	.04920	.00605	.290
Pulvinar	.07683	.00768	.07732	.00654	.798	.07540	.00570	.07350	.00848	.565	.07474	.00625	.07162	.00742	.556
VA	.03156	.00297	.03175	.00404	.868	.03288	.00229	.03343	.00302	.550	.03199	.00340	.03234	.00350	.979
VP	.02520	.00265	.02484	.00230	.631	.02593	.00264	.02329	.00244	.015	.02547	.00208	.02202	.00264	.009
VL	.04554	.00444	.04591	.00551	.810	.04858	.00363	.04578	.00585	.156	.04691	.00351	.04434	.00674	.268
Thalamus total, right	.32413	.02336	.32019	.02076	.567	.33124	.01278	.31827	.02027	.083	.32838	.02470	.31547	.02189	.257
LGN	.01136	.00138	.01143	.00134	.861	.01190	.00125	.01203	.002108	.947	.01177	.00096	.01160	.00211	.626
MGN	.01235	.00142	.01226	.00109	.790	.01268	.00096	.01262	.00148	.875	.01314	.00120	.01264	.00181	.581
Anterior nuclei	.00759	.00109	.00720	.00146	.283	.00749	.00070	.00792	.00068	.209	.00787	.00099	.00796	.00055	.912
Central nuclei	.00979	.00084	.00948	.00078	.218	.01003	.00060	.00968	.00075	.237	.01021	.00117	.00960	.00073	.224
Lateral dorsal nuclei	.00309	.00089	.00296	.00077	.570	.00299	.00058	.00329	.00064	.180	.00302	.00063	.00334	.00060	.084
Lateral posterior nuclei	.01683	.00247	.01672	.00216	.886	.01594	.00158	.01687	.00132	.213	.01708	.00147	.01680	.00124	.988
Medial dorsal nuclei	.04785	.00373	.04630	.00452	.226	.04823	.00430	.04647	.00435	.370	.04928	.00685	.04610	.00474	.222
Pulvinar	.09388	.00827	.09504	.00743	.569	.09443	.00553	.08914	.00799	.114	.09228	.00659	.08769	.00847	.307
VA	.03362	.00285	.03242	.00400	.246	.03532	.00326	.03405	.00280	.261	.03404	.00323	.03352	.00297	.509

VP	.03795 .00441	.02331 .00260	.753	.02382 .00180	.02196 .00257	.047	.02337 .00163	.02135 .00253	.054
VL	.03876 .00349	.03715 .00435	.221	.04071 .00302	.03818 .00468	.109	.03925 .00388	.03786 .00485	.339
Striatum total, left	.51914 .03450	.49659 .02327	.013*	.51636 .03540	.50261 .03202	.482	.49783 .02986	.50050 .03693	.936
Striatum total, right	.51211 .03543	.48445 .02920	.006*	.50521 .03297	.49679 .02506	.557	.49142 .02774	.49558 .02767	.917

Values represent means and standard deviations of volumes relative to estimated total incranial volume * 100. HC, healthy control subjects; MCI-S, stable mild cognitive impairment at baseline; MCI-CB, mild cognitive impairment converters at baseline; MCI-CC, mild cognitive impairment converters at time of conversion; eTIV, estimated total intracranial volume; CA, cornu ammonis; LGN, lateral geniculate nucleus; MGN, medial geniculate nucleus; VA, ventral anterior nuclei; VP, ventral posterior nuclei; VL, ventral lateral nuclei. * Significant p value test by using volumes relative to estimated total intracranial volume and multiplied by 100 as dependent variables, and including age and gender in the model, and after correction for multiple testing.

Table 3. Raw volume sizes for patient and control groups.

	Group 1			Group 2			Group 3		
	HC	MCI-S	*p*	HC	MCI-CB	*p*	HC	MCI-CC	*p*
eTIV, cm^3	1586.33 177.35	1546.71 155.10	.424	1499.99 155.00	1498.05 133.58	.976	1487.72 132.59	1507.66 133.52	.741
Hippocampus total, left	2238.28 260.63	2150.25 434.33	.390	2250.76 374.17	1687.81 274.65	.003*	2156.61 223.12	1609.17 247.38	.000*
Subiculum	332.02 44.55	304.09 62.10	.052	331.47 51.73	248.01 43.84	.001*	305.25 29.47	238.94 48.22	.002*
CA1	716.61 83.99	706.75 141.74	.785	727.14 132.45	548.12 89.81	.004*	692.32 81.86	542.17 95.77	.004*
CA2-CA3	133.94 27.55	130.89 31.18	.729	132.45 31.93	111.93 21.82	.150	134.26 16.94	98.11 20.69	.001*
CA4/Dentate gyrus	534.68 64.87	503.78 101.15	.215	538.14 86.87	414.63 75.53	.006*	522.28 73.58	390.57 67.95	.001*
Strata	521.03 69.33	504.74 118.25	.564	521.85 93.31	365.12 67.27	.001*	502.50 56.59	339.38 50.29	.000*
Hippocampus total, right	2234.65 300.09	2232.02 340.64	.993	2244.32 274.42	1858.63 335.92	.019*	2149.88 196.89	1775.68 280.26	.006*
Subiculum	304.93 34.75	293.59 52.12	.377	311.29 45.88	251.38 54.78	.027	296.18 38.27	239.80 47.82	.009*
CA1	743.04 108.48	751.13 117.96	.782	750.52 107.06	638.02 115.92	.057	722.65 74.27	628.90 115.45	.073
CA2-CA3	146.56 23.46	147.91 27.64	.844	143.55 22.07	125.88 26.26	.119	138.63 29.32	111.37 26.32	.057
CA4/Dentate gyrus	536.26 73.05	534.87 76.72	.980	531.92 70.60	443.88 73.45	.017	509.88 61.47	420.12 57.92	.008*
Strata	503.86 85.79	504.52 95.45	.945	507.04 57.00	399.47 85.29	.007*	482.54 45.84	375.49 64.85	.001*
Thalamus total, left	5126.73 503.34	5036.59 652.23	.565	4977.11 470.58	4854.86 547.58	.886	4887.31 330.22	4792.43 195.68	.870
LGN	111.36 15.48	108.48 15.57	.522	108.08 19.89	102.21 14.05	.525	105.67 13.19	98.15 11.26	.258

MGN	159.11	24.28	156.87	22.00	.706	151.80	18.91	143.73	15.72	.404	160.02	17.57	146.96	12.99	.148
Anterior nuclei	87.56	19.90	83.39	15.61	.361	79.87	13.58	83.20	15.85	.241	78.88	9.53	86.78	18.23	.104
Central nuclei	248.49	27.52	237.58	31.05	.147	239.37	30.15	224.34	25.28	.335	240.92	30.16	223.86	23.09	.871
Lateral dorsal nuclei	44.53	14.55	45.86	13.94	.761	42.85	13.33	48.56	9.44	.083	45.40	10.29	50.02	11.52	.105
Lateral posterior nuclei	355.06	68.93	366.43	60.36	.542	341.19	47.86	364.56	43.91	.099	349.79	21.34	361.28	42.25	.331
Medial dorsal nuclei	822.66	79.53	785.62	110.11	.178	790.30	67.28	753.79	102.32	.501	779.15	65.12	738.24	83.74	.508
Pulvinar	1212.08	126.63	1195.09	146.50	.655	1128.08	113.66	1101.08	160.98	.940	1109.93	118.10	1079.69	146.41	.800
VA	500.06	67.78	493.17	89.54	.755	493.21	61.80	500.08	56.84	.367	472.95	33.09	485.61	49.05	.399
VP	396.65	33.99	383.97	50.83	.275	386.85	34.62	348.36	44.33	.050	377.78	34.68	331.26	44.02	.041
VL	719.09	80.65	711.71	117.47	.799	725.58	56.69	684.07	92.85	.283	695.61	56.70	665.58	93.58	.551
Thalamus total, right	5122.67	493.57	4958.83	643.05	.280	4959.92	448.02	4758.09	417.01	.423	4864.32	321.10	4742.79	377.55	.839
LGN	179.37	23.03	176.95	28.31	.763	177.46	14.77	178.81	25.88	.873	174.31	10.92	173.45	23.64	.928
MGN	195.04	25.38	190.02	29.13	.439	189.86	19.72	188.17	20.73	.882	195.39	25.37	189.52	24.60	.956
Anterior nuclei	120.72	22.93	111.68	26.22	.168	112.40	16.29	119.18	18.36	.276	116.68	15.55	120.22	15.19	.468
Central nuclei	154.73	17.33	146.89	21.11	.118	150.24	16.51	144.89	16.56	.648	151.41	18.34	144.54	14.79	.625
Lateral dorsal nuclei	49.43	15.49	45.96	13.21	.374	45.14	11.29	49.85	12.83	.196	45.27	11.65	50.67	11.98	.087
Lateral posterior nuclei	267.29	47.20	259.55	47.31	.571	239.24	34.40	252.46	28.41	.234	253.76	28.45	252.63	23.74	.189
Medial dorsal nuclei	756.02	74.65	716.16	99.86	.104	720.75	68.41	693.40	61.79	.503	727.41	73.61	691.37	54.93	.385
Pulvinar	1484.26	165.02	1469.57	183.34	.749	1414.45	145.15	1331.68	137.33	.227	1370.91	138.16	1316.74	122.95	.781
VA	532.09	65.62	503.16	89.00	.204	527.86	53.61	510.49	66.36	.670	503.71	35.07	504.70	56.99	.813

VP	366.80	32.69	357.21	50.58	.402	356.18	34.07	327.49	34.56	.069	346.68	29.03	320.19	32.51	.123
VL	611.33	14.59	576.04	95.90	.156	608.29	51.25	569.12	60.62	.176	581.08	52.21	567.77	62.64	.684
Striatum total, left	8208.75	818.54	7688.01	897.51	.031*	7746.97	1003.05	7513.04	651.33	.844	7389.66	615.77	7527.29	689.44	.356
Striatum total, right	8095.68	805.24	7497.72	905.81	.015*	7575.03	917.71	7432.17	645.25	.989	7303.52	696.77	7453.16	554.69	.382

Values represent means and standard deviations of raw volumes mm3. HC, healthy control subjects; MCI-S, stable mild cognitive impairment at baseline; MCI-CB, mild cognitive impairment converters at baseline; MCI-CC, mild cognitive impairment converters at time of conversion; eTIV, estimated total intracranial volume; CA, cornu ammonis; LGN, lateral geniculate nucleus; MGN, medial geniculate nucleus; VA, ventral anterior nuclei; VP, ventral posterior nuclei; VL, ventral lateral nuclei. * Significant p value test by using raw volumes as dependent variable, and including age and gender in the model, and after correction for multiple testing.

Figure 1. Thalamic subnuclei.

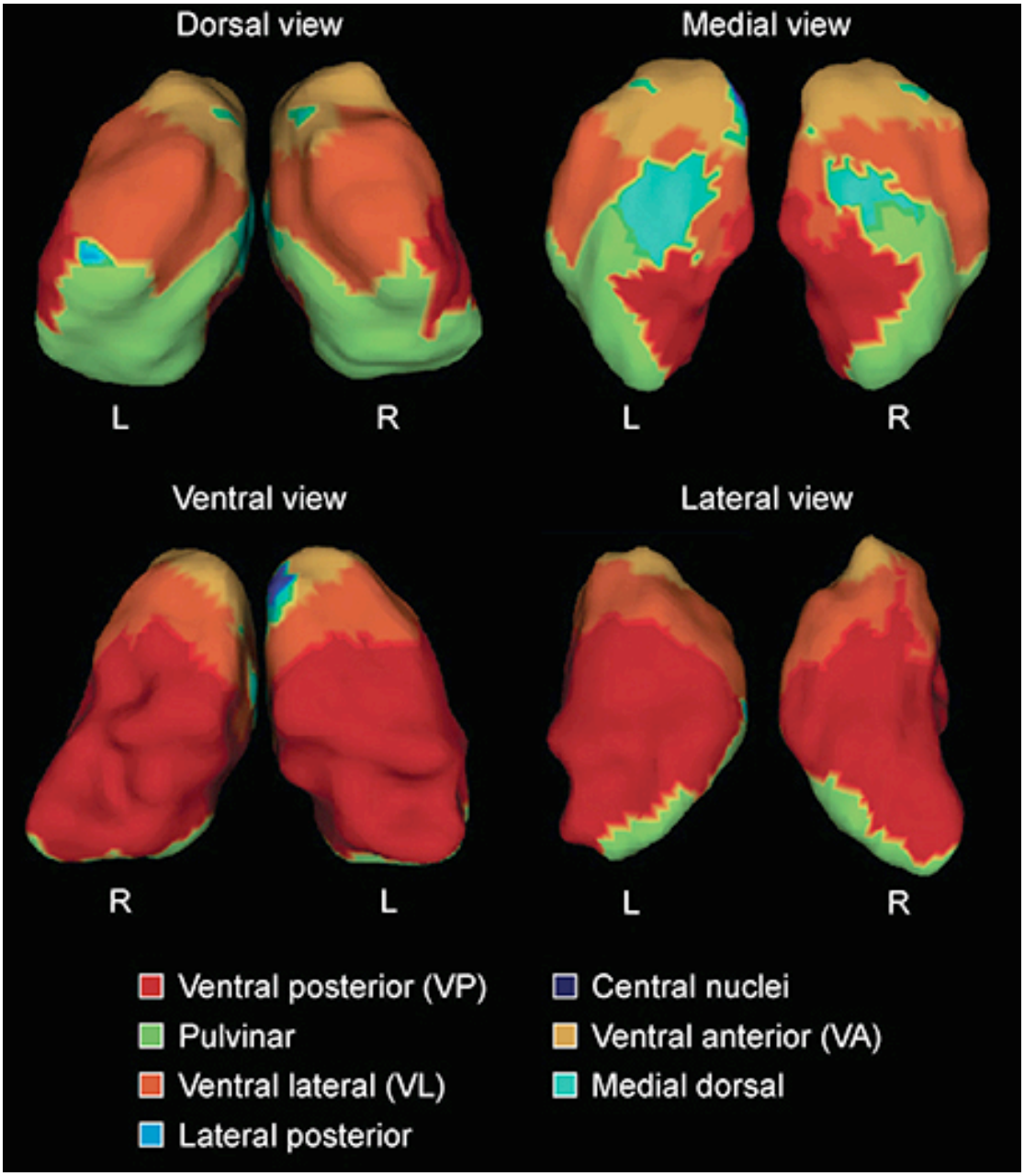

Figure 1. Surface labels for automated segmentation of thalamic subnuclei (L = left hemisphere; R = right hemisphere), based on expert neuroanatomical labeling of serial histology (Chakravarty et al., 2006).

Figure 2. Hippocampal subfield segmentation.

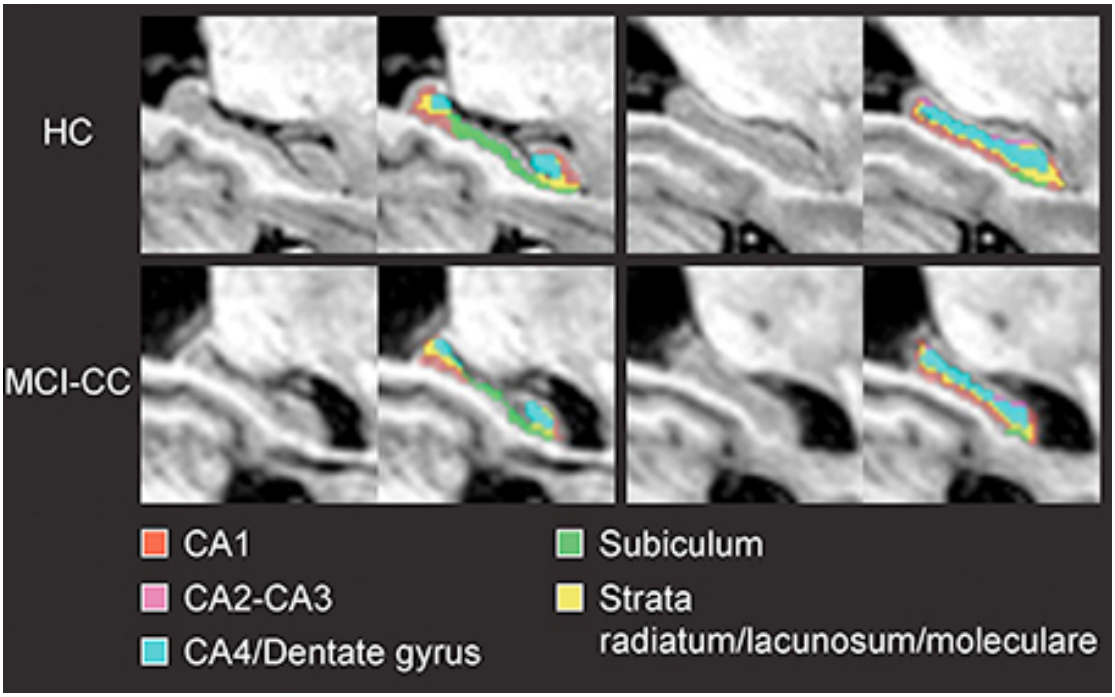

Figure 2. Coronal views of the hippocampus and hippocampal subfields in magnetic resonance images from a healthy control subject (HC) and a mild cognitive impairment converter subject at time of conversion (MCI-CC) of the present study.

Volumetric analyses in MCI-CB

In contrast, pronounced reductions in volumes relative to eTIV were found in MCI-CB (see Table 2). In particular, and apart from CA2-CA3 volumes, all bilateral hippocampal subfield volumes were smaller in MCI-CB compared to HC (right CA1 $t = 3.23$, $p = 0.005$; subiculum $t = 3.29$, $p = 0.005$; CA4/Dentate gyrus $t = 3.80$, $p = 0.002$; strata $t = 4.55$, $p < 0.001$/left CA1 $t = 5.18$, $p < 0.001$; subiculum $t = 4.96$, $p < 0.001$; CA4/Dentate gyrus $t = 4.66$, $p < 0.001$; strata $t = 5.91$, $p < 0.001$; $df = 3,16$) after correction for multiple testing. With regard to thalamic subnuclei, and although statistically significant, effects of volume reductions in bilateral VP in MCI-CB (right $p = 0.047$, left $p = 0.015$) did not survive the correction for multiple testing. Significance and p-values were similar when using raw volumes instead of volumes relative to eTIV. However, some of the right hemispheric differences in hippocampal subfield volumes did not quite achieve the level of significance (CA1 $p = 0.057$). Additionally, and although statistically significant, two right

hemispheric effects did not survive the correction for multiple comparisons (CA4/Dentate gyrus p = 0.017; subiculum p = 0.027) (see Table 3).

Vertex-wise cortical thickness analyses in MCI groups

Analyses on data corrected for multiple testing by using FDR at q < 0.10 revealed no cortical thinning in MCI-S compared to HC. Reduced cortical thickness, however, was found in MCI-CB and MCI-CC compared to HC (Figure 3, Table 4). Significant effects were limited to medial areas such as the left parahippocampal cortex, left subgenual cingulate, and left region of the uncus in MCI-CB. Similar regions revealed cortical thinning in the right hemisphere, with significance only at q < 0.15 though (Figure 4). Importantly, the pattern of cortical thinning extended to the right hemisphere in MCI-CC, where cortical thinning in bilateral parahippocampal cortices and bilateral regions of the uncus now achieved an appropriate level of significance.

Figure 3. Cortical thickness results.

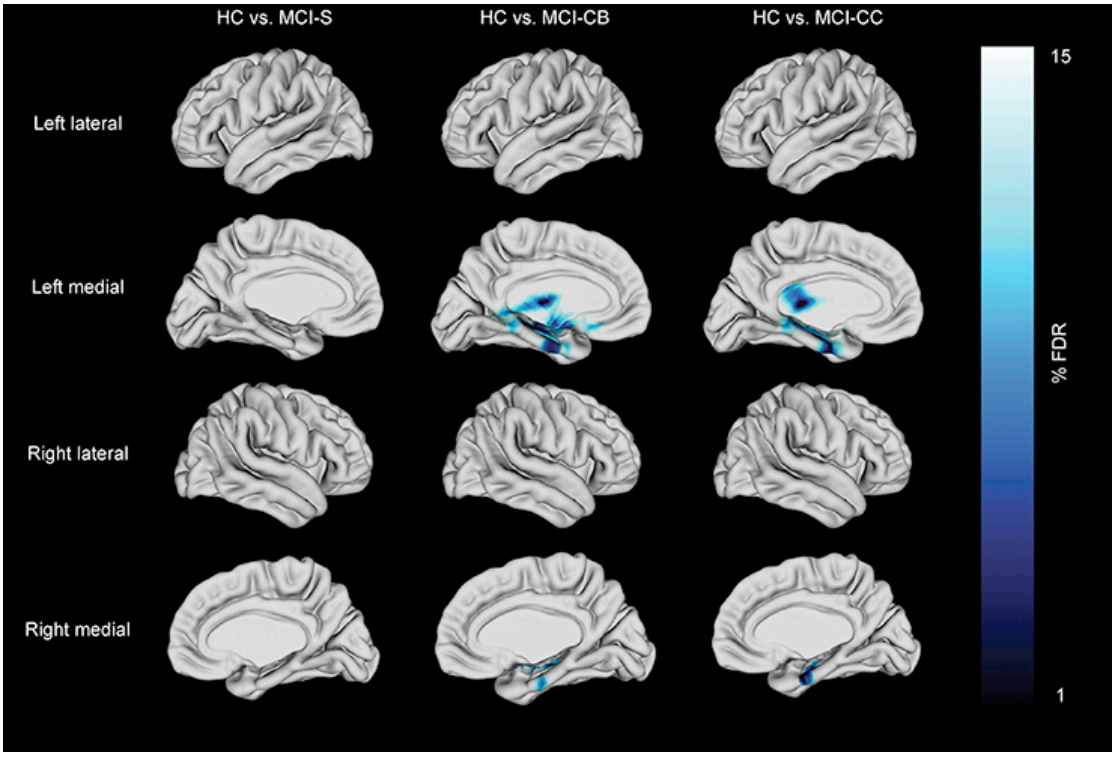

Figure 3. Cortical thickness differences in patients with stable mild cognitive impairment (MCI-S), future converters at baseline (MCI-CB) and converters at time of conversion (MCI-CC) when compared with healthy control subjects (HC). Images were generated after including age and gender in the model,

and after correction using FDR at q = 0.15 to better illustrate the anatomical localization. Bar shows FDR-values, with blue /light blue indicating reduced cortical thickness.

Table 4. Reduced cortical thickness in patient groups.

A

Anatomic localization	MNI coordinates (peak)			*t* statistic (peak)
	x	y	z	
Parahippocampal Cortex, left	-30	-16	-27	-5.77**
Subgenual Cingulate, left	-18	15	-14	-4.34**
Uncus, left	-29	-29	-8	-6.53**

B

Anatomic localization	MNI coordinates (peak)			*t* statistic (peak)
	x	y	z	
Parahippocampal Cortex, left	-25	-13	-32	-7.13**
Uncus, left	-31	-12	-23	-7.06**
Parahippocampal Cortex, right	29	-12	-28	-5.45*
Uncus, right	31	-10	-22	-5.20*

Anatomical localization of cortical thinning in mild cognitive impairment converters at baseline (A), and in mild cognitive impairment converters at time of conversion (B). MNI: Montreal Neurological Institute. * significant after including age and gender in the model, and after correction using False Discovery Rate at q<.10. ** significant after including age and gender in the model, and after correction using False Discovery Rate at q<.01.

Figure 4. Striatal and thalamic shape differences.

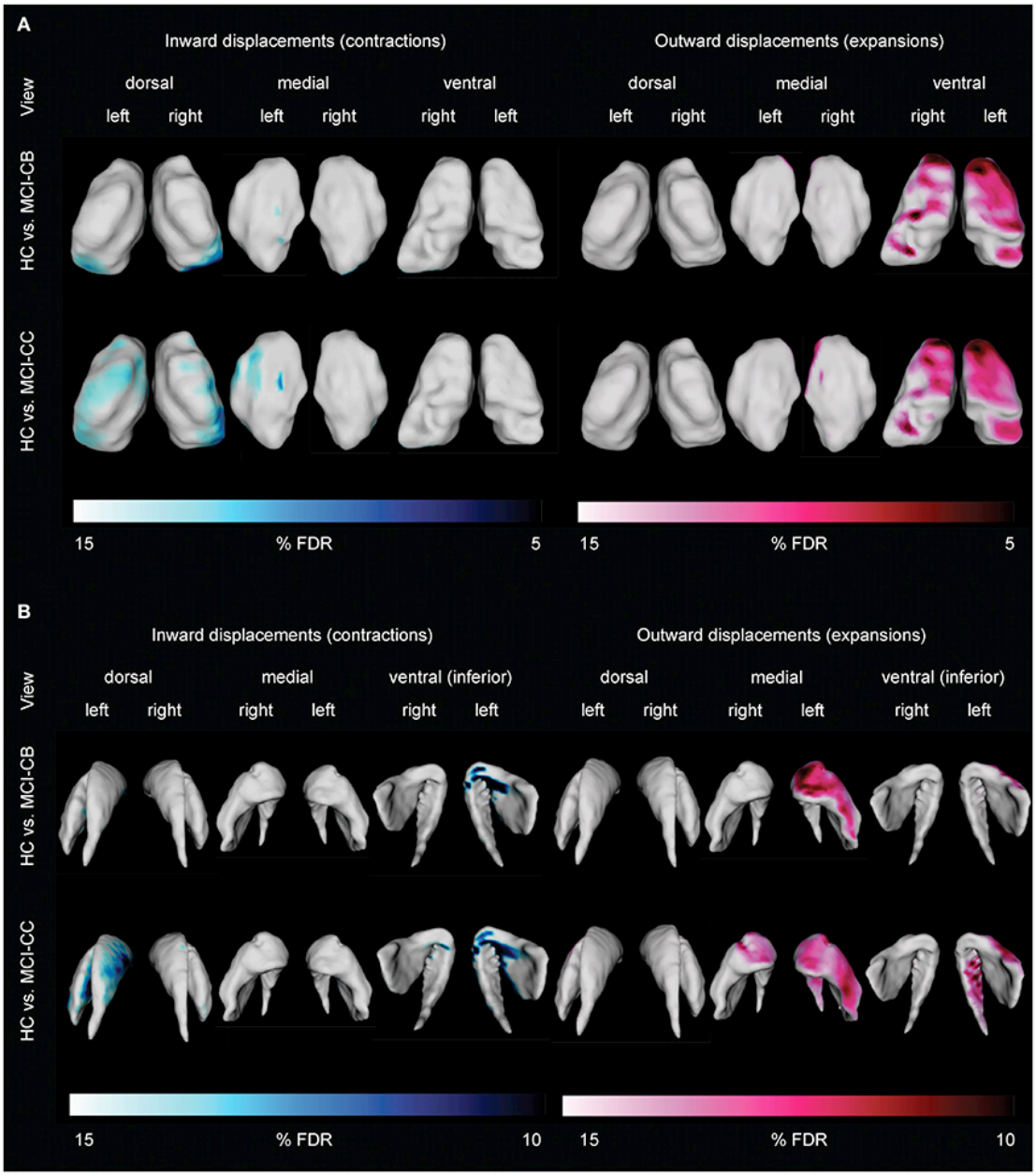

Figure 4. Differences in thalamic (A) and striatal (B) shape alterations in future converters at baseline (MCI-CB) and at time of conversion (MCI-CC) when compared with healthy control subjects (HC). Images were generated after including age and gender in the model, and after correction using FDR at q = 0.15 to better illustrate the anatomical localization. Bars show FDR-values, with blue/light blue indicating inward displacements (contractions) and pink/light pink indicating outward displacements (expansions).

Vertex-wise subcortical shape analyses in MCI groups

Analyses on data corrected for multiple testing by using FDR at $q < 0.10$ revealed no striatal or thalamic shape alterations in MCI-S, but pronounced striatal and thalamic displacements in MCI-CB and MCI-CC compared to HC.

Thalamic contractions and expansions are presented in Figure 4A. In contrast to MCI-S, MCI-CB, and MCI-CC revealed contractions which were limited to dorsal and medial parts, and were more pronounced in the left than in the right hemisphere. Specifically, MCI-CB exhibited contractions in bilateral dorsal aspects of the pulvinar, bilateral dorsal aspects of VP, and in left medial aspects of VP and medial dorsal nuclei. Again, the pattern of alterations had further continued in MCI-CC, exhibiting more pronounced contractions extending from dorsal aspects of the pulvinar and VP to dorsal aspects of VL, lateral posterior nuclei, and VA in the right hemisphere. In contrast, contractions in the left hemisphere were now limited to dorsal aspects of VL, VA, and medial dorsal nuclei. However, there was a tendency toward significant contractions ($q = 0.15$) in dorsal aspects of the pulvinar, VP and lateral posterior nuclei as well. Thalamic expansions in turn were limited to ventral and medial parts. MCI-CB revealed expansions in bilateral ventral aspects of the central nuclei, VA, VL, and VP. MCI-CC revealed the same, though more pronounced pattern of expansions in both hemispheres, with additional expansion in the medial aspect of the medial dorsal nuclei.

Striatal displacements are presented in Figure 4B. Again in contrast to MCI-S, the other groups displayed contractions, predominantly in the left hemisphere and most pronounced in ventral (inferior) aspects. More precisely, MCI-CB revealed contractions in medial parts of the putamen and anterior parts of the striatum (caudate head). The same pattern was found in MCI-CC, with more pronounced alterations in left ventral (inferior) medial parts of the putamen and with continued spreading to the left dorsal medial striatum (caudate body) and to right ventral (inferior) aspects of the anterior striatum (caudate head). Similar to the contractions, striatal expansions were more pronounced in the left hemisphere: MCI-CB showed pronounced expansions in ventral aspects of the anterior striatum (caudate head) and lateral putamen. MCI-CC showed a similar pattern, but with further continued expansions to

ventral (inferior) aspects of the left striatum (caudate tail), and to ventral aspects of the anterior striatum (caudate head) of the right hemisphere.

Discriminative accuracy of shape alterations and hippocampus volumes

For these analyses, between group t statistics from comparison between HC and MCI-CB were used. More precisely, for all vertices whose t-values constituted a local minimum (or maximum), the average of the displacement values in mm was computed for each subject. This was done separately for each structure and hemisphere. The analyses revealed contractions of the right thalamus and left striatum having an AUC of 0.98 (95% confidence interval [CI] 0.929-1.000, $p < 0.001$) and of 0.96 (95%CI 0.883-1.000, $p < 0.001$) for discriminating HC from MCI-CB (Figure 5), both AUC confirming excellent accuracy and high statistical significance similar to left hippocampus volume (raw volume AUC = 0.95, 95%CI 0.861-1.000, $p < 0.001$; volume relative to eTIV AUC = 0.95, 95%CI 0.848-1.000, $p < 0.001$) and increased accuracy and statistical significance when compared to the right hippocampus volume (raw volume AUC = 0.80, 95%CI 0.572-1.000, $p < 0.05$; volume relative to eTIV AUC = 0.84, 95%CI 0.633-1.000, $p < 0.05$). The same AUC analyses carried out for thalamic expansions (left AUC = 0.92 95%CI 0.767-1.000, $p = 0.001$; right AUC = 0.93 95%CI 0.816-1.000, $p = 0.001$), thalamic contractions left (AUC = 0.86, 95%CI 0.685-1.000, $p = 0.007$) and striatal expansions left (AUC = 0.88, 95%CI 0.730-1.000, $p = 0.004$) revealed lower but still statistically significant accuracy for discriminating HC from MCI-CB.

Figure 5. ROC curve analyses.

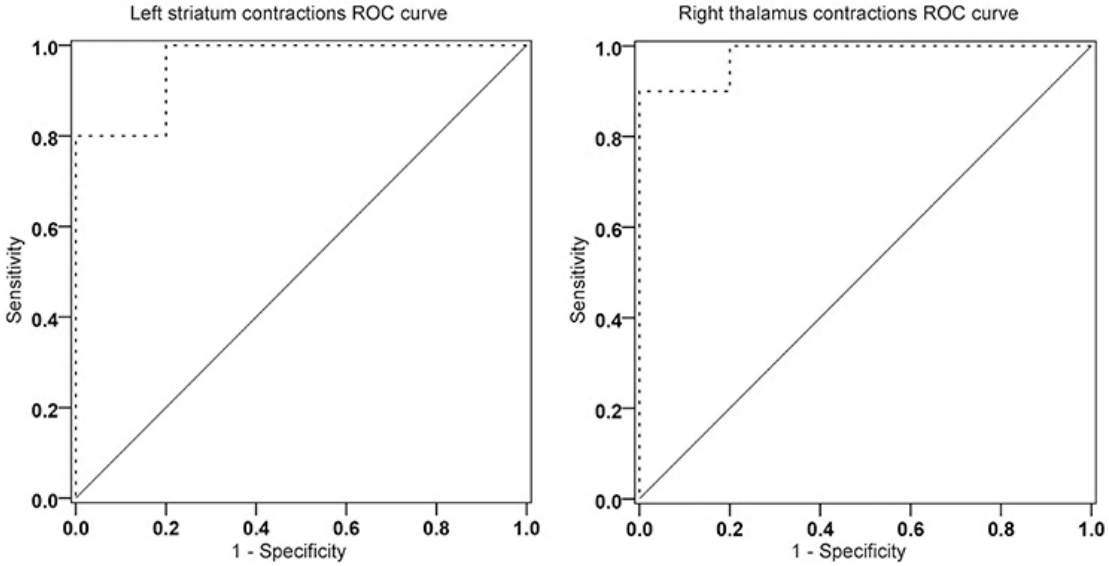

Figure 5. Receiver operating characteristic curve analyses of contractions in the left striatum (area under the curve [AUC] = 0.96, $p < 0.001$) and the right thalamus (AUC = 0.98, $p < 0.001$) for discriminating future converters at baseline from healthy control subjects. — — — — - ROC curvereference lines.

Discussion

In the current study, we used a combination of novel (thalamic and striatal shape indices) and well-established (cortical thickness and the volume of the hippocampus and its subfields) structural imaging techniques to characterize the neuroanatomy of MCI-to-AD converters. We examined the neuroanatomy in the MCI-to-AD converters using data acquired both at baseline and time of conversion. In addition, we compared baseline data from stable MCI subjects, comparing them with data from group-wise matched HC in a cross-sectional manner.

Cortical thinning in future converters

There was no significant difference in cortical thickness in MCI-S compared to HC, but in MCI-CB in left parahippocampal regions including the uncus with further propagation to bilateral regions in MCI-CC. This pattern is consistent with the literature (H. Braak & Braak, 1991b; Mitchell et al., 2002) and with morphometric changes previously associated with early stages of AD

(Drago et al., 2011; Mitchell et al., 2002). Like others (Lebedev et al., 2013), we also identified cortical thinning in the subgenual cingulate region in MCI-CB. Functionally, this region has been related to normal sadness reactions (Phan, Wager, Taylor, & Liberzon, 2002), and reduced volumes have been observed in patients with major depressive disorder (Drevets, Price, & Furey, 2008). Although clinically significant depression was one of the exclusion criteria in our study, very subtle and subclinical depressive symptoms that are difficult to quantify may be related to this finding in MCI-CB, leaving the exact mechanism unclear. This region has furthermore been associated with the uptake of serotonin (Lanzenberger et al., 2013). Serotonin is involved in the regulation of sleep (Portas, Bjorvatn, & Ursin, 2000) which is disturbed in AD (Westerberg et al., 2012).

Hippocampal atrophy in future converters

MCI-S revealed no global or local hippocampal volume reductions compared to HC. However, in accordance with the AD literature (Stepan-Buksakowska et al., 2014) and our expectations, we found reduced volumes of bilateral hippocampi in MCI-CB and MCI-CC as well as reduced local volumes of all but one (CA2-CA3) bilateral subfields already in MCI-CB, and of all bilateral subfields in MCI-CC.

Hippocampal atrophy represents the key imaging marker in AD research. The successful identification of hippocampal subfields by using high-field MRI, however, has offered a more refined approach (Antharam et al., 2012; Mueller et al., 2010; Mueller & Weiner, 2009; Wisse, Biessels, Heringa, et al., 2014; Yushkevich et al., 2009). Advances in segmentation and analysis techniques have now enabled the field to identify hippocampal subfield alterations on images obtained from standard clinical systems. Corresponding with the pattern of neurofibrillary tangle formation, predominant CA1 atrophy has been found in MCI (Apostolova, Dinov, et al., 2006; Atienza et al., 2011; La Joie et al., 2013; Pluta et al., 2012; Yushkevich, Pluta, et al., 2015), with some of these studies having reported additional subicular alterations (Atienza et al., 2011; La Joie et al., 2013) and alterations in additional subfields (Amaral, Park, Devenyi, Lynn, Pipitone, Winterburn, Chavez, Schira, Lobaugh, & Voineskos, 2016). A more extended pattern also

including CA2 and CA3 or even CA4/Dentate gyrus has been identified in AD (Apostolova, Dinov, et al., 2006; Frankó, Joly, & Initiative, 2013; Frisoni et al., 2008; Y.-D. Li, Dong, Xie, & Zhang, 2013). Importantly, alterations in these subfields have been related to impaired memory functions in amnestic MCI (Atienza et al., 2011; Ferrarini et al., 2014). Local analysis of the structure, therefore, has been suggested advantageous for the early detection of dementia (Tang et al., 2014).

Nevertheless, only a few studies have examined hippocampal subfields in future converters. Even though they have applied surface-based subfield imaging without providing volumetric information, results of alterations in CA1 and/or subiculum in future converters to MCI (Apostolova et al., 2010) or to AD (Apostolova, Dutton, et al., 2006; Gaël Chételat et al., 2008; Frankó et al., 2013) are in agreement with our own findings. In line with further progression of tangle accumulation (H. Braak & Braak, 1991b), we found similar bilateral CA2-CA3 volumes in MCI-CB but reduced bilateral CA2-CA3 volumes in MCI-CC compared to HC. Additionally, we found bilateral CA4/Dentate gyrus volumes were lowered not only in MCI-CC but also in MCI-CB. Although CA4/Dentate gyrus volume reduction has mainly been identified in dementia stages (Frankó et al., 2013; Y.-D. Li et al., 2013), earlier alterations in this subfield have also been reported by others (Pluta et al., 2012). We also identified reduced volumes of bilateral strata lacunosum/radiatum/moleculare in MCI-CB and MCI-CC, and our results are supported by studies reporting stratum radiatum and stratum lacunosum/moleculare of CA1 being affected by early tangle accumulation (E. Braak & Braak, 1997; H. Braak, Alafuzoff, Arzberger, Kretzschmar, & Del Tredici, 2006; Dietmar R. Thal et al., 2000) and atrophy in mild AD (Kerchner et al., 2010b). It shoud be further noted that only a few protocols exist allowing for the reliable, automated segmentation of hippocampal subfields (see (Wisse, Biessels, & Geerlings, 2014) for a critical discussion; (Yushkevich, Amaral, et al., 2015)). Here, we used a multi-atlas based segmentation approach (Chakravarty et al., 2013; Voineskos et al., 2015) that performs as well as other methods used in the field (Pipitone et al., 2014).

Thalamic alterations in future converters

MCI-S did not reveal any deviation from HC, neither in thalamic total or subfield volumes nor in shape alterations. Contrary to our expectation, the same was true for both total and local thalamus volumes in MCI-CB and MCI-CC. Indeed reduced thalamic total volumes have been reported in amnestic MCI (Hahn, Lee, Won, Joo, & Lim, 2016) and MCI-CB (Bossa, Zacur, & Olmos, 2011). However, thalamic atrophy in AD is debated, particularly in early disease stages (H. Braak & Braak, 1991a; Paskavitz, Lippa, Hamos, Pulaski-Salo, & Drachman, 1995; Xuereb et al., 1991), where only a few regions are affected by a small number of isolated neurofibrillary tangles (H. Braak & Braak, 1991b). Moreover, our results are in agreement with other studies having observed similar volumes in amnestic MCI, MCI and AD patients (Cho et al., 2014).

But first and foremost, and despite the absence of volumetric differences, we identified a widespread pattern of shape alterations in MCI-CB and MCI-CC with displacements showing similar if not improved discrimination between HC and MCI-CB compared to hippocampus volume. These findings may represent a critical MRI-based marker for AD. Confirming our expectation, the pronounced thalamic shape alterations in VA found in MCI-CB and MCI-CC cover regions that are affected from early neurofibrillary tangles and later occurring amyloid deposition (H. Braak & Braak, 1991a). Importantly, the thalamus plays a crucial role in the Papez circuit with the anterior thalamus and the pulvinar, both having shown shape alterations in MCI-CB and MCI-CC, being directly connected to the hippocampus (Zarei et al., 2010). Furthermore, frontostriatal circuits link dorsolateral prefrontal, anterior cingulate, and orbitofrontal cortex regions (Alexander, DeLong, & Strick, 1986) via the striatum / globus pallidus (Haber, 2003) to VA and medial dorsal aspects of the thalamus (Bonelli & Cummings, 2007; Tekin & Cummings, 2002), aspects that again have shown shape alterations in MCI-CB and MCI-CC. Further significant shape alterations were found in the VP, VL and lateral posterior nuclei connecting the structure with the somatosensory, motor, premotor and prefrontal and temporal and parietal cortices (Behrens et al., 2003; de Bourbon-Teles et al., 2014). Consistent with these extensive connections, thalamic regions affected from shape alterations in MCI-CB and MCI-CC have been linked with memory and frontal executive,

attention, visuospatial perception, and emotion processing (Arend, Henik, & Okon-Singer, 2015; de Bourbon-Teles et al., 2014; Saalmann, 2014; Wilke, Kagan, & Andersen, 2013), with all of these functions being impaired early in AD (Klekociuk, Summers, Vickers, & Summers, 2014).

To our knowledge, there has been only one other study investigating subcortical shape alterations in MCI-S and MCI-CB, without a HC group (Tang et al., 2014). The contractions found in the pulvinar and dorsal aspects of the VP in MCI-CB are consistent with contractions that have been identified in amnestic MCI by an earlier study of our group (Leh et al., 2016). Additionally, the authors have documented contractions in regions that remained unaffected in the present MCI-CB sample such as the VL and lateral posterior nuclei. These, however, revealed contractions in the MCI-CC group. Our finding of contractions in dorsal, medial dorsal and anterior regions with more pronounced results in the left than in the right hemisphere in MCI-CB and MCI-CC, contractions in the pulvinar and dorsal as well as medial dorsal regions in MCI-CC in turn are consistent with other study results (Cho et al., 2014; Hahn et al., 2016; Qiu, Fennema-Notestine, Dale, Miller, & Alzheimer's Disease Neuroimaging, 2009; Stepan-Buksakowska et al., 2014). The few results about thalamic expansions in MCI and AD are inconsistent. In contrast to expansions in ventral regions in both MCI-CB and MCI-CC, the earlier study from our group has identified expansions in more lateral aspects in amnestic MCI, whereas others have reported expansions in medial or even dorsal aspects in MCI and AD (Qiu et al., 2009). Further studies are warranted to find out whether there is a typical AD-related pattern of thalamic expansion.

Striatal alterations in future converters

Against our expectation, we observed reduced bilateral striatal volumes in MCI-S but similar volumes in MCI-CB and MCI-CC when compared to HC. The most plausible explanation for this seem to be age- and gender-related shrinking, or age-related changes in dopamine and frontostriatal networks (Klostermann, Braskie, Landau, O'Neil, & Jagust, 2012) resulting in reduced striatal volumes. Due to age- and gender-matched MCI-S and HC groups, however, this is rather unlikely in the present study. Rather, the result may

indicate non-AD pathology in our MCI-S sample. This assumption is further supported by cognitive profiles differing between MCI-S and MCI-CB. In comparison with their respective HC group, MCI-S showed significantly reduced cognitive scores not only in memory tests but also in tests assessing executive functions, attention and language abilities (see Table 1). In contrast, and apart from impaired memory functions, MCI-CB performed worse than their respective HC in the category fluency task and in the boston naming test but not in attentional tasks. Both, the category fluency task and the boston naming test have closely been linked with semantic knowledge (Delis & Kaplan, 2001), which in turn is thought to rely on temporal brain regions (Levy, Bayley, & Squire, 2004) known to be affected early in AD (Tondelli et al., 2012b). Genereally speaking, MCI-S in our study might indeed represent non-AD cognitive impairment mainly based on attentional deficits influencing other cognitive processes and leading to a more widespread pattern of cognitive impairment whereas our MCI-CB group showed an AD-typical pattern of cognitive impairment.

Normal striatal volumes in MCI-CB and MCI-CC in turn are most likely attributable to the early disease stages of each group: striatal amyloid deposition and tangle formation have evidenced at late histopathological disease stages, and mainly after dementia onset (Beach et al., 2012; H. Braak & Braak, 1990, 1991a, 1991b; Dietmar R Thal, Rüb, Orantes, & Braak, 2002). Hence, the striatum in MCI-CB and MCI-CC may still be free of typical AD pathology. Correspondingly, similar volumes of the striatum, putamen and caudate in MCI and future converters compared to HC have been reported by others (Bossa et al., 2011; J. H. Roh et al., 2011).

As expected, however, shape analyses showed no alterations in the striatum in MCI-S but pronounced displacements in MCI-CB and MCI-CC. The observed shape alterations were limited to the left striatum in MCI-CB, but displacements had propagated within the structure and to the right hemisphere in MCI-CC. Furthermore, and as with the thalamic shape alterations, these striatal shape alterations revealed similar abilities for discriminating HC from MCI-CB compared to hippocampus volume. Aspects of the striatum showing most pronounced contractions and expansions such as the caudate head, body and tail as well as medial and lateral putamen

have been linked to a wide range of cognitive functions. These regions are involved in attention, planning and memory (Cummings, 1995), all of which are impaired early in AD (Klekociuk et al., 2014).

Again, the study from Tang et al. (Tang et al., 2014) represents the only study we are aware of having documented shape alterations in MCI-S and MCI-CB; however no HCs were compared in this study. In agreement with other studies, however, they demonstrated patterns of striatal contractions in MCI and AD patients (de Jong et al., 2011; Qiu et al., 2009; Tang et al., 2014) that were comparable to the patterns found in the current study. Interestingly, only a few studies have documented striatal expansions in general (de Jong et al., 2011; Tang et al., 2014), though these expansions were less pronounced than in the present study (visual inspection).

It is beyond the aim of our study to draw direct inferences about the neuronal correlate of shape alterations. Given the pronounced connections with other disease-relevant structures (Leh, Chakravarty, & Ptito, 2008), however, striatal and thalamic shape alterations may represent secondary downstream effects. A similar effect has been proposed by Stepan-Buksakowska et al. (Stepan-Buksakowska et al., 2014). Specifically, volume reductions in the hippocampus and other early affected cortical regions may have caused subsequent morphometric changes in connected regions such as the thalamus and the striatum, without generating volume reductions yet. Although we cannot rule out the possibility of contractions representing atrophy-related alterations, the applied surface-based shape analyses provide local, but not fully comprehensive information about the entire structure. Accordingly, and as it has been shown in the present study, structural shape alterations are not necessarily associated with corresponding volume changes. Hence, our results of shape differences in the absence of volume differences highlight the importance of considering shape changes along with established volume measures.

Limitations

The authors are fully aware of other studies investigating subcortical shape alterations in MCI and/or AD patients (Cho et al., 2014; Hahn et al.,

2016; Stepan-Buksakowska et al., 2014; Tang et al., 2014). However, and apart from the study from Tang et al. (Tang et al., 2014), we are not aware of other studies investigating thalamic and striatal shape abnormalities in MCI-S, MCI-CB, and MCI-CC in a single comparative study, and of no study comparing these shape abnormalities with measures from age—and gender matched HC. More importantly, we are not aware of any other study providing evidence of thalamic/striatal shape alterations at such early stages of AD (MCI-CB)—with absent thalamic/striatal shape alterations in MCI-S at the same time. Thus, our work provides support for these novel morphometric measures representing a potential and very sensitive early marker for AD. Additionally, and compared with emerging techniques such as hippocampal subfield volume analysis and already established techniques such as cortical thickness analysis, shape analysis represents an advanced and novel technique. Accordingly, the number of studies investigating subcortical shape alterations in MCI/AD subjects is limited (Cho et al., 2014; de Jong et al., 2011; Hahn et al., 2016; Qiu et al., 2009; Tang et al., 2014). Furthermore, the comparability of results remains difficult due to different imaging processing algorithms and different MRI acquisition modalities (i.e., with field strength of scanners varying from 1.5 T in our own study to 7 T in the study from Tang et al., 2014, and with other high-sample studies using images acquired from various scanners in the study from Qiu et al., 2009). Thus, contractions and expansions represent a novel way to quantify the morphometry of brain regions, with shape alterations having been associated with memory performance in our previous study (Voineskos et al., 2015).

Although other groups have also reported shape analysis results obtained from studies consisting of similarly small sample sizes (i.e., Stepan-Buksakowska et al., 2014, 12 AD, 13 HC), the small group sizes may have prevented the detection of small effects in this study. However, we believe that the reliability of our findings are supported by low standard deviations across our measures (see Tables 2, 3) as well as by the overall characteristic of the results obtained using well-established analyses techniques (the volume of the hippocampus and its subfields and cortical thickness) and being perfectly in line with the literature. Furthermore, statistically significant differences in shape alterations between small groups indicate that even more

pronounced effects might be expected in future studies using larger sample sizes. In sum, and despite the small group sizes, we consider the present study results important to investigate whether shape alteration can help localizing differences associated with the stability or progression of cognitive impairment. However, further studies are required to confirm our results in larger samples. This is also true for our ROC analyses, whose AUC values were remarkably high for measures of striatal and thalamic shape and left hippocampus and may represent an overestimation of discriminative ability due to small sample size.

The approach of using three different control groups might indeed increase chances of coincidental findings, and thus represent a limitating factor. However, and for the present study, MCI subjects were selected from a study aiming to characterize future converters to AD. The study did not consist of HC. Therefore, it was necessary to recruit HC restrospectively, rendering the acquisition of longitudinal data and performance of longitudinal statistical analyses impossible. Furthermore, MCI-CB differed from MCI-S with respect to age and gender, both having previously been associated with morphometric measures. Thus, and in order to prevent the use of a high number of covariates in statistical analyses (and the risk to further reduce statistical power), control subjects were recruited for group-wise matching to each patient group with respect to these potentially confounding factors.

Additionally, the comparison of the data between MCI-S and MCI-CB, and between MCI-CB and MCI-CC would be of high interest. However, and apart from the cross-sectional nature of the present study, these analyses require accounting for confounding variables (i.e., variable times to conversion), and increase the number of comparisons. Generally speaking, and in consideration of the rather low sample sizes in the present study, additional analyses would further reduce the power of the present results. Similarly, ROC analyses discriminating MCI-CB from MCI-SB based on striatal and thalamic shape alterations is relevant. However, and for similar reasons and consistency, the main aim of the ROC analyses in the present study was to demonstrate similar if not improved abilities of striatal / thalamic shape alterations compared to hippocampal volumes for AD to discriminate between MCI-CB from HC. But first and foremost, the aim of the present study

was to investigate morphometric differences between patient and well matched control groups to establish the sophisticated analysis techniques on images obtained from a 1.5 Tesla scanner. Nevertheless, further studies are now required to confirm our results in larger samples allowing for additional and more advanced statistical models.

MCI-S has been described as a potential early stage of AD (Bossa et al., 2011). However, apart from slightly reduced striatal volumes, MCI-S demonstrated no morphometric changes when compared to HC in the present study, rendering this notion unlikely. At the same time, MCI-S, consisting of amnestic MCI multiple domain subjects only, showed a more widespread pattern of cognitive impairment than MCI-CB, consisting of both, amnestic MCI single domain (n = 3) and amnestic MCI multiple domain subjects (n = 7). More precisely, both MCI groups showed memory impairment and impairment in a language-related function (confrontation naming) as well as in semantic memory and executive functioning (animal fluency). Interestingly, however, MCI-S but not MCI-CB showed further impairments in additional executive tasks (letter fluency, digit span backwards) as well as in attentional abilities (TMT A and TMT B). These attentional deficits in MCI-S might be at the basis of the other cognitive deficits in this group, resulting in a more widespread and global pattern of cognitive impairment when compared with MCI-CB–with remaining abilities for everyday life at the same time. Generally speaking, these findings might represent non-typical-AD pathology rather than early stage AD in the present MCI-S group, and this assumption is further supported by the morphometric findings in this group (reduced striatal volumes, no other morphometric abnormalities). However, the AD typical cognitive impairment, the pattern of cortical thinning and hippocampal atrophy in MCI-CB and MCI-CC, together with a cognitive profile uncharacteristic for AD and the absence of morphometric alterations in MCI-S, is supportive of AD pathology in MCI-CB and MCI-CC. Additional markers of neurodegeneration such as CSF levels of phosphorylated Tau together with amyloid imaging may provide additional information on this matter in future longitudinal studies. Also, vascular risk factors such as hypertension, diabetes mellitus, hyperlipidemia, etc. represent main risk factors for the development of

dementia. This information, however, was not available for all subjects and could therefore not be added in the statistical models.

The similarity of patterns of morphometric alterations in MCI-CB and MCI-CC is most likely due to both groups consisting of the same subjects, with MCI-CC data having been obtained at time of conversion. Hence, the time lag of approximately 20.8 months between MRI at baseline and at time of conversion might have been too short to reveal progression of morphometric alterations.

Conclusion

In conclusion, the simultaneous presence of highly accurate thalamic and striatal shape alterations, AD typical cortical thinning and hippocampal atrophy in MCI-CB but not in MCI-S highlights the value of subcortical shape alterations as early marker for AD, and emphasizes the importance to consider regional morphological information of subcortical structures. It is necessary to find ways allowing the implementation of advanced segmentation and analysis techniques in everyday clinical practice in the near future.

Ethics statement

The study protocol was approved by the cantonal ethics committee Zurich, Switzerland, and the study was carried out in accordance with good clinical practice guidelines issued by the committee. All subjects gave written informed consent in accordance with the Declaration of Helsinki.

Author contributions

Research questions and study design were formulated by SL, RN, AG, CH, and AK. Data acquisition was carried out by AK, LM, CS, SB, SK, AG, and SL. Data analyses were performed by AK, MP, MC, JL, LM, CS, and SL. All authors contributed to the interpretation of data and to the manuscript drafting, writing and revising.

Funding

This study was made possible by SNF SPUM Grant No. 33CM30-124111, by the Molecular Imaging Network Zürich (MINZ), and by an International Short Visits Grant from the SNF to SL (IZK0Z3_151124). MC is funded by the Canadian Institutes of Health Research, National Sciences and Engineering Research Council of Cananda, Weston Brain Institute, Alzheimer's Society, and the Michael J. Fox Foundation for Parkinson's Research. RN and CH are founder/co-founder and board members of Neurimmune Holding AG, Schlieren.

Conflict of interest statement

The authors declare that the research was conducted in the absence of any commercial or financial relationships that could be construed as a potential conflict of interest.

RN and CH are founder/co-founder and board members of Neurimmune Holding AG, Schlieren.

Acknowledgments

We thank the participants and their families for their generous support. We furthermore thank Isabella Blum, Esmeralda Gruber and Faith Sieber (study nurses), Sara Kroll and Marc Bächinger (research assistants), Sabine Spoerri, Stefan Kluge and Stefan Doppler (data management), Daniel Summermatter (neuropsychologist) and all study physicians for their help with the data acquisition, and Manuel Gersbacher for improving the figures. The content of this study first appeared in the doctoral thesis of the manuscripts' first author (Kälin, 2015).

Abbreviations

CA, Cornu ammonis; eTIV, estimated total intracranial volume; HC, Healthy controls; ICBM, International consortium for brain mapping; ICV, intracranial volume; INSECT, Intensity-Normalized Stereotaxic Environment for Classification of Tissues; LGN, lateral geniculate nucleus; MAGeT, Multiple automatically generated templates; MCI-CB, mild cognitive impairment to AD converters at baseline; MCI-CC, mild cognitive impairment converters to AD at time of conversion; MCI-S, stable mild cognitive

impairment at baseline; MGN, medial geniculate nucleus; NINCDS-ADRDA, National Institute of Neurological and Communicative Disorders and Stroke and the Alzheimer's Disease and Related Disorders Association; RMINC, R for Medical Imaging NetCDF; VA, ventral anterior nucleus; VL, ventral lateral nucleus; VP, ventral posterior nucleus.

4.3 Informing participants about the study purpose: A hidden peril in studies of resting state fMRI connectivity?

Clemens Schroeder[1¶], Sandra E. Leh[1¶], Andrea M. Kälin[1], Christoph Hock[1], Lars Michels[2+**], Spyros Kollias[2**]

[1]Division of Psychiatry Research, University of Zurich, Zurich, Zurich, Switzerland
[2]Clinic of Neuroradiology, University Hospital Zurich, Zurich, Zurich, Switzerland

+ Corresponding author
lars.michels@usz.ch

¶ These authors contributed equally to this work
** shared-senior authorship

Keywords: functional connectivity, resting-state, dynamic connectivity, elderly

Abstract

Objective: Resting state functional magnetic resonance imaging (rsfMRI) is a widely used technique to investigate task-unrelated brain networks. Yet, even in rsfMRI studies there is considerable variation regarding study purpose and instruction, which might affect neuronal sources linked to the brain's resting state. This may have far-reaching consequences for the comparability of different studies on the same topic. The objective of the present study was to systematically investigate the influence of providing information on the study purpose on static and dynamic resting-state functional connectivity (rs-FC).

Methods: Thirty right-handed healthy elderly volunteers (61-80 years) were scanned during an eyes-closed rsfMRI run. One group was informed about a particular study aim ("we study an important brain function") immediately before the rsfMRI run, whereas the other group was not

informed. Static regional (i.e., Brodmann areas) as well as network-specific rs-FC using independent-component analysis (ICA) was performed. Additionally, dynamic functional network connectivity was compared between the two groups to examine inter-network connectivity.

Results: Participants informed before the rsfMRI scan showed both increased and decreased regional rs-FC compared to participants informed after scanning in several Brodmann areas (BA 8-11, 17, 20, 44-45, $p < 0.05$, corrected). Using a group ICA analysis, participants of the group informed after scanning revealed higher rs-FC of the medial prefrontal and anterior cingulate cortex component. Further, the strongest effect of the dynamic functional network connectivity analysis was seen for this frontal component, reflected by its increased connectivity to the left central executive network in the group informed after scanning ($p < 0.05$, corrected).

Conclusion: Our results suggest that informing participants about the study purpose before rsfMRI influences subsequent task-unrelated brain activation within and between functional networks. Hence, we conclude that subject information prior to rsfMRI should be taken into consideration when comparing rs-FC findings between existing studies.

Introduction

Initial work using task-unrelated resting state functional magnetic resonance imaging (rsfMRI) has identified a number of functional networks in the human brain that were consistently reproduced in following studies. These networks are termed default mode network (DMN), central executive network (CEN) or task-positive dorsal attention system (M. D. Fox et al., 2005), sensorimotor network (SMN), salience network (SN), and primary visual and auditory network (Damoiseaux et al., 2006; M. D. Fox et al., 2005; Lee, Smyser, & Shimony, 2013; Seeley et al., 2007; Sridharan, Levitin, & Menon, 2008). Analyses of resting state networks have been conducted to various topics, such as bipolar disorder (Vargas, Lopez-Jaramillo, & Vieta, 2013), epilepsy (Centeno & Carmichael, 2014), stroke (Rehme & Grefkes, 2013), Alzheimer disease (AD) (Gomez-Ramirez & Wu, 2014), states of

consciousness (Heine et al., 2012), aging (Dennis & Thompson, 2014) and normal brain development and young adults (Barber, Caffo, Pekar, & Mostofsky, 2013; Chai, Ofen, Gabrieli, & Whitfield-Gabrieli, 2014).

The body of research on resting state networks is rapidly growing with increasing relevance in various disciplines. In order to secure comparability of results across studies, it is of great interest to identify and remove confounding influences in rsfMRI data. Because there are a number of possible "resting states", it is highly relevant to estimate the extent to which different resting states feature differences in network connectivity. Several aspects of study design have already been identified as factors influencing resting-state functional connectivity (rs-FC): In a study by Patriat et al. (2013), higher auditory network connectivity was found in an eyes-closed condition than an eyes-open and an eyes-fixated condition. Another study revealed higher DMN connectivity in an eyes-open and an eyes-fixated condition compared to an eyes-closed condition (Yan et al., 2009). Findings of another study revealed marginally significant differences between eyes-closed and eyes-fixated conditions for the DMN and the CEN (K. Van Dijk et al., 2010).

Here, we assessed whether participant information about the study purpose prior to rsfMRI is sufficient to alter rs-FC while keeping the instruction constant (keep your eyes closed, lie still, and do not move). Specifically, prior to scanning we informed all participants that an important brain function was going to be investigated during one of the subsequent measurements. We then particularly assessed the effect of providing information about the study purpose immediately before *versus* after scanning on rs-FC (using rsfMRI) within and between several resting state networks as well as on the whole-brain level. We assume that delivering controlled information about the study aim had an impact on cognitive arousal, resulting in between-group differences in rs-FC.

Specifically, we expected the informed participants to more strongly monitor and invest effort in their behavioural compliance (keep your eyes closed, lie still, do not move), and therefore to engage more in cognitive processes such as motor inhibition and self-control, and to engage less in thought processes typically associated with brain activity during rest, such as mind wandering (Christoff, Gordon, Smallwood, Smith, & Schooler, 2009;

Mason et al., 2007). Therefore, we hypothesized the following between-group rs-FC differences for these Brodmann areas (BA), comparing the after *versus* before group: decreased rs-FC between bilateral dorsolateral prefrontal cortex (DLPFC: BA 9 and 46), ventrolateral prefrontal cortex (VLPFC: BA 44 and 45), which are involved in motor inhibition (Leung & Cai, 2007); decreased rs-FC between bilateral inferior frontal gyrus (IFG: same BA as VLPFC), which is activated in motor inhibition, and medial prefrontal cortex (MPFC: BA 8 and 11), which is deactivated in motor inhibition (Rodrigo et al., 2014) and involved in inhibitory control (Mulligan, Kristjansson, Reiersen, Parra, & Anokhin, 2014). Additionally, we expected increased recruitment of the medial prefrontal default network area (MPFC), which is involved in mind wandering (Christoff et al., 2009), to be reflected in rs-FC differences between groups. Accordingly, we hypothesized between-group rs-FC differences in the following networks: The CEN, which includes the DLPFC (Sridharan et al., 2008); the SN, which includes the ACC (Menon & Uddin, 2010; Seeley et al., 2007); and the DMN, which includes the MPFC and ACC (M. D. Fox et al., 2005).

Materials and Methods

Participants

Thirty cognitively healthy subjects were recruited from ongoing longitudinal studies at the Memory Clinic of the Division of Psychiatry Research and Psychogeriatric Medicine, University of Zurich. For the present study, inclusion criteria were: cognitive health ascertained by clinical work up and neuropsychological testing, mini-mental state examination (MMSE) scores > 27 and a Hamilton depression scale German version (Ham-D) score < 12, MRI suitability, and right handedness. No subject took caffeine or nicotine on the day of examination or exceeded the limit for head movements of 1.5 millimetres (= half of the fMRI voxel recording size) during scanning. The final sample consisted of 30 individuals (61-80 years, 12 female). The final groups consisted of 16 participants (9 female) informed after scanning and 14 participants (4 female) informed before scanning. Detailed demographic information is presented in Table 1.

Table 1. Participant demographical and control variables.

Variable	Condition	M (SD)	Statistic, p-value
Age	Informed before scanning	72.1 (4.8)	t(24.3) = -2.7, p = 0.566
	Informed after scanning	71.1 (5.3)	
Education	Informed before scanning	16.2 (2.9)	t(27.9) = -0.6, p = 0.012*
	Informed after scanning	13.6 (2.2)	
MMSE	Informed before scanning	29.5 (0.7)	t(25.8) = 0.0, p = 1.000
	Informed after scanning	29.5 (0.9)	
Ham-D	Informed before scanning	1.1 (1.8)	t(28.0) = -0.5, p = 0.631
	Informed after scanning	1.4 (1.6)	
Digit span backward	Informed before scanning	5.9 (1.5)	t(27.9) = -2.0, p = 0.055
	Informed after scanning	6.9 (1.4)	
Corsi block backward	Informed before scanning	27.1 (8.5)	t(27.8) = -0.1, p = 0.898
	Informed after scanning	32.0 (11.9)	
Verbal fluency - categorical	Informed before scanning	23.7 (4.1)	t(24.4) = -0.5, p = 0.621
	Informed after scanning	24.6 (5.3)	
Verbal fluency - phonetic	Informed before scanning	27.1 (8.5)	t(23.2) = -1.3, p = 0.214
	Informed after scanning	32.0 (11.9)	
Stroop interference	Informed before scanning	2.1 (0.6)	t(23.5) = 0.7, p = 0.471
	Informed after scanning	2.0 (0.3)	
TMT ratio	Informed before scanning	2.6 (0.6)	t(27.7) = 1.3, p = 0.217
	Informed after scanning	2.3 (0.6)	

*$p < 0.05$

Descriptive statistics of control variables for both groups and results of statistical tests between groups.

Ethics statement

This study was approved by the cantonal ethics committee of canton Zurich (E22/2009, SNF-Nr 33CM30-1124111,), Switzerland, and in accordance with the Helsinki Declaration. All participants provided written informed consent prior to study inclusion.

Control variables

Control variables compared between groups (Table 1) included age, gender, education (in years) and scores on the MMSE, the Ham-D and a number of tests on working memory and executive function. These neuropsychological tests were conducted to exclude the possibility that differences between groups in neural activity during rest are attributable to differences in cognitive functions related to self-control and inhibition. Neuropsychological measures included scores on the digit span backward and block-tapping backward test (Wechsler Memory Scale-Revised Edition, Wechsler 1987) assessing working memory and the interference score (time required for inconsistent condition minus time required for naming coloured circles) of the Stroop test (Stroop, 1935), a score of categorical fluency (number of animals named within 1 minute; Goodglass & Kaplan 1972) a phonetic fluency score (number of words starting with S named within 3 minutes; adapted from the Thurstone Word Fluency Test; Thurstone & Thurstone 1938), and the trail making test (TMT; ratio: time required for TMT B divided by time required for TMT A) assessing different executive functions. Gender was compared between groups using the Chi-square test. All other control variables were compared between groups using the Welch two sample t-tests. For these analyses, the R software package (R version 2.13.1: http://www.r-project.org/) was used.

Experimental manipulation

Prior to any scan, all participants were informed that the study purpose of one measurement was the investigation of an important brain function, which was going to be revealed at a suitable time along the investigation. One group of participants was informed about the study purpose immediately

before the rsfMRI scan (before group) whereas the other group was informed after all MRI measurements (after group).

Data acquisition

Participants were instructed to relax and keep their eyes closed during a six-minute rsfMRI scan conducted on a 1.5T Philips Achieva (The Netherlands) scanner. fMRI imaging parameters were: echo-planar imaging, time of repetition = 3s, time of echo = 50 ms, flip angle = 90°, field of view = 220 mm, 128 x 128 scan matrix, slice thickness 3 mm, 34 slices, voxel size 1.72 x 1.72 mm, 120 scans, SENSE (sensitivity encoding for fast MRI (Pruessmann et al., 1999)) imaging with a SENSE factor of 1.5, and scan duration: 372s. A structural T1-weighted scan (inversion recovery turbo field echo, time of repetition = 6.9 s, time of echo = 3.1 s, flip angle = 8°, field of view = 240 mm, 400 x 400 scan matrix, slice thickness 1.2 mm, 166 slices, voxel size 0.6 x 0.6 mm) was acquired after the rs-fMRI scan.

Data processing and Analysis

Static connectivity

Whole-brain connectivity was assessed using the functional connectivity toolbox CONN (version 14h; http://www.nitrc.org/projects/conn/). Pre-processing steps included realignment, temporal filtering (0.01 – 0.1 Hz, Biswal et al. (1995)), detrending, slice-timing correction, coregistration, segmentation, normalisation, and spatial smoothing (8 mm). The CONN toolbox uses the anatomical component-based noise correction (aCompCor) method (Behzadi et al., 2007) to correct for physiological noise. This method identifies voxels consisting of mainly white matter or cerebrospinal fluid in order to model signal fluctuations not attributable to neural activation. This approach was shown to be superior to global signal correction (Chai et al., 2012) and increases the validity, sensitivity and specificity of functional connectivity MRI analyses (Whitfield-Gabrieli & Nieto-Castanon, 2012). CONN uses the general linear model for second-level analyses. Here, we separately analysed the interactions of group assignment with each of the control variables to determine whether any connectivity differences between groups

were attributable to the interaction with a control variable. Second analysis was applied on spherical regions of interest (ROI) predefined by CONN (i.e., 84 Brodmann areas) using Talairach Daemon (http://www.talairach.org/daemon.html) labels. In brief, the fMRI signal was averaged across all voxels within a ROI for each time point to calculate an average time series. Bivariate correlation coefficients were calculated for each pairing of ROIs. These coefficients were Fisher transformed prior to second-level analysis (Whitfield-Gabrieli & Nieto-Castanon, 2012).

Group level independent component analysis (ICA) was performed using the Group ICA of fMRI Toolbox (GIFT; version 3.0a; http://mialab.mrn.org/software/gift/). For pre-processing, removal of mean per time point was chosen. A mask was calculated using all subject and session files. Principal component analysis was run on the dataset of each subject before group ICA. For group ICA, two data reduction steps were chosen with the first step resulting in 30 and the second step resulting in 20 independent components. These components were estimated by the infomax algorithm (Bell & Sejnowski, 1995) and then submitted to spectral group comparison, allowing for significance testing of group differences in non-artefact (neuronal) components. FDR-corrected p values of $p < 0.05$ were considered significant. Correction was performed in R (http://www.r-project.org/).Group ICA was also performed separately for both groups in order to assess correspondence of independent components between the two groups. Resting state networks were identified by visual inspection using MRIcron (http://www.nitrc.org/projects/mricron). To determine the reliability of the ICA algorithm, we used the ICASSO toolbox (research.ics.aalto.fi/ica/icasso) to run the algorithm 20 times, starting with different initial values and using a bootstrap technique (minimal cluster size 16, maximal cluster size 20). This analysis indicated excellent reliability (lowest stability index 0.94).

Dynamic connectivity

In order to take into account variability of rs-FC over time, we compared groups using the dynamic FC (dyn-FC) toolbox (Allen et al., 2014). We submitted the described neuronal ICs (from the group ICA) to the dyn-FC analysis. Pre-processing included detrending and despiking, which was done

using 3dDespike (http://afni.nimh.nih.gov/afni), and low-pass filtering at 0.15 Hz using a fifth-order Butterworth filter. Accurate identification of cognitive states has been shown for window sizes of 30-60 s (Shirer, Ryali, Rykhlevskaia, Menon, & Greicius, 2012). Because variation of window size from 30 to 120 s has been shown to affect dynamics only slightly (C. Chang & Glover, 2010; Hutchison, Womelsdorf, Gati, Everling, & Menon, 2013) and a recent study found a window size of 22 TR = 44s to be optimal (Allen et al. 2014), we chose to use a window size of 20 TR = 60 s. Regularization was performed using GLASSO (http://cran.r-project.org/web/packages/glasso) (Friedman, Hastie, & Tibshirani, 2008), imposing an L1 (lasso) penalty on the estimation of the inverse covariance matrix to facilitate sparseness. We divided the time course of our resting-state acquisitions into the default number of 6 clusters using the k-means clustering algorithm (Lloyd, 1982) and compared between-network (IC-specific) connectivity across groups within the most dominant cluster, which accounted for 25.7 percent of total dwell time. A FDR-corrected p-value of $p < 0.05$ was considered significant.

Results

Control variables

There was a significant difference between groups in education (p = 0.012). There were no significant differences between groups in gender (X^2 = 1.3, p = 0.247), age, MMSE, Ham-D, semantic fluency, phonetic fluency, digit span backward, Corsi block backward, Stroop interference, and the TMT ratio between groups (all $p > 0.05$, see Table 1).

Static rs-FC: ROI-to-ROI analysis

ROI-to-ROI whole-brain rs-FC connectivity differed between groups for several pairings of ROIs (Figure 1). Stronger connectivity was found in the after group for the following connections: left BA 20 (inferior temporal area) - BA 9 (DLPFC), left BA 20 - BA 10 (including MPFC and ACC), and left BA 45 (IFG) - BA 17 (primary visual cortex). Decreased rs-FC was found between left BA 17 - right BA 29 (retrosplenial cortex), left BA 17 - right BA 34 (superior

temporal gyrus), right BA 17 - BA 29, right BA 45 - left BA 31, left BA 44 (IFG) - BA 45, left BA 44 - right BA 45, right BA 45 left BA 11 (MPFC), left BA 44 - BA 8 (MPFC) and left BA 44 - BA 9. None of these differences was attributable to the interaction of group assignment with any control variable (p-FDR > 0.05) even for education, which differed significantly between groups.

Figure 1. Whole-brain static ROI-to-ROI connectivity differences.

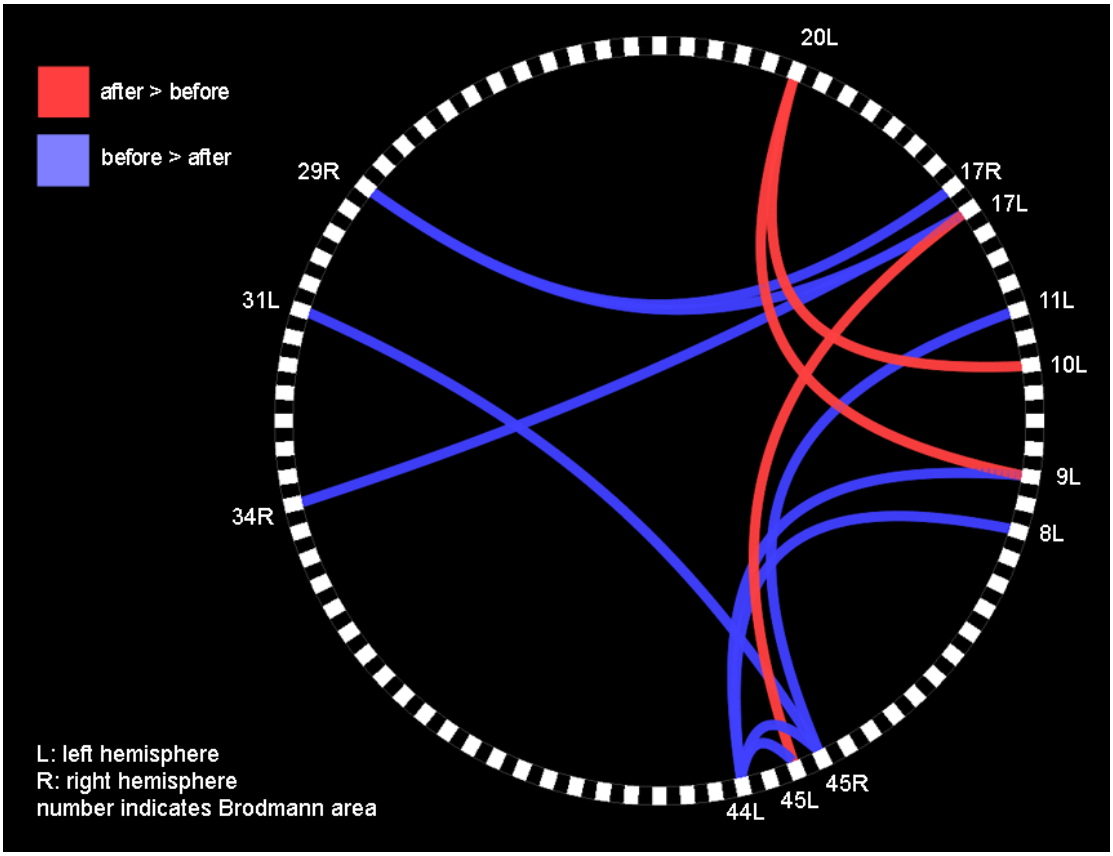

Connectivity between Brodmann areas was altered in several instances and in both directions. Results of two-sided testing with a threshold of p-FDR=0.05 are displayed.

Static rs-FC: Group ICA

In order to ensure comparability of the two groups with respect to meaningful ICs, group ICA was first performed separately for each group. Out of 20 ICs, 12 reflected non-neuronal physiological artefacts (respiration or pulse) or head motion. Visual inspection of the ICs revealed high correspondence between groups (Figure 2).

Figure 2. Independent components in both groups.

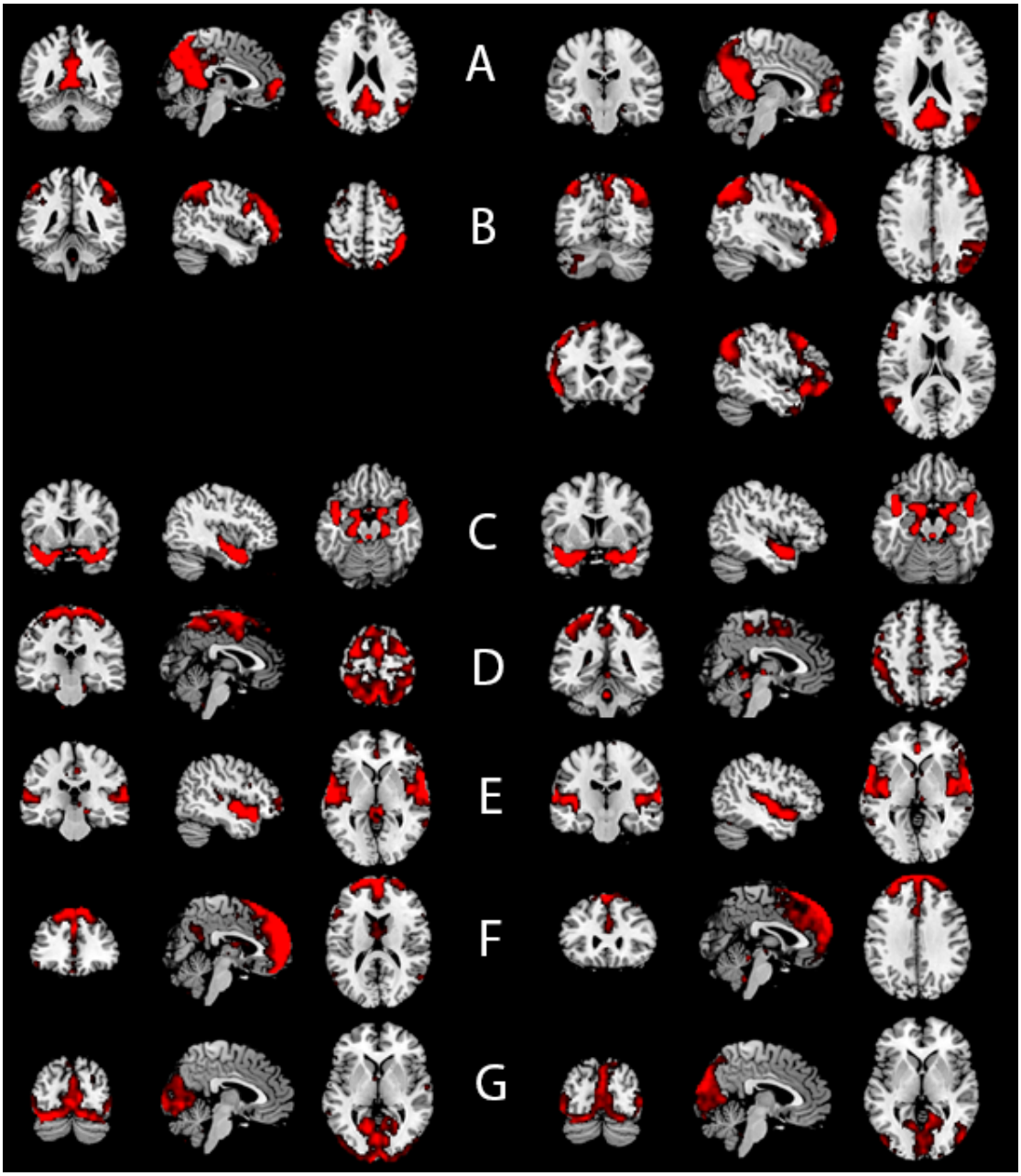

Independent components (ICs) correspond well between the before (left hand side) and after (right hand side) group. These ICs are the default mode network (DMN: A), the central executive network (CEN: B), the salience network (SN, C), the sensory/motor component (SMN, D), the auditory component (E), and the medial prefrontal cortex/anterior cingulate cortex component (MPFC/ACC: F), and the visual component (G).

The subsequent whole-sample group ICA resulted in identification of the same resting state networks that were found within the two groups, with

the exception that two separate salience components were extracted (Figure 3). Results from the ensuing spectral group comparison revealed a significant difference in ACC/MPFC (part of the DMN) connectivity with higher rs-FC in the after group (Figure 3, Table 2).

Figure 3. Static resting state connectivity differences between groups.

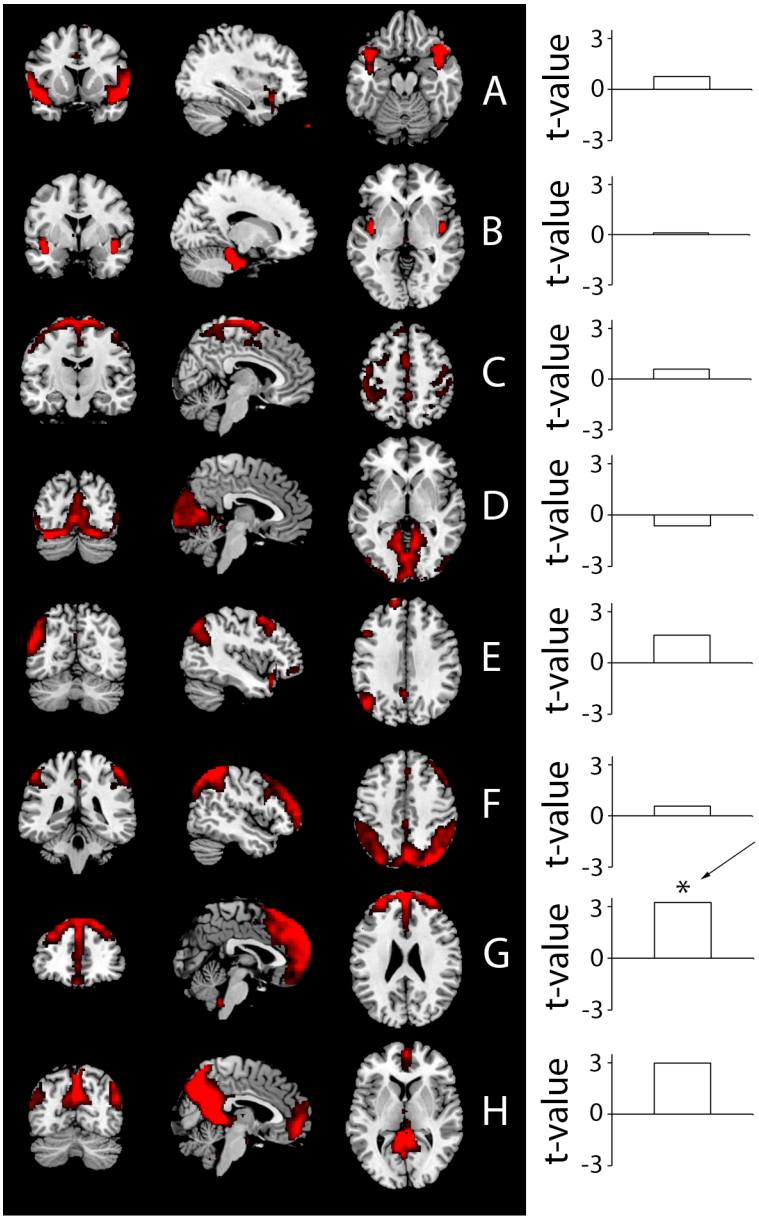

Whole sample ICs (left hand side) are auditory (A), salience (B, B'), SMN (C), visual (D), left CEN (E), right CEN (F), MPFC/ACC (G) and DMN (H) component. Bar graphs show t-values from spectral group comparison (after *versus* before). The after group shows stronger connectivity in the MPFC/ACC and the DMN component.

Table 2. Spectral group comparison statistics.

Component		p	
	t	FDR-corrected	uncorrected
Auditory	0.76	1	0.455
Salience 1	0.11	1	0.912
Salience 2	0.96	1	0.343
Sensory/motor	0.59	1	0.557
Visual	-0.64	1	0.528
CEN left	1.62	1	0.116
CEN right	0.57	1	0.570
MPFC/ACC	3.23	0.027[a]	0.003
DMN	2.98	0.053	0.006

T-values resulting from between groups comparison and FDR-corrected p-values.

[a]Significant difference, p-FDR <0.05

Dynamic rs-FC

The dyn-FC analysis revealed group differences among several pairs of networks: We found the most accentuated difference between ACC/MPFC - left CEN, with increased connectivity in the after group (relative to the before group). Additionally, connectivity was increased between the left CEN - DMN, auditory network - SMN, auditory - visual network, and auditory network - right CEN. Dyn-FC was decreased between the SMN - left CEN and SMN - DMN in the after group (**Figure 4**). Results for clusters 1 (8.7 percent of total dwell time) and 2 (15.6 percent of total dwell time) are shown in Supplementary Figure 1.

Figure 4. Differences between groups in dynamic functional network connectivity.

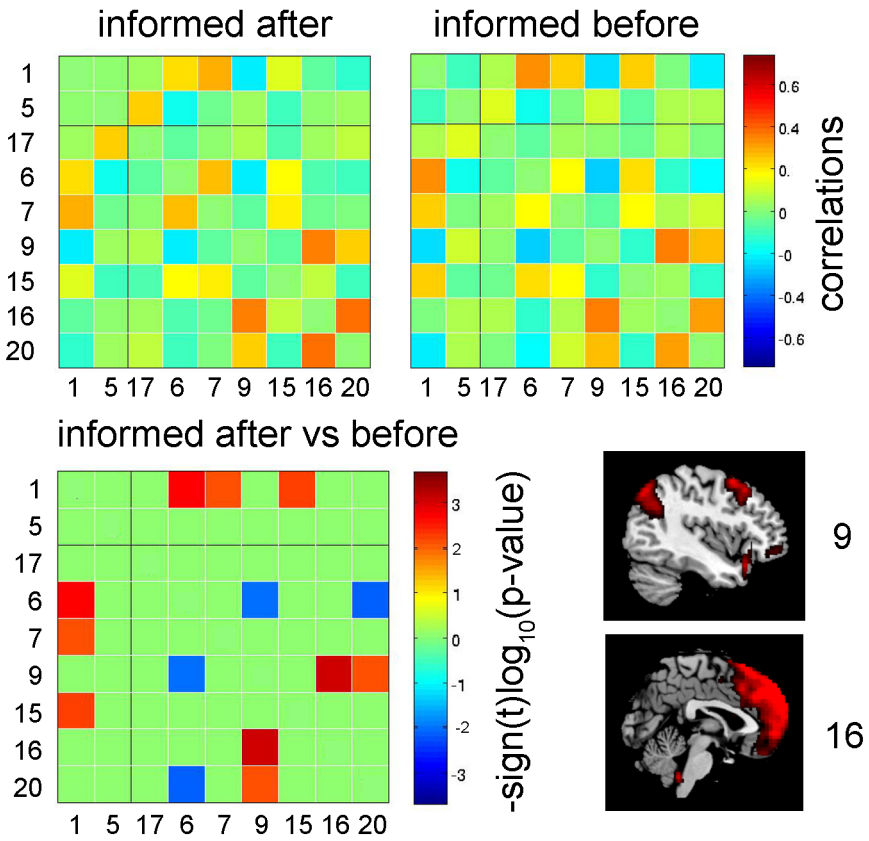

1 = auditory, 5 and 17 = salience, 6 = sensory-motor, 7 = visual, 9 and 15 = left and right CEN, 16 = ACC/MPFC, 20 = DMN. The first row shows correlations between components within groups for the dominant cluster. The second row shows significance of differences in these correlations between groups. The strongest difference was found for connectivity between left CEN and ACC/MPFC.

Discussion

The main question of this study was how resting-state functional connectivity changes in healthy elderly volunteers as a consequence of manipulating participant information before scanning. We hypothesized that regions involved in motor inhibition, self-control and cognitive processes associated with cognition during rest (for example, mind wandering), such as MPFC, ACC, DLPFC and IFG, would be affected by our manipulation. We

further hypothesized that functional connectivity within DMN would be affected because MPFC and ACC constitute part of DMN.

Static connectivity

We found no difference for DMN connectivity between the before and after group. However, group ICA revealed an ACC/MPFC component (as part of the DMN) that significantly differed between groups. This component was found to show differential connectivity between groups to a CEN component within the dominant cluster of our dynamic FC analysis. Moreover, the whole-brain connectivity analysis revealed significant differences in connectivity between left BA 9 and 44 and BA 44 and 45, which are parts of DLPFC (Levesque et al., 2003; Lissek, Glaubitz, Uengoer, & Tegenthoff, 2013) and IFG (Doeller et al., 2003; Zhuang, Tyler, Randall, Stamatakis, & Marslen-Wilson, 2014). Importantly, additional results indicate that none of these differences can be attributed to differences in working memory, executive function, interactions between either of these and group.

Informing participants about the true study purpose reveals that adherence to instructions is crucial to the study. Therefore, although actual adherence was expected to be similar in both groups, we hypothesized increased effort to adhere to instructions in the before group. ACC/MPFC network connectivity differed significantly between groups in our group ICA. The areas constituting this network have been shown to be involved in behavioural inhibition (Fu et al., 2008). Furthermore, the whole-brain analysis revealed greater connectivity in the before group for BA 8, 9, 44 and 45, contributing to MPFC, DLPFC or IFG, which are involved in behavioural inhibition and self-monitoring (Hollmann et al., 2012; Ochsner et al., 2004). Hence, these group differences may reflect increased motor inhibition in the participants of the before group. This difference in static rs-FC is not attributable to pre-existing differences in cognitive function because there was no significant between-group difference in neuropsychological test performance (Table 1).

We found no between-group difference in either of our salience network ICs, which is explained by the fact that ACC activity was captured separately in an ACC/MPFC IC.

Both right BA 29 (retrosplenial cortex) and right BA 34 (dorsal entorhinal) showed stronger rs-FC to BA 17 (primary visual cortex) in the before group. Taking into account that participants had kept their eyes closed during scanning, this finding may be attributable to between-group differences in visual mind wandering processes during rsfMRI. In addition, in the ICA analysis we found stronger (although not significant) rs-FC in the before group within the visual IC, underlying the dominance of more mental visual processing operations in this group. The retrosplenial cortex is part of a network known to be involved in remembering the past and imagining the future (Schacter, Addis, & Buckner, 2007). Considering previous findings of primary visual cortex being relevant for allocentric representation of the environment (Miller, Vedder, Law, & Smith, 2014) and of dorsal entorhinal cortex regions being associated with spatial information processing (Gaskin & White, 2010), our finding suggests that the before group may have spent more time remembering or imagining navigating through an environment.

Increased functional connectivity in the before group between left BA 11 and right BA 45, which is involved in behavioural inhibition, may be explained by increased self-control in these individuals. However, it is unclear why connectivity is increased between contralateral and not ipsilateral regions. Therefore, this finding may represent a false positive.

The rs-FC of the DMN did not differ between groups, neither for the regional connectivity analysis nor for the group ICA analysis. Together with reported findings of DMN connectivity not differing between an eyes-closed, an eyes-open, and a fixation condition (R. Patriat, E. K. Molloy, et al., 2013) or simply an eyes-closed and an eyes-open condition (Greicius, Krasnow, Reiss, & Menon, 2003), this suggests that the DMN is relatively stable with regard to procedural aspects of resting-state studies. However, other studies comparing eyes-closed, eyes-open, and fixation did find differences in DMN connectivity (K. R. Van Dijk et al., 2010; Yan et al., 2009). Additionally, considering that the p-value in our study was only slightly above the statistical threshold, our failure to find this difference may be attributable to small sample size. These inconsistent results create a need for further research concerning the impact of participant instruction and participant information on DMN connectivity (see Limitations).

Dynamic connectivity

Research on dynamic changes in functional connectivity has demonstrated notable fluctuations of between-networks connectivity over time (C. Chang & Glover, 2010). Considering the fact that cognitive processes are unconstrained in the resting-state paradigm, this finding is plausible and suggests that investigations using this paradigm should consider such fluctuations. Our results from the dyn-FC analysis extend the findings from the static rs-FC (group ICA) analysis, demonstrating that there are considerable between-group differences in connectivity within the dominant (MPFC/ACC) cluster, suggesting that participant information prior to scanning influences connectivity during scanning between resting-state networks. The most significant difference in connectivity occurred between a frontal part of the DMN (ACC/MPFC) and left CEN. The functional relevance of connectivity between these networks has been demonstrated in a recent study using transcranial magnetic stimulation and rsfMRI, which found a causal relationship between CEN and medial prefrontal activity, thereby demonstrating an (inhibitory) influence of the CEN on DMN activity, which was exerted via its medial prefrontal aspect (A. C. Chen et al., 2013). Given the importance of these networks for cognition and the array of disorders DMN connectivity is associated with, our finding that connectivity between these networks is affected by participant information prior to scanning suggests that this study feature deserves considerable attention when planning and interpreting studies of rs-FC.

Differences between groups in dyn-FC occurred in six additional pairs of networks. Our finding of increased connectivity between left CEN and DMN in the after group parallels the finding of increased connectivity between left CEN and ACC/MPFC. Increased connectivity was also present between the auditory network and SMN as well as between the auditory and visual network. Functional connectivity between these regions facilitates the integration of sensory and cognitive processes. The interaction of components of the auditory network and the right CEN, which also showed increased rs-FC in the after *versus* before group, is necessary during multisensory attention (T. Chen et al., 2014). Finally, the after group displayed decreased

rs-FC between the SMN and both left CEN and DMN. Thus, participant information potentially influences results from research on a wide range of topics and deserves careful consideration when comparing and interpreting findings form different studies.

Limitations

Functional connectivity shows age dependent changes (Balsters et al., 2013; Fair et al., 2008). Given that we examined two groups of healthy elderly volunteers, caution needs to be exercised when generalising our findings for both static and dynamic functional connectivity to populations of younger participants. Another limitation is that we studied only one resting state condition (i.e., eyes-closed), which makes it difficult to judge about the generalizability of the observed connectivity differences across various resting states. Finally, we provided only true and meaningful information on the task purpose, mainly to ensure that participants' stayed focused in the scanner. It is debatable, but difficult to examine in a systematic way, if only this type of information lead to the observed functional connectivity pattern or whether the information could be also invalid or non-context dependent.

Conclusions

Future rsfMRI investigations should take into account the influence of the type of information given to the participant on subsequent task-unrelated functional connectivity. Our results show that connectivity between areas associated with inhibition and control is higher in subjects informed before than in subjects informed after scanning. These findings suggest that participants of rsfMRI studies will show increased effort to comply with pre-scanning instructions if they are informed about the study purpose before scanning. Therefore, participant information prior to scanning significantly influences rsfMRI results and should be taken into consideration both when designing and comparing studies on resting-state connectivity. This applies to

connectivity both within and between networks and measures of both static and dynamic connectivity.

Acknowledgements

We are grateful to Elena Allen, PhD and Angela Martina Müller, PhD for their helpful methodological advice. Furthermore, we hereby express our gratitude towards all individuals who chose to participate in our study.

Figure S1. Results for clusters with second- and third-most dwell time.

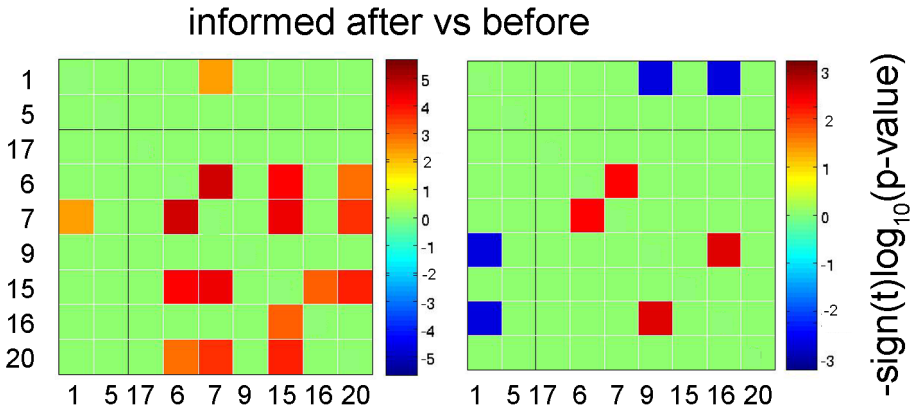

Results for clusters 1 (8.7 percent of total dwell time; left-hand side) and 2 (15.6 percent of total dwell time; right-hand side). 1 = auditory, 5 and 17 = salience, 6 = sensory-motor, 7 = visual, 9 and 15 = left and right CEN, 16 = ACC/MPFC, 20 = DMN.

Table S2. Brodmann area ROIs involved in between group connectivity differences.

Brodmann area	Structure	ROI center x y z
8	Left dorsal frontal cortex	-23 30 44
9	Left dorsolateral prefrontal cortex	-27 35 29
10	Left anterior prefrontal cortex	-22 56 7
11	Left orbitofrontal cortex	-15 43 -18
17	Left primary visual cortex	13 -88 2
17	Right primary visual cortex	13 -88 2
20	Left inferior temporal gyrus	-48 -20 -25
23	Left ventral posterior cingulate cortex	-4 -38 23
25	Subgenual cortex	-5 14 -12
29	Left retrosplenial cingulate cortex	-6 -46 11
29	Right retrosplenial cingulate cortex	7 -45 12
44	Left inferior frontal cortex, pars opercularis	-51 10 12
45	Left inferior frontal cortex, pars triangularis	-50 23 10
45	Right inferior frontal cortex, pars triangularis	52 23 10

ROIs showing differences in connectivity with at least one other BA ROI between groups.

5 Discussion

One goal of the present work was to examine hippocampal, thalamic, and striatal shape and surface area as well as cortical thickness as potential biomarkers in preclinical AD and MCI. Whereas surface area did not correlate with amyloid burden, hippocampal and thalamic shape as well as entorhinal cortical thickness were related to measures of Aβ load in cognitively normal elderly individuals. Moreover, individuals with MCI who later converted to AD differed from healthy controls with respect to striatal and thalamic shape and left hemispheric cortical thinning as well as hippocampal total and subfield atrophy. In an ROC analysis, hippocampal shape improved upon volume-based classification of individuals from these two groups. The implications of these findings will be discussed in the first part of this section.

Because rsfMRI may provide preclinical AD biomarkers that change prior to Aβ deposition (Jack et al., 2013) and RSN connectivity and reliability have been shown to change as a result of variations in participant instruction (R. Patriat, Molloy EK, et al., 2013; K. Van Dijk et al., 2010; Yan et al., 2009), another goal of the present work was to investigate the influence of participant information on functional connectivity within and between RSNs in healthy elderly subjects. We found significant differences in connectivity within a component including the mPFC, which is part of the DMN (Michael D Fox et al., 2005), and between this component and the left CEN. The implications of these findings will be discussed in the second part of this section.

The results presented in this work are subject to several limitations and give rise to a number of possible directions to take in future research projects. Limitations and directions of future research are discussed in the third part of this section, followed by a general conclusion.

5.1 Implications: localized structural MRI measures in MCI and preclinical AD

According to a recent changepoint model of morphometric changes in preclinical AD, entorhinal cortical atrophy may accelerate up to 10 years before clinical symptom onset (Younes et al., 2014). In our research, cortical

thickness did not significantly differ between individuals with stable MCI and a healthy control group, but there were significant parahippocampal cortical thickness differences between MCI converters at baseline and healthy controls. This is consistent with our finding of bilateral associations of entorhinal cortical thickness with cortical SUVR in cognitively healthy elderly subjects. Our findings are in agreement with previous with previous reports on AD related cortical thinning in asymptomatic individuals (Dickerson et al., 2008; Dickerson et al., 2011) and the progression of tau-related neuropathology (H. Braak & Braak, 1991b; Mitchell et al., 2002). The results of the present work have repeatedly indicated early involvement of cortical thickness in the parahippocampal region in AD progression, considerably strengthening the evidence for cortical thickness as a preclinical biomarker in AD research.

In our investigation of individuals with MCI, no hippocampal volume reductions compared to healthy controls were present in individuals with stable MCI. In contrast and according to our expectations, converters already differed at baseline from their healthy control group in bilateral hippocampal volumes. Previous research including individuals with MCI has repeatedly indicated predominant involvement of the CA1 (Apostolova, Dinov, et al., 2006; Apostolova, Dutton, et al., 2006; La Joie et al., 2013; Pluta et al., 2012; Yushkevich, Pluta, et al., 2015) and subiculum (Apostolova, Dutton, et al., 2006; Frankó et al., 2013). These findings are corroborated by our results in cognitively healthy elderly individuals. An association between hippocampal shape and CSF Aβ in healthy elderly individuals has been reported in one previous study (Carmichael et al., 2012). We have shown that left hippocampal shape in areas corresponding with its CA1 and subiculum subfields was associated with amyloid burden in this region, which is in line with previous findings in MCI patients (de Flores et al., 2015) a previous study on progression of non-demented elderly individuals to dementia due to AD (Csernansky et al., 2005). One possible explanation for our result is provided by a study using transgenic mice, where amyloid deposits added to the terminal zone of perforant pathway axons of neurons containing pathological tau increased axon dystrophy in these neurons and strongly altered their connectivity (Pooler et al., 2013). Additionally, in a recent study hippocampal

amyloid burden in cognitively normal elderly subjects was associated with fluid attenuated inversion recovery intensities, indicating tissue edema (Schreiner et al., 2014). Hence, our results represent an important finding in support of hippocampal shape as an MRI biomarker in preclinical AD.

As an important part of the Papez circuit, the anterior thalamus plays an important role in memory (Jankowski et al., 2013; Zarei et al., 2010). Yet, the thalamus has received little attention in preclinical AD research (Aggleton et al., 2016) despite the fact that its anterior nuclei contain a large number of NFT in AD (H. Braak & Braak, 1991a). In the present work, we found thalamic shape differences between elderly individuals with MCI who later converted to AD dementia and a healthy control group. For these two groups, thalamic shape reached excellent classification performance in our ROC analysis. In healthy elderly individuals, we found significant associations between left anterior thalamic shape and cortical SUVR, extending previously reported between-group differences in left anterior thalamic shape comparing aMCI subjects to a healthy control group (Hahn et al., 2016). Hence, our findings may indicate that thalamic shape is a useful measure for prediction of AD at the preclinical stage.

Our results on striatal shape in MCI add to previously published findings indicating striatal shape changes in individuals with MCI (Tang et al., 2014) and dementia due to AD (Cho et al., 2014; de Jong et al., 2011). Striatal shape also achieved excellent classification performance between MCI converters and healthy control subjects in our ROC analysis. Yet, we found no associations between striatal shape and striatal or cortical amyloid burden in healthy elderly individuals. In addition, results from simultaneous investigations of multiple structures suggest comparatively late striatal involvement in AD progression (Jee Hoon Roh et al., 2011; Tang et al., 2014), in line with AD neuropathological stageing (H. Braak & Braak, 1991b). Thus, striatal shape may be of limited value as a preclinical AD biomarker.

5.2 Implications: the stability of rsfMRI and its future in preclinical AD research

Although rsfMRI provides promising measures in preclinical AD (Chhatwal et al., 2013; Greicius et al., 2004; Thomas et al., 2014) biomarker research possibly preceding Aβ biomarkers (Jagust & Mormino, 2011), it is not yet incorporated in AD biomarker change models (Counts et al., 2017; Jack et al., 2013) or in the proposed framework for stageing of the preclinical phase of AD by the NIA-AA working group (Sperling, Aisen, et al., 2011). To date, only few studies have investigated rsfMRI in preclinical AD, and reliability and reproducibility are affected by pooling of data acquired by different scanners (Teipel et al., 2017), and variation in participant instruction (R Patriat et al., 2013; Yan et al., 2009). In the present work, we found that variation in participant information also affects rsfMRI measurement, providing an important extension of these previous findings. The MPFC is a part of the DMN and we found that connectivity within ACC/MPFC as well as connectivity between ACC/PFC and left CEN significantly differed between groups. Our analyses also revealed greater connectivity in individuals informed before scanning between areas involved in behavioural inhibition and self-monitoring, suggesting that participants in this group showed increased effort to comply with pre-scanning instructions. Hence, our findings imply that participant information prior to scanning significantly influences rsfMRI results and should be taken into consideration both when designing and comparing studies on resting-state connectivity. They also suggest that different centers conducting preclinical AD biomarker research using rsfMRI should find a consensus regarding study design in order to ensure reliability and reproducibility of their results, which is an important prerequisite for establishing this method in the broader field of AD biomarker research and for conclusive evidence on the exact stage of AD progression at which DMN functional connectivity becomes abnormal.

5.3 Limitations and directions of future research

In the second and third study, sample sizes were small, which may explain why the DMN component, in contrast to the ACC/MPFC component,

did not significantly differ between groups in our spectral group comparison. The generalizability of our findings in the third study is also limited, since we investigated only one instruction condition (i.e., eyes-closed). Hence, future studies on the influence of participant information on rsfMRI measures should incorporate the "eyes-open" and "eyes fixated on a cross" conditions.

One limitation of the first two studies is their cross-sectional nature. Longitudinal design and the analysis of change parameters would have increased the validity of our findings on early AD biomarkers. In addition, future studies should investigate which morphological feature best predicts conversion from no cognitive impairment to amnestic MCI in cognitively unimpaired individuals, using a classifier method such as the ROC analysis employed in the second study of the present work. These studies are also limited by the resolution of the acquired PET and MRI data: An increase in PET spatial resolution allowing for reliable SUVR readout of separate hippocampal subregions would enable a more intricate assessment of associations between features of hippocampal subfield morphology and regional amyloid burden, and an increase in MRI spatial resolution would further enhance the quality of automated segmentation using the MAGeT Brain algorithm. Future research should also incorporate entorhinal shape as a potential early AD biomarker.

Additionally, a promising avenue of future research is the combination of measures from functional and structural MRI to evaluate whether prediction performance is enhanced by a joint measure of functional and structural change.

5.4 Conclusions

The findings of the present work suggest that localized changes in entorhinal, hippocampal, and thalamic morphology may be valuable predictors of cognitive decline and eventually progression to AD dementia in cognitively unimpaired elderly individuals. Striatal shape was not associated with measures of amyloid burden in this group, but achieved excellent classification performance in our ROC analysis including individuals with MCI, indicating that this measure may be a valuable prediction feature for

progression at the MCI stage. Our findings also extended on previously reported pitfalls of rsfMRI research, informing future investigations on potential rsfMRI biomarkers in preclinical AD.

In conclusion, our work makes a notable contribution to early AD biomarker research.

6 References

Ad-Dab'bagh, Y., Lyttelton, O., Muehlboeck, J., Lepage, C., Einarson, D., Mok, K., . . . Fombonne, E. (2006). *The CIVET image-processing environment: a fully automated comprehensive pipeline for anatomical neuroimaging research.* Paper presented at the Proceedings of the 12th annual meeting of the organization for human brain mapping.

Aggleton, J. P., Desimone, R., & Mishkin, M. (1986). The origin, course, and termination of the hippocampothalamic projections in the macaque. *J Comp Neurol, 243*(3), 409-421. doi:10.1002/cne.902430310

Aggleton, J. P., Pralus, A., Nelson, A. J., & Hornberger, M. (2016). Thalamic pathology and memory loss in early Alzheimer's disease: moving the focus from the medial temporal lobe to Papez circuit. *Brain, 139*(Pt 7), 1877-1890. doi:10.1093/brain/aww083

Albert, M. S., DeKosky, S. T., Dickson, D., Dubois, B., Feldman, H. H., Fox, N. C., . . . Phelps, C. H. (2011). The diagnosis of mild cognitive impairment due to Alzheimer's disease: recommendations from the National Institute on Aging-Alzheimer's Association workgroups on diagnostic guidelines for Alzheimer's disease. *Alzheimers Dement, 7*(3), 270-279. doi:10.1016/j.jalz.2011.03.008

Alexander, G. E., DeLong, M. R., & Strick, P. L. (1986). Parallel organization of functionally segregated circuits linking basal ganglia and cortex. *Annu Rev Neurosci, 9*, 357-381. doi:10.1146/annurev.ne.09.030186.002041

Aljabar, P., Heckemann, R. A., Hammers, A., Hajnal, J. V., & Rueckert, D. (2009). Multi-atlas based segmentation of brain images: atlas selection and its effect on accuracy. *NeuroImage, 46*(3), 726-738. doi:10.1016/j.neuroimage.2009.02.018

Allen, E. A., Damaraju, E., Plis, S. M., Erhardt, E. B., Eichele, T., & Calhoun, V. D. (2014). Tracking whole-brain connectivity dynamics in the resting state. *Cereb Cortex, 24*(3), 663-676. doi:10.1093/cercor/bhs352

Alzheimer's Association. (2017). 2017 Alzheimer's disease facts and figures. *Alzheimer's & dementia, 13*(4), 325-373.

Amaral, R., Park, M. T. M., Devenyi, G. A., Lynn, V., Pipitone, J., Winterburn, J., . . . Voineskos, A. N. (2016). Manual segmentation of the fornix, fimbria, and alveus on high-resolution 3T MRI: Application via fully-automated mapping of the human memory circuit white and grey matter in healthy and pathological aging. *NeuroImage*.

Amaral, R., Park, M. T. M., Devenyi, G. A., Lynn, V., Pipitone, J., Winterburn, J., . . . Chakravarty, M. M. (2016). Manual segmentation of the fornix, fimbria, and alveus on high-resolution 3T MRI: Application via fully-automated mapping of the human memory circuit white and grey matter in healthy and pathological aging. *NeuroImage*. doi:https://doi.org/10.1016/j.neuroimage.2016.10.027

Amunts, K., Kedo, O., Kindler, M., Pieperhoff, P., Mohlberg, H., Shah, N. J., . . . Zilles, K. (2005). Cytoarchitectonic mapping of the human amygdala, hippocampal region and entorhinal cortex: intersubject variability and probability maps. *Anat Embryol (Berl), 210*(5-6), 343-352. doi:10.1007/s00429-005-0025-5

Antharam, V., Collingwood, J. F., Bullivant, J. P., Davidson, M. R., Chandra, S., Mikhaylova, A., . . . Dobson, J. (2012). High field magnetic resonance microscopy of the human hippocampus in Alzheimer's disease: quantitative imaging and correlation with iron. *NeuroImage, 59*(2), 1249-1260. doi:10.1016/j.neuroimage.2011.08.019

Apostolova, L. G., Dinov, I. D., Dutton, R. A., Hayashi, K. M., Toga, A. W., Cummings, J. L., & Thompson, P. M. (2006). 3D comparison of hippocampal atrophy in amnestic mild cognitive impairment and Alzheimer's disease. *Brain, 129*(Pt 11), 2867-2873. doi:10.1093/brain/awl274

Apostolova, L. G., Dutton, R. A., Dinov, I. D., Hayashi, K. M., Toga, A. W., Cummings, J. L., & Thompson, P. M. (2006). Conversion of mild cognitive impairment to Alzheimer disease predicted by hippocampal atrophy maps. *Arch Neurol, 63*(5), 693-699. doi:10.1001/archneur.63.5.693

Apostolova, L. G., Mosconi, L., Thompson, P. M., Green, A. E., Hwang, K. S., Ramirez, A., . . . de Leon, M. J. (2010). Subregional hippocampal atrophy predicts Alzheimer's dementia in the cognitively normal. *Neurobiol Aging, 31*(7), 1077-1088. doi:10.1016/j.neurobiolaging.2008.08.008

Arend, I., Henik, A., & Okon-Singer, H. (2015). Dissociating emotion and attention functions in the pulvinar nucleus of the thalamus. *Neuropsychology, 29*(2), 191-196. doi:10.1037/neu0000139

Army Individual Test Battery. Manual of Directions and Scoring. 1944. Washington, DC: War Department, Adjutant General's Office.

Atienza, M., Atalaia-Silva, K. C., Gonzalez-Escamilla, G., Gil-Neciga, E., Suarez-Gonzalez, A., & Cantero, J. L. (2011). Associative memory deficits in mild cognitive impairment: the role of hippocampal formation. *NeuroImage, 57*(4), 1331-1342. doi:10.1016/j.neuroimage.2011.05.047

Bakkour, A., Morris, J. C., & Dickerson, B. C. (2009). The cortical signature of prodromal AD: regional thinning predicts mild AD dementia. *Neurology, 72*(12), 1048-1055. doi:10.1212/01.wnl.0000340981.97664.2f

Balsters, J. H., O'Connell, R. G., Galli, A., Nolan, H., Greco, E., Kilcullen, S. M., . . . Robertson, I. H. (2013). Changes in resting connectivity with age: a simultaneous electroencephalogram and functional magnetic resonance imaging investigation. *Neurobiol Aging, 34*(9), 2194-2207. doi:10.1016/j.neurobiolaging.2013.03.004

Barber, A. D., Caffo, B. S., Pekar, J. J., & Mostofsky, S. H. (2013). Developmental changes in within- and between-network connectivity between late childhood and adulthood. *Neuropsychologia, 51*(1), 156-167. doi:10.1016/j.neuropsychologia.2012.11.011

Beach, T. G., Sue, L. I., Walker, D. G., Sabbagh, M. N., Serrano, G., Dugger, B. N., . . . Souders, L. (2012). Striatal amyloid plaque density predicts Braak neurofibrillary stage and clinicopathological Alzheimer's disease: implications for amyloid imaging. *J Alzheimers Dis, 28*(4), 869-876. doi:10.3233/JAD-2011-111340

Behrens, T., Johansen-Berg, H., Woolrich, M., Smith, S., Wheeler-Kingshott, C., Boulby, P., . . . Matthews, P. (2003). Non-invasive mapping of connections between human thalamus and cortex using diffusion imaging. *Nature Neuroscience, 6*, 750-757.

Behzadi, Y., Restom, K., Liau, J., & Liu, T. T. (2007). A component based noise correction method (CompCor) for BOLD and perfusion based fMRI. *Neuroimage, 37*(1), 90-101. doi:10.1016/j.neuroimage.2007.04.042

Bell, A. J., & Sejnowski, T. J. (1995). An information-maximization approach to blind separation and blind deconvolution. *Neural Comput, 7*(6), 1129-1159.

Besson, F. L., La Joie, R., Doeuvre, L., Gaubert, M., Mezenge, F., Egret, S., . . . Chetelat, G. (2015). Cognitive and Brain Profiles Associated with Current Neuroimaging Biomarkers of Preclinical Alzheimer's Disease. *J Neurosci, 35*(29), 10402-10411. doi:10.1523/JNEUROSCI.0150-15.2015

Birks, J. (2006). Cholinesterase inhibitors for Alzheimer's disease. *Cochrane Database Syst Rev*(1), CD005593. doi:10.1002/14651858.CD005593

Biswal, B., Yetkin, F. Z., Haughton, V. M., & Hyde, J. S. (1995). Functional connectivity in the motor cortex of resting human brain using echo-planar MRI. *Magn Reson Med, 34*(4), 537-541.

Bonelli, R. M., & Cummings, J. L. (2007). Frontal-subcortical circuitry and behavior. *Dialogues Clin Neurosci, 9*(2), 141-151.

Borghammer, P., Ostergaard, K., Cumming, P., Gjedde, A., Rodell, A., Hall, N., & Chakravarty, M. M. (2010). A deformation-based morphometry study of patients with early-stage Parkinson's disease. *Eur J Neurol, 17*(2), 314-320. doi:10.1111/j.1468-1331.2009.02807.x

Bossa, M., Zacur, E., & Olmos, S. (2011). Statistical analysis of relative pose information of subcortical nuclei: application on ADNI data. *NeuroImage, 55*(3), 999-1008.

Braak, E., & Braak, H. (1997). Alzheimer's disease: transiently developing dendritic changes in pyramidal cells of sector CA1 of the Ammon's horn. *Acta Neuropathol, 93*(4), 323-325.

Braak, H., Alafuzoff, I., Arzberger, T., Kretzschmar, H., & Del Tredici, K. (2006). Staging of Alzheimer disease-associated neurofibrillary pathology using paraffin sections and immunocytochemistry. *Acta Neuropathol, 112*(4), 389-404.

Braak, H., & Braak, E. (1990). Alzheimer's disease: striatal amyloid deposits and neurofibrillary changes. *J Neuropathol Exp Neurol, 49*(3), 215-224.

Braak, H., & Braak, E. (1991a). Alzheimer's disease affects limbic nuclei of the thalamus. *Acta Neuropathol, 81*(3), 261-268.

Braak, H., & Braak, E. (1991b). Neuropathological stageing of Alzheimer-related changes. *Acta Neuropathol, 82*(4), 239-259.

Braak, H., Zetterberg, H., Del Tredici, K., & Blennow, K. (2013). Intraneuronal tau aggregation precedes diffuse plaque deposition, but amyloid-beta changes occur before increases of tau in cerebrospinal fluid. *Acta Neuropathol, 126*(5), 631-641. doi:10.1007/s00401-013-1139-0

Buckner, R. L., Head, D., Parker, J., Fotenos, A. F., Marcus, D., Morris, J. C., & Snyder, A. Z. (2004). A unified approach for morphometric and functional data analysis in young, old, and demented adults using automated atlas-based head size normalization: reliability and validation against manual measurement of total intracranial volume. *NeuroImage, 23*(2), 724-738. doi:10.1016/j.neuroimage.2004.06.018

Carmichael, O., Xie, J., Fletcher, E., Singh, B., DeCarli, C., & Alzheimer's Disease Neuroimaging, I. (2012). Localized hippocampus measures are associated with Alzheimer pathology and cognition independent of total hippocampal volume. *Neurobiol Aging, 33*(6), 1124 e1131-1141. doi:10.1016/j.neurobiolaging.2011.08.016

Centeno, M., & Carmichael, D. W. (2014). Network Connectivity in Epilepsy: Resting State fMRI and EEG-fMRI Contributions. *Front Neurol, 5*, 93. doi:10.3389/fneur.2014.00093

Chai, X. J., Castanon, A. N., Ongur, D., & Whitfield-Gabrieli, S. (2012). Anticorrelations in resting state networks without global signal regression. *Neuroimage, 59*(2), 1420-1428. doi:10.1016/j.neuroimage.2011.08.048

Chai, X. J., Ofen, N., Gabrieli, J. D., & Whitfield-Gabrieli, S. (2014). Selective development of anticorrelated networks in the intrinsic functional organization of the human brain. *J Cogn Neurosci, 26*(3), 501-513. doi:10.1162/jocn_a_00517

Chakravarty, M. M., Bertrand, G., Hodge, C. P., Sadikot, A. F., & Collins, D. L. (2006). The creation of a brain atlas for image guided neurosurgery using serial histological data. *NeuroImage, 30*(2), 359-376. doi:10.1016/j.neuroimage.2005.09.041

Chakravarty, M. M., Rapoport, J. L., Giedd, J. N., Raznahan, A., Shaw, P., Collins, D. L., . . . Gogtay, N. (2015). Striatal shape abnormalities as novel neurodevelopmental endophenotypes in schizophrenia: a longitudinal study. *Hum Brain Mapp, 36*(4), 1458-1469.

Chakravarty, M. M., Sadikot, A. F., Germann, J., Hellier, P., Bertrand, G., & Collins, D. L. (2009). Comparison of piece-wise linear, linear, and nonlinear atlas-to-patient warping techniques: analysis of the labeling of subcortical nuclei for functional neurosurgical applications. *Hum Brain Mapp, 30*(11), 3574-3595. doi:10.1002/hbm.20780

Chakravarty, M. M., Steadman, P., van Eede, M. C., Calcott, R. D., Gu, V., Shaw, P., . . . Lerch, J. P. (2013). Performing label-fusion-based segmentation using multiple automatically generated templates. *Hum Brain Mapp, 34*(10), 2635-2654. doi:10.1002/hbm.22092

Chang, C., & Glover, G. H. (2010). Time-frequency dynamics of resting-state brain connectivity measured with fMRI. *NeuroImage, 50*(1), 81-98. doi:10.1016/j.neuroimage.2009.12.011

Chang, Y. T., Huang, C. W., Chang, Y. H., Chen, N. C., Lin, K. J., Yan, T. C., . . . Chang, C. C. (2015). Amyloid burden in the hippocampus and default mode network: relationships with gray matter volume and cognitive performance in mild stage Alzheimer disease. *Medicine (Baltimore), 94*(16), e763. doi:10.1097/MD.0000000000000763

Chen, A. C., Oathes, D. J., Chang, C., Bradley, T., Zhou, Z. W., Williams, L. M., . . . Etkin, A. (2013). Causal interactions between fronto-parietal central executive and default-mode networks in humans. *Proceedings of the National Academy of Sciences of the United States of America, 110*(49), 19944-19949. doi:DOI 10.1073/pnas.1311772110

Chen, T., Michels, L., Supekar, K., Kochalka, J., Ryali, S., & Menon, V. (2014). Role of the anterior insular cortex in integrative causal signaling during multisensory auditory-visual attention. *Eur J Neurosci*. doi:10.1111/ejn.12764

Chételat, G., Fouquet, M., Kalpouzos, G., Denghien, I., De La Sayette, V., Viader, F., . . . Eustache, F. (2008). Three-dimensional surface mapping of hippocampal atrophy progression from MCI to AD and over normal aging as assessed using voxel-based morphometry. *Neuropsychologia, 46*(6), 1721-1731.

Chételat, G., Landeau, B., Eustache, F., Mézenge, F., Viader, F., de la Sayette, V., . . . Baron, J. C. (2005). Using voxel-based morphometry to map the structural changes associated with rapid conversion in MCI: A longitudinal MRI study. *NeuroImage, 27*(4), 934-946. doi:https://doi.org/10.1016/j.neuroimage.2005.05.015

Chhatwal, J. P., Schultz, A. P., Johnson, K., Benzinger, T. L., Jack, C., Ances, B. M., . . . Koeppe, R. A. (2013). Impaired default network functional connectivity in autosomal dominant Alzheimer disease. *Neurology, 81*(8), 736-744.

Cho, H., Kim, J. H., Kim, C., Ye, B. S., Kim, H. J., Yoon, C. W., . . . Seo, S. W. (2014). Shape changes of the basal ganglia and thalamus in Alzheimer's disease: a three-year longitudinal study. *J Alzheimers Dis, 40*(2), 285-295. doi:10.3233/JAD-132072

Christoff, K., Gordon, A. M., Smallwood, J., Smith, R., & Schooler, J. W. (2009). Experience sampling during fMRI reveals default network and executive system contributions to mind wandering. *Proc Natl Acad Sci U S A, 106*(21), 8719-8724. doi:10.1073/pnas.0900234106

Chung, M. K., & Taylor, J. (2004). *Diffusion smoothing on brain surface via finite element method.* Paper presented at the Biomedical imaging: nano to macro, 2004. IEEE International Symposium on.

Collins, D. L., Neelin, P., Peters, T. M., & Evans, A. C. (1994). Automatic 3D intersubject registration of MR volumetric data in standardized Talairach space. *J Comput Assist Tomogr, 18*(2), 192-205.

Collins, D. L., & Pruessner, J. C. (2010). Towards accurate, automatic segmentation of the hippocampus and amygdala from MRI by augmenting ANIMAL with a template library and label fusion. *NeuroImage, 52*(4), 1355-1366. doi:10.1016/j.neuroimage.2010.04.193

Counts, S. E., Ikonomovic, M. D., Mercado, N., Vega, I. E., & Mufson, E. J. (2017). Biomarkers for the Early Detection and Progression of Alzheimer's Disease. *Neurotherapeutics, 14*(1), 35-53. doi:10.1007/s13311-016-0481-z

Csernansky, J. G., Wang, L., Swank, J., Miller, J. P., Gado, M., McKeel, D., . . . Morris, J. C. (2005). Preclinical detection of Alzheimer's disease: hippocampal shape and volume predict dementia onset in the elderly. *NeuroImage, 25*(3), 783-792. doi:10.1016/j.neuroimage.2004.12.036

Cummings, J. L. (1995). Anatomic and behavioral aspects of frontal-subcortical circuits. *Ann N Y Acad Sci, 769*, 1-13.

Damoiseaux, J. S., Rombouts, S. A., Barkhof, F., Scheltens, P., Stam, C. J., Smith, S. M., & Beckmann, C. F. (2006). Consistent resting-state networks across healthy subjects. *Proc Natl Acad Sci U S A, 103*(37), 13848-13853.

de Bourbon-Teles, J., Bentley, P., Koshino, S., Shah, K., Dutta, A., Malhotra, P., . . . Soto, D. (2014). Thalamic control of human attention driven by memory and learning. *Curr Biol, 24*(9), 993-999. doi:10.1016/j.cub.2014.03.024

de Flores, R., La Joie, R., & Chetelat, G. (2015). Structural imaging of hippocampal subfields in healthy aging and Alzheimer's disease. *Neuroscience, 309*, 29-50. doi:10.1016/j.neuroscience.2015.08.033

de Jong, L. W., Ferrarini, L., van der Grond, J., Milles, J. R., Reiber, J. H., Westendorp, R. G., . . . van Buchem, M. A. (2011). Shape abnormalities of the striatum in Alzheimer's disease. *J Alzheimers Dis, 23*(1), 49-59. doi:10.3233/JAD-2010-101026

de Oliveira, M. S., Balthazar, M. L., D'Abreu, A., Yasuda, C. L., Damasceno, B. P., Cendes, F., & Castellano, G. (2011). MR imaging texture analysis of the corpus callosum and thalamus in amnestic mild cognitive impairment and mild Alzheimer disease. *AJNR Am J Neuroradiol, 32*(1), 60-66. doi:10.3174/ajnr.A2232

Delis, D., & Kaplan, E. (2001). Delis-Kaplan executive function battery. *San Antonio, TX: Psychological Corporation*.

Dennis, E. L., & Thompson, P. M. (2014). Functional brain connectivity using fMRI in aging and Alzheimer's disease. *Neuropsychol Rev, 24*(1), 49-62. doi:10.1007/s11065-014-9249-6

Devanand, D. P., Pradhaban, G., Liu, X., Khandji, A., De Santi, S., Segal, S., . . . de Leon, M. J. (2007). Hippocampal and entorhinal atrophy in mild cognitive impairment: prediction of Alzheimer disease. *Neurology, 68*(11), 828-836. doi:10.1212/01.wnl.0000256697.20968.d7

Dickerson, B. C., Bakkour, A., Salat, D. H., Feczko, E., Pacheco, J., Greve, D. N., . . . Rosas, H. D. (2008). The cortical signature of Alzheimer's disease: regionally specific cortical thinning relates to symptom severity in very mild to mild AD dementia and is detectable in asymptomatic amyloid-positive individuals. *Cerebral cortex, 19*(3), 497-510.

Dickerson, B. C., Stoub, T. R., Shah, R. C., Sperling, R. A., Killiany, R. J., Albert, M. S., . . . Detoledo-Morrell, L. (2011). Alzheimer-signature MRI biomarker predicts AD dementia in cognitively normal adults. *Neurology, 76*(16), 1395-1402. doi:10.1212/WNL.0b013e3182166e96

Doeller, C. F., Opitz, B., Mecklinger, A., Krick, C., Reith, W., & Schroger, E. (2003). Prefrontal cortex involvement in preattentive auditory deviance detection: neuroimaging and electrophysiological evidence. *NeuroImage, 20*(2), 1270-1282. doi:10.1016/S1053-8119(03)00389-6

Dorr, A., Lerch, J. P., Spring, S., Kabani, N., & Henkelman, R. M. (2008). High resolution three-dimensional brain atlas using an average magnetic resonance image of 40 adult C57Bl/6J mice. *NeuroImage, 42*(1), 60-69.

Drago, V., Babiloni, C., Bartrés-Faz, D., Caroli, A., Bosch, B., Hensch, T., . . . Jovicich, J. (2011). Disease tracking markers for Alzheimer's disease at the prodromal (MCI) stage. *Journal of Alzheimer's Disease, 26*(s3), 159-199.

Drevets, W. C., Price, J. L., & Furey, M. L. (2008). Brain structural and functional abnormalities in mood disorders: implications for neurocircuitry models of depression. *Brain Struct Funct, 213*(1-2), 93-118. doi:10.1007/s00429-008-0189-x

Drzezga, A., Grimmer, T., Riemenschneider, M., Lautenschlager, N., Siebner, H., Alexopoulus, P., . . . Kurz, A. (2005). Prediction of individual clinical outcome in MCI by means of genetic assessment and (18)F-FDG PET. *J Nucl Med, 46*(10), 1625-1632.

Dubois, B., Feldman, H. H., Jacova, C., DeKosky, S. T., Barberger-Gateau, P., Cummings, J., . . . Jicha, G. (2007). Research criteria for the diagnosis of Alzheimer's disease: revising the NINCDS–ADRDA criteria. *The Lancet Neurology, 6*(8), 734-746.

Fagan, A. M., Roe, C. M., Xiong, C., Mintun, M. A., Morris, J. C., & Holtzman, D. M. (2007). Cerebrospinal fluid tau/β-amyloid42 ratio as a prediction of cognitive decline in nondemented older adults. *Archives of Neurology, 64*(3), 343-349.

Fair, D. A., Cohen, A. L., Dosenbach, N. U., Church, J. A., Miezin, F. M., Barch, D. M., . . . Schlaggar, B. L. (2008). The maturing architecture of the brain's default network. *Proc Natl Acad Sci U S A, 105*(10), 4028-4032. doi:10.1073/pnas.0800376105

Ferrarini, L., van Lew, B., Reiber, J. H., Gandin, C., Galluzzo, L., Scafato, E., . . . Group, I. W. (2014). Hippocampal atrophy in people with memory deficits: results from the population-based IPREA study. *Int Psychogeriatr, 26*(7), 1067-1081. doi:10.1017/S1041610213002627

Fox, M. D., Snyder, A. Z., Vincent, J. L., Corbetta, M., Van Essen, D. C., & Raichle, M. E. (2005). The human brain is intrinsically organized into dynamic, anticorrelated functional networks. *Proceedings of the National Academy of Sciences of the United States of America, 102*(27), 9673-9678.

Fox, M. D., Snyder, A. Z., Vincent, J. L., Corbetta, M., Van Essen, D. C., & Raichle, M. E. (2005). The human brain is intrinsically organized into dynamic, anticorrelated functional networks. *Proc Natl Acad Sci U S A, 102*(27), 9673-9678.

Frankó, E., Joly, O., & Initiative, A. s. D. N. (2013). Evaluating Alzheimer's disease progression using rate of regional hippocampal atrophy. *PLOS ONE, 8*(8), e71354.

Frey, S., Pandya, D. N., Chakravarty, M. M., Bailey, L., Petrides, M., & Collins, D. L. (2011). An MRI based average macaque monkey stereotaxic atlas and space (MNI monkey space). *NeuroImage, 55*(4), 1435-1442. doi:10.1016/j.neuroimage.2011.01.040

Friedman, J., Hastie, T., & Tibshirani, R. (2008). Sparse inverse covariance estimation with the graphical lasso. *Biostatistics, 9*(3), 432-441. doi:10.1093/biostatistics/kxm045

Frisoni, G. B., Fox, N. C., Jack, C. R., Scheltens, P., & Thompson, P. M. (2010). The clinical use of structural MRI in Alzheimer disease. *Nature Reviews Neurology, 6*(2), 67-77.

Frisoni, G. B., Ganzola, R., Canu, E., Rüb, U., Pizzini, F. B., Alessandrini, F., . . . Thompson, P. M. (2008). Mapping local hippocampal changes in Alzheimer's disease and normal ageing with MRI at 3 Tesla. *Brain, 131*(12), 3266-3276.

Fu, L. P., Bi, G. H., Zou, Z. T., Wang, Y., Ye, E. M., Ma, L., . . . Yang, Z. (2008). Impaired response inhibition function in abstinent heroin dependents: An fMRI study. *Neuroscience Letters, 438*(3), 322-326. doi:DOI 10.1016/j.neulet.2008.04.033

Galimberti, D., & Scarpini, E. (2011). Disease-modifying treatments for Alzheimer's disease. *Ther Adv Neurol Disord, 4*(4), 203-216. doi:10.1177/1756285611404470

Gaskin, S., & White, N. M. (2010). Temporary inactivation of the dorsal entorhinal cortex impairs acquisition and retrieval of spatial information. *Neurobiology of Learning and Memory, 93*(2), 203-207. doi:DOI 10.1016/j.nlm.2009.09.012

Gietl, A. F., Warnock, G., Riese, F., Kälin, A. M., Saake, A., Gruber, E., . . . Burger, C. (2015). Regional cerebral blood flow estimated by early PiB uptake is reduced in mild cognitive impairment and associated with age in an amyloid-dependent manner. *Neurobiol Aging, 36*(4), 1619-1628.

Gloor, P. (1997). *The temporal lobe and limbic system*: Oxford University Press, USA.

Golde, T. E., Schneider, L. S., & Koo, E. H. (2011). Anti-abeta therapeutics in Alzheimer's disease: the need for a paradigm shift. *Neuron, 69*(2), 203-213. doi:10.1016/j.neuron.2011.01.002

Gomez-Ramirez, J., & Wu, J. (2014). Network-based biomarkers in Alzheimer's disease: review and future directions. *Front Aging Neurosci, 6*, 12. doi:10.3389/fnagi.2014.00012

Goodglass, H., & Kaplan, E. (1972). *Assessment of aphasia and related disorders*. Philadelphia: Lea & Febiger.

Gordon, B. A., Blazey, T., Su, Y., Fagan, A. M., Holtzman, D. M., Morris, J. C., & Benzinger, T. L. (2016). Longitudinal beta-Amyloid Deposition and Hippocampal Volume in Preclinical Alzheimer Disease and Suspected Non-Alzheimer Disease Pathophysiology. *JAMA Neurol, 73*(10), 1192-1200. doi:10.1001/jamaneurol.2016.2642

Gousias, I. S., Rueckert, D., Heckemann, R. A., Dyet, L. E., Boardman, J. P., Edwards, A. D., & Hammers, A. (2008). Automatic segmentation of brain MRIs of 2-year-olds into 83 regions of interest. *NeuroImage, 40*(2), 672-684.

Greicius, M., Krasnow, B., Reiss, A. L., & Menon, V. (2003). Functional connectivity in the resting brain: a network analysis of the default mode hypothesis. *Proc Natl Acad Sci U S A, 100*(1), 253-258. doi:10.1073/pnas.0135058100

Greicius, M., Srivastava, G., Reiss, A. L., & Menon, V. (2004). Default-mode network activity distinguishes Alzheimer's disease from healthy aging: evidence from functional MRI. *Proceedings of the National Academy of Sciences of the United States of America, 101*(13), 4637-4642.

Grundman, M., Sencakova, D., Jack, C. R., Jr., Petersen, R. C., Kim, H. T., Schultz, A., . . . Alzheimer's Disease Cooperative, S. (2002). Brain MRI hippocampal volume and prediction of clinical status in a mild cognitive impairment trial. *J Mol Neurosci, 19*(1-2), 23-27. doi:10.1007/s12031-002-0006-6

Haber, S. N. (2003). The primate basal ganglia: parallel and integrative networks. *J Chem Neuroanat, 26*(4), 317-330.

Hahn, C., Lee, C. U., Won, W. Y., Joo, S. H., & Lim, H. K. (2016). Thalamic Shape and Cognitive Performance in Amnestic Mild Cognitive Impairment. *Psychiatry Investig, 13*(5), 504-510. doi:10.4306/pi.2016.13.5.504

Hammers, A., Allom, R., Koepp, M. J., Free, S. L., Myers, R., Lemieux, L., . . . Duncan, J. S. (2003). Three-dimensional maximum probability atlas of the human brain, with particular reference to the temporal lobe. *Hum Brain Mapp, 19*(4), 224-247. doi:10.1002/hbm.10123

Härting, C., Markowitsch, H. J., Neufeld, H., Calabrese, P., Deisinger, K., & Kessler, J. (2000). Wechsler Gedächtnis Test-Revidierte Fassung (WMS-R). *Bern: Huber*.

Heine, L., Soddu, A., Gomez, F., Vanhaudenhuyse, A., Tshibanda, L., Thonnard, M., . . . Demertzi, A. (2012). Resting state networks and consciousness: alterations of multiple resting state network connectivity in physiological, pharmacological, and pathological consciousness States. *Front Psychol, 3*, 295. doi:10.3389/fpsyg.2012.00295

Helmstaedter, C., Lendt, M., & Lux, S. (2001). *VLMT: Verbaler Lern-und Merkfähigkeitstest*: Beltz Test.

Herrup, K. (2010). Reimagining Alzheimer's disease--an age-based hypothesis. *J Neurosci, 30*(50), 16755-16762. doi:10.1523/JNEUROSCI.4521-10.2010

Hirai, T., & Jones, E. G. (1989). A new parcellation of the human thalamus on the basis of histochemical staining. *Brain Res Brain Res Rev, 14*(1), 1-34.

Hollmann, M., Hellrung, L., Pleger, B., Schlogl, H., Kabisch, S., Stumvoll, M., . . . Horstmann, A. (2012). Neural correlates of the volitional regulation of the desire for food. *International Journal of Obesity, 36*(5), 648-655. doi:Doi 10.1038/Ijo.2011.125

Hsu, P. J., Shou, H., Benzinger, T., Marcus, D., Durbin, T., Morris, J. C., & Sheline, Y. I. (2015). Amyloid burden in cognitively normal elderly is associated with preferential hippocampal subfield volume loss. *Journal of Alzheimer's Disease, 45*(1), 27-33.

Hutchison, R. M., Womelsdorf, T., Gati, J. S., Everling, S., & Menon, R. S. (2013). Resting-state networks show dynamic functional connectivity in awake humans and anesthetized macaques. *Hum Brain Mapp, 34*(9), 2154-2177. doi:10.1002/hbm.22058

Hyman, B. T., Phelps, C. H., Beach, T. G., Bigio, E. H., Cairns, N. J., Carrillo, M. C., . . . Montine, T. J. (2012). National Institute on Aging-Alzheimer's Association guidelines for the neuropathologic assessment of Alzheimer's disease. *Alzheimers Dement, 8*(1), 1-13. doi:10.1016/j.jalz.2011.10.007

Hyman, B. T., & Trojanowski, J. Q. (1997). Consensus recommendations for the postmortem diagnosis of Alzheimer disease from the National Institute on Aging and the Reagan Institute Working Group on diagnostic criteria for the neuropathological assessment of Alzheimer disease. *J Neuropathol Exp Neurol, 56*(10), 1095-1097.

Hyman, B. T., Van Hoesen, G., Kromer, L., & Damasio, A. (1986). Perforant pathway changes and the memory impairment of Alzheimer's disease. *Annals of neurology, 20*(4), 472-481.

Jack, C. R., Jr., Albert, M. S., Knopman, D. S., McKhann, G. M., Sperling, R. A., Carrillo, M. C., . . . Phelps, C. H. (2011). Introduction to the recommendations from the National Institute on Aging-Alzheimer's Association workgroups on diagnostic guidelines for Alzheimer's disease. *Alzheimers Dement, 7*(3), 257-262. doi:10.1016/j.jalz.2011.03.004

Jack, C. R., Jr., Knopman, D. S., Jagust, W. J., Petersen, R. C., Weiner, M. W., Aisen, P. S., . . . Trojanowski, J. Q. (2013). Tracking pathophysiological processes in Alzheimer's disease: an updated

hypothetical model of dynamic biomarkers. *Lancet Neurol, 12*(2), 207-216. doi:10.1016/S1474-4422(12)70291-0
Jagust, W. J., & Mormino, E. C. (2011). Lifespan brain activity, β-amyloid, and Alzheimer's disease. *Trends in cognitive sciences, 15*(11), 520-526.
Janes, A. C., Park, M. T. M., Farmer, S., & Chakravarty, M. M. (2015). Striatal morphology is associated with tobacco cigarette craving. *Neuropsychopharmacology, 40*(2), 406-411.
Jankowski, M. M., Ronnqvist, K. C., Tsanov, M., Vann, S. D., Wright, N. F., Erichsen, J. T., . . . O'Mara, S. M. (2013). The anterior thalamus provides a subcortical circuit supporting memory and spatial navigation. *Frontiers in systems neuroscience, 7*.
Johnson, K. A., Schultz, A., Betensky, R. A., Becker, J. A., Sepulcre, J., Rentz, D., . . . Papp, K. (2016). Tau positron emission tomographic imaging in aging and early Alzheimer disease. *Annals of neurology, 79*(1), 110-119.
Julkunen, V., Niskanen, E., Koikkalainen, J., Herukka, S. K., Pihlajamaki, M., Hallikainen, M., . . . Hilkka, S. (2010). Differences in cortical thickness in healthy controls, subjects with mild cognitive impairment, and Alzheimer's disease patients: a longitudinal study. *J Alzheimers Dis, 21*(4), 1141-1151.
Kelemen, E., & Fenton, A. A. (2010). Dynamic grouping of hippocampal neural activity during cognitive control of two spatial frames. *PLoS Biol, 8*(6), e1000403. doi:10.1371/journal.pbio.1000403
Kerchner, G., Hess, C., Hammond-Rosenbluth, K., Xu, D., Rabinovici, G., Kelley, D., . . . Miller, B. (2010a). Hippocampal CA1 apical neuropil atrophy in mild Alzheimer disease visualized with 7-T MRI. *Neurology, 75*(15), 1381-1387.
Kerchner, G., Hess, C. P., Hammond-Rosenbluth, K. E., Xu, D., Rabinovici, G. D., Kelley, D. A., . . . Miller, B. L. (2010b). Hippocampal CA1 apical neuropil atrophy in mild Alzheimer disease visualized with 7-T MRI. *Neurology, 75*(15), 1381-1387. doi:10.1212/WNL.0b013e3181f736a1
Kim, J. S., Singh, V., Lee, J. K., Lerch, J., Ad-Dab'bagh, Y., MacDonald, D., . . . Evans, A. C. (2005). Automated 3-D extraction and evaluation of the inner and outer cortical surfaces using a Laplacian map and partial volume effect classification. *NeuroImage, 27*(1), 210-221.
Klekociuk, S. Z., Summers, J. J., Vickers, J. C., & Summers, M. J. (2014). Reducing false positive diagnoses in mild cognitive impairment: the importance of comprehensive neuropsychological assessment. *Eur J Neurol, 21*(10), 1330-1336, e1382-1333. doi:10.1111/ene.12488
Klostermann, E. C., Braskie, M. N., Landau, S. M., O'Neil, J. P., & Jagust, W. J. (2012). Dopamine and frontostriatal networks in cognitive aging. *Neurobiol Aging, 33*(3), 623 e615-624. doi:10.1016/j.neurobiolaging.2011.03.002
La Joie, R., Perrotin, A., de La Sayette, V., Egret, S., Doeuvre, L., Belliard, S., . . . Chetelat, G. (2013). Hippocampal subfield volumetry in mild cognitive impairment, Alzheimer's disease and semantic dementia. *Neuroimage Clin, 3*, 155-162. doi:10.1016/j.nicl.2013.08.007
Lanzenberger, R., Baldinger, P., Hahn, A., Ungersboeck, J., Mitterhauser, M., Winkler, D., . . . Frey, R. (2013). Global decrease of serotonin-1A receptor binding after electroconvulsive therapy in major depression

measured by PET. *Mol Psychiatry, 18*(1), 93-100. doi:10.1038/mp.2012.93
Laske, C. (2014). Phase 3 trials of solanezumab and bapineuzumab for Alzheimer's disease. *N Engl J Med, 370*(15), 1459. doi:10.1056/NEJMc1402193#SA1
Laske, C., Sohrabi, H. R., Frost, S. M., Lopez-de-Ipina, K., Garrard, P., Buscema, M., . . . O'Bryant, S. E. (2015). Innovative diagnostic tools for early detection of Alzheimer's disease. *Alzheimers Dement, 11*(5), 561-578. doi:10.1016/j.jalz.2014.06.004
Lebedev, A. V., Westman, E., Beyer, M., Kramberger, M., Aguilar, C., Pirtosek, Z., & Aarsland, D. (2013). Multivariate classification of patients with Alzheimer's and dementia with Lewy bodies using high-dimensional cortical thickness measurements: an MRI surface-based morphometric study. *Journal of neurology, 260*(4), 1104-1115.
Lee, M. H., Smyser, C. D., & Shimony, J. S. (2013). Resting-state fMRI: a review of methods and clinical applications. *AJNR Am J Neuroradiol, 34*(10), 1866-1872. doi:10.3174/ajnr.A3263
Leh, S. E., Chakravarty, M. M., & Ptito, A. (2008). The connectivity of the human pulvinar: a diffusion tensor imaging tractography study. *Int J Biomed Imaging, 2008*, 789539. doi:10.1155/2008/789539
Leh, S. E., Kälin, A. M., Schroeder, C., Park, M. T. M., Chakravarty, M. M., Freund, P., . . . Hock, C. (2016). Volumetric and shape analysis of the thalamus and striatum in amnestic mild cognitive impairment. *Journal of Alzheimer's Disease, 49*(1), 237-249.
Lerch, J., Carroll, J. B., Spring, S., Bertram, L. N., Schwab, C., Hayden, M. R., & Henkelman, R. M. (2008). Automated deformation analysis in the YAC128 Huntington disease mouse model. *NeuroImage, 39*(1), 32-39. doi:10.1016/j.neuroimage.2007.08.033
Lerch, J., & Evans, A. C. (2005). Cortical thickness analysis examined through power analysis and a population simulation. *NeuroImage, 24*(1), 163-173.
Lerch, J., & Nikelski, J. (2009). Package RMINC: Voxel-Wise Morphometry Using RMINC. *McGill University, Montreal, QC, Canada.* https://github*. com/Mouse-Imaging-Centre/RMINC*.
Lerch, J., Pruessner, J., Zijdenbos, A. P., Collins, D. L., Teipel, S. J., Hampel, H., & Evans, A. C. (2008). Automated cortical thickness measurements from MRI can accurately separate Alzheimer's patients from normal elderly controls. *Neurobiol Aging, 29*(1), 23-30.
Leung, H. C., & Cai, W. (2007). Common and differential ventrolateral prefrontal activity during inhibition of hand and eye movements. *J Neurosci, 27*(37), 9893-9900. doi:10.1523/JNEUROSCI.2837-07.2007
Levesque, J., Eugene, F., Joanette, Y., Paquette, V., Mensour, B., Beaudoin, G., . . . Beauregard, M. (2003). Neural circuitry underlying voluntary suppression of sadness. *Biological Psychiatry, 53*(6), 502-510. doi:Doi 10.1016/S0002-3223(03)01817-6
Levy, D. A., Bayley, P. J., & Squire, L. R. (2004). The anatomy of semantic knowledge: medial vs. lateral temporal lobe. *Proc Natl Acad Sci U S A, 101*(17), 6710-6715. doi:10.1073/pnas.0401679101
Li, Y., Wang, Y., Wu, G., Shi, F., Zhou, L., Lin, W., . . . Initiative, A. s. D. N. (2012). Discriminant analysis of longitudinal cortical thickness changes

in Alzheimer's disease using dynamic and network features. *Neurobiol Aging, 33*(2), 427. e415-427. e430.
Li, Y.-D., Dong, H.-B., Xie, G.-M., & Zhang, L.-j. (2013). Discriminative analysis of mild Alzheimer's disease and normal aging using volume of hippocampal subfields and hippocampal mean diffusivity: an in vivo magnetic resonance imaging study. *American Journal of Alzheimer's Disease & Other Dementias®, 28*(6), 627-633.
Liao, W., Long, X., Jiang, C., Diao, Y., Liu, X., Zheng, H., . . . Alzheimer's Disease Neuroimaging, I. (2014). Discerning mild cognitive impairment and Alzheimer Disease from normal aging: morphologic characterization based on univariate and multivariate models. *Acad Radiol, 21*(5), 597-604. doi:10.1016/j.acra.2013.12.001
Lissek, S., Glaubitz, B., Uengoer, M., & Tegenthoff, M. (2013). Hippocampal activation during extinction learning predicts occurrence of the renewal effect in extinction recall. *NeuroImage, 81*, 131-143. doi:10.1016/j.neuroimage.2013.05.025
Liu, E., Schmidt, M. E., Margolin, R., Sperling, R., Koeppe, R., Mason, N. S., . . . Fox, N. C. (2015). Amyloid-β 11C-PiB-PET imaging results from 2 randomized bapineuzumab phase 3 AD trials. *Neurology, 85*(8), 692-700.
Lloyd, S. P. (1982). Least-Squares Quantization in Pcm. *Ieee Transactions on Information Theory, 28*(2), 129-137. doi:Doi 10.1109/Tit.1982.1056489
Madsen, S. K., Ho, A. J., Hua, X., Saharan, P. S., Toga, A. W., Jack, C. R., Jr., . . . Alzheimer's Disease Neuroimaging, I. (2010). 3D maps localize caudate nucleus atrophy in 400 Alzheimer's disease, mild cognitive impairment, and healthy elderly subjects. *Neurobiol Aging, 31*(8), 1312-1325. doi:10.1016/j.neurobiolaging.2010.05.002
Magon, S., Chakravarty, M. M., Amann, M., Weier, K., Naegelin, Y., Andelova, M., . . . Sprenger, T. (2014). Label-fusion-segmentation and deformation-based shape analysis of deep gray matter in multiple sclerosis: the impact of thalamic subnuclei on disability. *Hum Brain Mapp, 35*(8), 4193-4203. doi:10.1002/hbm.22470
Mai, J. K., Majtanik, M., & Paxinos, G. (2015). *Atlas of the human brain*: Academic Press.
Masdeu, J. C., Kreisl, W. C., & Berman, K. F. (2012). The neurobiology of Alzheimer disease defined by neuroimaging. *Curr Opin Neurol, 25*(4), 410-420. doi:10.1097/WCO.0b013e3283557b36
Mason, M. F., Norton, M. I., Van Horn, J. D., Wegner, D. M., Grafton, S. T., & Macrae, C. N. (2007). Wandering minds: the default network and stimulus-independent thought. *Science, 315*(5810), 393-395. doi:10.1126/science.1131295
Mattsson, N., Zetterberg, H., Hansson, O., Andreasen, N., Parnetti, L., Jonsson, M., . . . Ewers, M. (2009). CSF biomarkers and incipient Alzheimer disease in patients with mild cognitive impairment. *Jama, 302*(4), 385-393.
Mazziotta, J. C., Toga, A., Evans, A., Fox, P., Lancaster, J., Zilles, K., . . . Mazoyer, B. (2001). A probabilistic atlas and reference system for the human brain: International Consortium for Brain Mapping (ICBM). *Philos Trans R Soc Lond B Biol Sci, 356*(1412), 1293-1322. doi:10.1098/rstb.2001.0915

Mazziotta, J. C., Toga, A. W., Evans, A., Fox, P., & Lancaster, J. (1995). A probabilistic atlas of the human brain: Theory and rationale for its development: The international consortium for brain mapping (icbm). *NeuroImage, 2*(2), 89-101.

McKhann, G. M., Knopman, D. S., Chertkow, H., Hyman, B. T., Jack, C. R., Jr., Kawas, C. H., . . . Phelps, C. H. (2011). The diagnosis of dementia due to Alzheimer's disease: recommendations from the National Institute on Aging-Alzheimer's Association workgroups on diagnostic guidelines for Alzheimer's disease. *Alzheimers Dement, 7*(3), 263-269. doi:10.1016/j.jalz.2011.03.005

McShane, R., Areosa Sastre, A., & Minakaran, N. (2006). Memantine for dementia. *Cochrane Database Syst Rev*(2), CD003154. doi:10.1002/14651858.CD003154.pub5

Menon, V., & Uddin, L. Q. (2010). Saliency, switching, attention and control: a network model of insula function. *Brain Struct Funct, 214*(5-6), 655-667. doi:10.1007/s00429-010-0262-0

Miller, A. M., Vedder, L. C., Law, L. M., & Smith, D. M. (2014). Cues, context, and long-term memory: the role of the retrosplenial cortex in spatial cognition. *Front Hum Neurosci, 8*, 586. doi:10.3389/fnhum.2014.00586

Mitchell, T. W., Mufson, E. J., Schneider, J. A., Cochran, E. J., Nissanov, J., Han, L. Y., . . . Arnold, S. E. (2002). Parahippocampal tau pathology in healthy aging, mild cognitive impairment, and early Alzheimer's disease. *Ann Neurol, 51*(2), 182-189.

Mormino, E., Kluth, J., Madison, C., Rabinovici, G., Baker, S., Miller, B., . . . Jagust, W. (2008). Episodic memory loss is related to hippocampal-mediated β-amyloid deposition in elderly subjects. *Brain, 132*(5), 1310-1323.

Morris, J. C. (1993). The Clinical Dementia Rating (CDR): current version and scoring rules. *Neurology, 43*(11), 2412-2414.

Mosconi, L., Perani, D., Sorbi, S., Herholz, K., Nacmias, B., Holthoff, V., . . . Pupi, A. (2004). MCI conversion to dementia and the APOE genotype: a prediction study with FDG-PET. *Neurology, 63*(12), 2332-2340.

Mueller, S. G., Schuff, N., Yaffe, K., Madison, C., Miller, B., & Weiner, M. W. (2010). Hippocampal atrophy patterns in mild cognitive impairment and Alzheimer's disease. *Hum Brain Mapp, 31*(9), 1339-1347. doi:10.1002/hbm.20934

Mueller, S. G., & Weiner, M. W. (2009). Selective effect of age, Apo e4, and Alzheimer's disease on hippocampal subfields. *Hippocampus, 19*(6), 558-564. doi:10.1002/hipo.20614

Mulligan, R. C., Kristjansson, S. D., Reiersen, A. M., Parra, A. S., & Anokhin, A. P. (2014). Neural correlates of inhibitory control and functional genetic variation in the dopamine D4 receptor gene. *Neuropsychologia, 62*, 306-318. doi:10.1016/j.neuropsychologia.2014.07.033

Nussbaum, J. M., Seward, M. E., & Bloom, G. S. (2013). Alzheimer disease: a tale of two prions. *Prion, 7*(1), 14-19. doi:10.4161/pri.22118

Ochsner, K. N., Ray, R. D., Cooper, J. C., Robertson, E. R., Chopra, S., Gabrieli, J. D. E., & Gross, J. J. (2004). For better or for worse: neural systems supporting the cognitive down- and up-regulation of negative emotion. *Neuroimage, 23*(2), 483-499. doi:DOI 10.1016/j.neuroimage.2004.06.030

Paskavitz, J. F., Lippa, C. F., Hamos, J. E., Pulaski-Salo, D., & Drachman, D. A. (1995). Role of the dorsomedial nucleus of the thalamus in Alzheimer's disease. *J Geriatr Psychiatry Neurol, 8*(1), 32-37.
Patriat, R., EK, M., TB, M., GR, K., VA, N., ME, M., . . . RM, B. (2013). The effect of resting condition on resting-state fMRI reliability and consistency: a comparison between resting with eyes open, closed, and fixated. *NeuroImage, 78*, 463-473.
Patriat, R., Molloy, E., Meier, T., Kirk, G., VA, N., ME, M., . . . RM, B. (2013). The effect of resting condition on resting-state fMRI reliability and consistency: a comparison between resting with eyes open, closed, and fixated. *NeuroImage, 78*, 463-473.
Patriat, R., Molloy, E. K., Meier, T. B., Kirk, G. R., Nair, V. A., Meyerand, M. E., . . . Birn, R. M. (2013). The effect of resting condition on resting-state fMRI reliability and consistency: a comparison between resting with eyes open, closed, and fixated. *Neuroimage, 78*, 463-473. doi:10.1016/j.neuroimage.2013.04.013
Petersen, R. C. (2004). Mild cognitive impairment as a diagnostic entity. *J Intern Med, 256*(3), 183-194. doi:10.1111/j.1365-2796.2004.01388.x
Phan, K. L., Wager, T., Taylor, S. F., & Liberzon, I. (2002). Functional neuroanatomy of emotion: a meta-analysis of emotion activation studies in PET and fMRI. *NeuroImage, 16*(2), 331-348. doi:10.1006/nimg.2002.1087
Pimplikar, S. W., Nixon, R. A., Robakis, N. K., Shen, J., & Tsai, L. H. (2010). Amyloid-independent mechanisms in Alzheimer's disease pathogenesis. *J Neurosci, 30*(45), 14946-14954. doi:10.1523/JNEUROSCI.4305-10.2010
Pipitone, J., Park, M. T. M., Winterburn, J., Lett, T. A., Lerch, J. P., Pruessner, J. C., . . . Initiative, A. s. D. N. (2014). Multi-atlas segmentation of the whole hippocampus and subfields using multiple automatically generated templates. *NeuroImage, 101*, 494-512.
Pluta, J., Yushkevich, P., Das, S., & Wolk, D. (2012). In vivo analysis of hippocampal subfield atrophy in mild cognitive impairment via semi-automatic segmentation of T2-weighted MRI. *J Alzheimers Dis, 31*(1), 85-99. doi:10.3233/JAD-2012-111931
Pooler, A. M., Polydoro, M., Wegmann, S. K., Pitstick, R., Kay, K. R., Sanchez, L., . . . Spires‐Jones, T. L. (2013). Tau‐amyloid interactions in the rTgTauEC model of early Alzheimer's disease suggest amyloid‐induced disruption of axonal projections and exacerbated axonal pathology. *Journal of Comparative Neurology, 521*(18), 4236-4248.
Portas, C. M., Bjorvatn, B., & Ursin, R. (2000). Serotonin and the sleep/wake cycle: special emphasis on microdialysis studies. *Prog Neurobiol, 60*(1), 13-35.
Prince, M., Comas-Herrera, A., Knapp, M., Guerchet, M., & Karagiannidou, M. (2016). World Alzheimer report 2016: improving healthcare for people living with dementia: coverage, quality and costs now and in the future.
Pruessmann, K. P., Weiger, M., Scheidegger, M. B., & Boesiger, P. (1999). SENSE: sensitivity encoding for fast MRI. *Magn Reson Med, 42*(5), 952-962.
Qiu, A., Fennema-Notestine, C., Dale, A. M., Miller, M. I., & Alzheimer's Disease Neuroimaging, I. (2009). Regional shape abnormalities in mild

cognitive impairment and Alzheimer's disease. *NeuroImage, 45*(3), 656-661.
R Core Team. (2014). R: A language and environment for statistical computing. Vienna, Austria: R Foundation for Statistical Computing; 2014.
Raznahan, A., Shaw, P. W., Lerch, J. P., Clasen, L. S., Greenstein, D., Berman, R., . . . Giedd, J. N. (2014). Longitudinal four-dimensional mapping of subcortical anatomy in human development. *Proceedings of the National Academy of Sciences, 111*(4), 1592-1597.
Regard, M., Strauss, E., & Knapp, P. (1982). Children's production on verbal and non-verbal fluency tasks. *Perceptual and motor skills, 55*(3), 839-844.
Rehme, A. K., & Grefkes, C. (2013). Cerebral network disorders after stroke: evidence from imaging-based connectivity analyses of active and resting brain states in humans. *J Physiol, 591*(Pt 1), 17-31. doi:10.1113/jphysiol.2012.243469
Reitan, R. M. (1958). Validity of the Trail Making Test as an indicator of organic brain damage. *Perceptual and motor skills, 8*(3), 271-276.
Rodrigo, A. H., Di Domenico, S. I., Ayaz, H., Gulrajani, S., Lam, J., & Ruocco, A. C. (2014). Differentiating functions of the lateral and medial prefrontal cortex in motor response inhibition. *Neuroimage, 85*, 423-431. doi:DOI 10.1016/j.neuroimage.2013.01.059
Roh, J. H., Qiu, A., Seo, S. W., Soon, H. W., Kim, J. H., Kim, G. H., . . . Na, D. L. (2011). Volume reduction in subcortical regions according to severity of Alzheimer’s disease. *Journal of neurology, 258*(6), 1013-1020. doi:10.1007/s00415-010-5872-1
Roh, J. H., Qiu, A., Seo, S. W., Soon, H. W., Kim, J. H., Kim, G. H., . . . Na, D. L. (2011). Volume reduction in subcortical regions according to severity of Alzheimer's disease. *J Neurol, 258*(6), 1013-1020. doi:10.1007/s00415-010-5872-1
Rullmann, M., Dukart, J., Hoffmann, K.-T., Luthardt, J., Tiepolt, S., Patt, M., . . . Schulz-Schaeffer, W. J. (2016). Partial-volume effect correction improves quantitative analysis of 18F-Florbetaben β-amyloid PET scans. *Journal of Nuclear Medicine, 57*(2), 198-203.
Saalmann, Y. B. (2014). Intralaminar and medial thalamic influence on cortical synchrony, information transmission and cognition. *Front Syst Neurosci, 8*, 83. doi:10.3389/fnsys.2014.00083
Schacter, D. L., Addis, D. R., & Buckner, R. L. (2007). Remembering the past to imagine the future: the prospective brain. *Nature Reviews Neuroscience, 8*(9), 657-661. doi:Doi 10.1038/Nrn2213
Schaltenbrand, G. S., & Wahren, W. (1977). Atlas for stereotaxy of the human brain. *Georg Thieme Publishers*.
Schreiner, S. J., Liu, X., Gietl, A. F., Wyss, M., Steininger, S. C., Gruber, E., . . . Leh, S. E. (2014). Regional Fluid-Attenuated Inversion Recovery (FLAIR) at 7 Tesla correlates with amyloid beta in hippocampus and brainstem of cognitively normal elderly subjects. *Frontiers in Aging Neuroscience, 6*.
Seeley, W. W., Menon, V., Schatzberg, A. F., Keller, J., Glover, G. H., Kenna, H., . . . Greicius, M. D. (2007). Dissociable intrinsic connectivity

networks for salience processing and executive control. *J Neurosci, 27*(9), 2349-2356. doi:10.1523/JNEUROSCI.5587-06.2007
Serrano-Pozo, A., Frosch, M. P., Masliah, E., & Hyman, B. T. (2011). Neuropathological alterations in Alzheimer disease. *Cold Spring Harb Perspect Med, 1*(1), a006189. doi:10.1101/cshperspect.a006189
Sevigny, J., Chiao, P., Bussière, T., Weinreb, P. H., Williams, L., Maier, M., . . . Ling, Y. (2016). The antibody aducanumab reduces Aβ plaques in Alzheimer's disease. *Nature, 537*(7618), 50-56.
Sevigny, J., Chiao, P., Bussiere, T., Weinreb, P. H., Williams, L., Maier, M., . . . Sandrock, A. (2016). The antibody aducanumab reduces Abeta plaques in Alzheimer's disease. *Nature, 537*(7618), 50-56. doi:10.1038/nature19323
Sevigny, J., Chiao, P., Bussiere, T., Weinreb, P. H., Williams, L., Maier, M., . . . Sandrock, A. (2017). Addendum: The antibody aducanumab reduces Abeta plaques in Alzheimer's disease. *Nature, 546*(7659), 564. doi:10.1038/nature22809
Shattuck, D. W., Mirza, M., Adisetiyo, V., Hojatkashani, C., Salamon, G., Narr, K. L., . . . Toga, A. W. (2008). Construction of a 3D probabilistic atlas of human cortical structures. *NeuroImage, 39*(3), 1064-1080.
Shaw, P., Sharp, W., Sudre, G., Wharton, A., Greenstein, D., Raznahan, A., . . . Rapoport, J. (2015). Subcortical and cortical morphological anomalies as an endophenotype in obsessive-compulsive disorder. *Molecular psychiatry, 20*(2), 224.
Shirer, W. R., Ryali, S., Rykhlevskaia, E., Menon, V., & Greicius, M. D. (2012). Decoding subject-driven cognitive states with whole-brain connectivity patterns. *Cereb Cortex, 22*(1), 158-165. doi:10.1093/cercor/bhr099
Sled, J. G., Zijdenbos, A. P., & Evans, A. C. (1998). A nonparametric method for automatic correction of intensity nonuniformity in MRI data. *IEEE Trans Med Imaging, 17*(1), 87-97. doi:10.1109/42.668698
Smith, S. M. (2002). Fast robust automated brain extraction. *Hum Brain Mapp, 17*(3), 143-155.
Solbach, C., Uebele, M., Reischl, G., & Machulla, H.-J. (2005). Efficient radiosynthesis of carbon-11 labelled uncharged thioflavin T derivatives using [11 C] methyl triflate for β-amyloid imaging in Alzheimer's disease with PET. *Applied radiation and isotopes, 62*(4), 591-595.
Sperling, R. A., Aisen, P. S., Beckett, L. A., Bennett, D. A., Craft, S., Fagan, A. M., . . . Montine, T. J. (2011). Toward defining the preclinical stages of Alzheimer's disease: Recommendations from the National Institute on Aging-Alzheimer's Association workgroups on diagnostic guidelines for Alzheimer's disease. *Alzheimer's & dementia, 7*(3), 280-292.
Sperling, R. A., Jack, C. R., & Aisen, P. S. (2011). Testing the right target and right drug at the right stage. *Science translational medicine, 3*(111), 111cm133-111cm133.
Sridharan, D., Levitin, D. J., & Menon, V. (2008). A critical role for the right fronto-insular cortex in switching between central-executive and default-mode networks. *Proc Natl Acad Sci U S A, 105*(34), 12569-12574. doi:0800005105 [pii]

Steininger, S. C., Liu, X., Gietl, A., Wyss, M., Schreiner, S., Gruber, E., . . . Buck, A. (2014). Cortical amyloid beta in cognitively normal elderly adults is associated with decreased network efficiency within the cerebro-cerebellar system. *Frontiers in Aging Neuroscience, 6*.

Stepan-Buksakowska, I., Szabo, N., Horinek, D., Toth, E., Hort, J., Warner, J., . . . Kincses, Z. T. (2014). Cortical and subcortical atrophy in Alzheimer disease: parallel atrophy of thalamus and hippocampus. *Alzheimer Dis Assoc Disord, 28*(1), 65-72. doi:10.1097/WAD.0b013e318299d3d6

Stroop, J. R. (1935). Studies of interference in serial verbal reactions. *Journal of Experimental Psychology, 18*, 643-662. doi:Doi 10.1037/H0054651

Studholme, C., Hill, D. L. G., & Hawkes, D. J. (1999). An overlap invariant entropy measure of 3D medical image alignment. *Pattern Recognition, 32*(1), 71-86. doi:https://doi.org/10.1016/S0031-3203(98)00091-0

Tang, X., Holland, D., Dale, A. M., Younes, L., Miller, M. I., & Alzheimer's Disease Neuroimaging, I. (2014). Shape abnormalities of subcortical and ventricular structures in mild cognitive impairment and Alzheimer's disease: detecting, quantifying, and predicting. *Hum Brain Mapp, 35*(8), 3701-3725. doi:10.1002/hbm.22431

Tapiola, T., Pennanen, C., Tapiola, M., Tervo, S., Kivipelto, M., Hänninen, T., . . . Soininen, H. (2008). MRI of hippocampus and entorhinal cortex in mild cognitive impairment: A follow-up study. *Neurobiol Aging, 29*(1), 31-38. doi:https://doi.org/10.1016/j.neurobiolaging.2006.09.007

Teipel, S. J., Wohlert, A., Metzger, C., Grimmer, T., Sorg, C., Ewers, M., . . . Dyrba, M. (2017). Multicenter stability of resting state fMRI in the detection of Alzheimer's disease and amnestic MCI. *Neuroimage Clin, 14*, 183-194. doi:10.1016/j.nicl.2017.01.018

Tekin, S., & Cummings, J. L. (2002). Frontal-subcortical neuronal circuits and clinical neuropsychiatry: an update. *J Psychosom Res, 53*(2), 647-654.

Thal, D. R., Holzer, M., Rub, U., Waldmann, G., Gunzel, S., Zedlick, D., & Schober, R. (2000). Alzheimer-related tau-pathology in the perforant path target zone and in the hippocampal stratum oriens and radiatum correlates with onset and degree of dementia. *Exp Neurol, 163*(1), 98-110. doi:10.1006/exnr.2000.7380

Thal, D. R., Rüb, U., Orantes, M., & Braak, H. (2002). Phases of Aβ-deposition in the human brain and its relevance for the development of AD. *Neurology, 58*(12), 1791-1800.

Thalmann, B., Monsch, A., Bernasconi, F., Berres, M., Schneitter, M., Ermini-Fünfschilling, D., . . . Stähelin, H. (1997). CERAD–Consortium to Establish a Registry for Alzheimer's Disease Assessment Battery–deutsche Fassung. *Basel: Geriatrische Universitätsklinik*.

Thomas, J. B., Brier, M. R., Bateman, R. J., Snyder, A. Z., Benzinger, T. L., Xiong, C., . . . Mayeux, R. (2014). Functional connectivity in autosomal dominant and late-onset Alzheimer disease. *JAMA neurology, 71*(9), 1111-1122.

Thompson, P. M., Hayashi, K. M., De Zubicaray, G., Janke, A. L., Rose, S. E., Semple, J., . . . Doddrell, D. M. (2003). Dynamics of gray matter loss in Alzheimer's disease. *Journal of neuroscience, 23*(3), 994-1005.

Thurstone, L. L., & Thurstone, T. G. (1938). *Primary Mental Abilities* Chicago: Univ. of Chicago Press

Tohka, J., Zijdenbos, A., & Evans, A. (2004). Fast and robust parameter estimation for statistical partial volume models in brain MRI. *NeuroImage, 23*(1), 84-97.
Tondelli, M., Wilcock, G. K., Nichelli, P., De Jager, C. A., Jenkinson, M., & Zamboni, G. (2012a). Structural MRI changes detectable up to ten years before clinical Alzheimer's disease. *Neurobiol Aging, 33*(4), 825.e825-825.e836. doi:https://doi.org/10.1016/j.neurobiolaging.2011.05.018
Tondelli, M., Wilcock, G. K., Nichelli, P., De Jager, C. A., Jenkinson, M., & Zamboni, G. (2012b). Structural MRI changes detectable up to ten years before clinical Alzheimer's disease. *Neurobiol Aging, 33*(4), 825. e825-825. e836.
Trojanowski, J. Q., Vandeerstichele, H., Korecka, M., Clark, C. M., Aisen, P. S., Petersen, R. C., . . . Lewczuk, P. (2010). Update on the biomarker core of the Alzheimer's Disease Neuroimaging Initiative subjects. *Alzheimer's & dementia, 6*(3), 230-238.
Trujillo-Estrada, L., Dávila, J. C., Sánchez-Mejias, E., Sánchez-Varo, R., Gomez-Arboledas, A., Vizuete, M., . . . Gutiérrez, A. (2014). Early neuronal loss and axonal/presynaptic damage is associated with accelerated amyloid-β accumulation in AβPP/PS1 Alzheimer's disease mice subiculum. *Journal of Alzheimer's Disease, 42*(2), 521-541.
Van Dijk, K., Hedden, T., Venkataraman, A., Evans, K. C., Lazar, S. W., & Buckner, R. L. (2010). Intrinsic functional connectivity as a tool for human connectomics: theory, properties, and optimization. *Journal of neurophysiology, 103*(1), 297-321.
Van Dijk, K. R., Hedden, T., Venkataraman, A., Evans, K. C., Lazar, S. W., & Buckner, R. L. (2010). Intrinsic functional connectivity as a tool for human connectomics: theory, properties, and optimization. *J Neurophysiol, 103*(1), 297-321. doi:10.1152/jn.00783.2009
Vargas, C., Lopez-Jaramillo, C., & Vieta, E. (2013). A systematic literature review of resting state network--functional MRI in bipolar disorder. *J Affect Disord, 150*(3), 727-735. doi:10.1016/j.jad.2013.05.083
Villemagne, V. L., Burnham, S., Bourgeat, P., Brown, B., Ellis, K. A., Salvado, O., . . . Maruff, P. (2013). Amyloid β deposition, neurodegeneration, and cognitive decline in sporadic Alzheimer's disease: a prospective cohort study. *The Lancet Neurology, 12*(4), 357-367.
Voineskos, A. N., Winterburn, J. L., Felsky, D., Pipitone, J., Rajji, T. K., Mulsant, B. H., & Chakravarty, M. M. (2015). Hippocampal (subfield) volume and shape in relation to cognitive performance across the adult lifespan. *Hum Brain Mapp, 36*(8), 3020-3037. doi:10.1002/hbm.22825
Volz-Sidiropoulou, E., Poll, E., Forkmann, T., & Gauggel, S. (2010). Erweiterte Altersnormen zum Verbalen Lern-und Merkfähigkeitstest (VLMT). *Klin Diagn Eval, 3*, 226-243.
Wang, L., Swank, J. S., Glick, I. E., Gado, M. H., Miller, M. I., Morris, J. C., & Csernansky, J. G. (2003). Changes in hippocampal volume and shape across time distinguish dementia of the Alzheimer type from healthy aging☆. *NeuroImage, 20*(2), 667-682.
Wechsler, D. (1987). *Wechsler Memory Scale - Revised Edition*. New York: The Psychological Corporation.

Westerberg, C. E., Mander, B. A., Florczak, S. M., Weintraub, S., Mesulam, M. M., Zee, P. C., & Paller, K. A. (2012). Concurrent impairments in sleep and memory in amnestic mild cognitive impairment. *J Int Neuropsychol Soc, 18*(3), 490-500. doi:10.1017/S135561771200001X

Westman, E., Aguilar, C., Muehlboeck, J. S., & Simmons, A. (2013). Regional magnetic resonance imaging measures for multivariate analysis in Alzheimer's disease and mild cognitive impairment. *Brain Topogr, 26*(1), 9-23. doi:10.1007/s10548-012-0246-x

Westman, E., Muehlboeck, J. S., & Simmons, A. (2012). Combining MRI and CSF measures for classification of Alzheimer's disease and prediction of mild cognitive impairment conversion. *NeuroImage, 62*(1), 229-238. doi:10.1016/j.neuroimage.2012.04.056

Westman, E., Simmons, A., Muehlboeck, J. S., Mecocci, P., Vellas, B., Tsolaki, M., . . . Alzheimer's Disease Neuroimaging Initiative. (2011). AddNeuroMed and ADNI: similar patterns of Alzheimer's atrophy and automated MRI classification accuracy in Europe and North America. *NeuroImage, 58*(3), 818-828. doi:10.1016/j.neuroimage.2011.06.065

Wheeler, A. L., Lerch, J. P., Chakravarty, M. M., Friedel, M., Sled, J. G., Fletcher, P. J., . . . Frankland, P. W. (2013). Adolescent cocaine exposure causes enduring macroscale changes in mouse brain structure. *J Neurosci, 33*(5), 1797-1803a. doi:10.1523/JNEUROSCI.3830-12.2013

Whitfield-Gabrieli, S., & Nieto-Castanon, A. (2012). Conn: a functional connectivity toolbox for correlated and anticorrelated brain networks. *Brain Connect, 2*(3), 125-141. doi:10.1089/brain.2012.0073

Wilke, M., Kagan, I., & Andersen, R. A. (2013). Effects of pulvinar inactivation on spatial decision-making between equal and asymmetric reward options. *Journal of cognitive neuroscience, 25*(8), 1270-1283.

Winblad, B., Palmer, K., Kivipelto, M., Jelic, V., Fratiglioni, L., Wahlund, L. O., . . . Petersen, R. C. (2004). Mild cognitive impairment--beyond controversies, towards a consensus: report of the International Working Group on Mild Cognitive Impairment. *J Intern Med, 256*(3), 240-246. doi:10.1111/j.1365-2796.2004.01380.x

Winterburn, J. L., Pruessner, J. C., Chavez, S., Schira, M. M., Lobaugh, N. J., Voineskos, A. N., & Chakravarty, M. M. (2013). A novel in vivo atlas of human hippocampal subfields using high-resolution 3T magnetic resonance imaging. *NeuroImage, 74*, 254-265.

Wisse, L. E., Biessels, G. J., & Geerlings, M. I. (2014). A Critical Appraisal of the Hippocampal Subfield Segmentation Package in FreeSurfer. *Front Aging Neurosci, 6*, 261. doi:10.3389/fnagi.2014.00261

Wisse, L. E., Biessels, G. J., Heringa, S. M., Kuijf, H. J., Luijten, P. R., Geerlings, M. I., & Group, U. V. C. I. V. S. (2014). Hippocampal subfield volumes at 7T in early Alzheimer's disease and normal aging. *Neurobiol Aging, 35*(9), 2039-2045.

Wohlert, A., Dyrba, M., Heine, C., Grothe, M. J., Grimmer, T., Sorg, C., . . . Borchardt, V. (2016). ALTERED FUNCTIONAL CONNECTIVITY OF THE DEFAULT MODE NETWORK IN ALZHEIMER'S DEMENTIA AND MILD COGNITIVE IMPAIRMENT: RESULTS FROM A LARGE-SCALE MULTICENTER RESTING-STATE FMRI STUDY. *Alzheimer's & Dementia: The Journal of the Alzheimer's Association, 12*(7), P945.

Wright, N. F., Erichsen, J. T., Vann, S. D., O'mara, S. M., & Aggleton, J. P. (2010). Parallel but separate inputs from limbic cortices to the mammillary bodies and anterior thalamic nuclei in the rat. *Journal of Comparative Neurology, 518*(12), 2334-2354.

Xuereb, J. H., Perry, R. H., Candy, J. M., Perry, E. K., Marshall, E., & Bonham, J. R. (1991). Nerve cell loss in the thalamus in Alzheimer's disease and Parkinson's disease. *Brain, 114 (Pt 3)*, 1363-1379.

Yan, C., Liu, D., He, Y., Zou, Q., Zhu, C., Zuo, X., . . . Zang, Y. (2009). Spontaneous brain activity in the default mode network is sensitive to different resting-state conditions with limited cognitive load. *PLOS ONE, 4*(5), e5743.

Ye, B. S., Seo, S. W., Yang, J. J., Kim, H. J., Kim, Y. J., Yoon, C. W., . . . Na, D. L. (2014). Comparison of cortical thickness in patients with early-stage versus late-stage amnestic mild cognitive impairment. *Eur J Neurol, 21*(1), 86-92. doi:10.1111/ene.12251

Yi, H.-A., Möller, C., Dieleman, N., Bouwman, F. H., Barkhof, F., Scheltens, P., . . . Vrenken, H. (2015). Relation between subcortical grey matter atrophy and conversion from mild cognitive impairment to Alzheimer's disease. *J Neurol Neurosurg Psychiatry*, jnnp-2014-309105.

Younes, L., Albert, M., Miller, M. I., & BIOCARD Research Team. (2014). Inferring changepoint times of medial temporal lobe morphometric change in preclinical Alzheimer's disease. *NeuroImage: Clinical, 5*, 178-187.

Yushkevich, P. A., Amaral, R. S., Augustinack, J. C., Bender, A. R., Bernstein, J. D., Boccardi, M., . . . Hippocampal Subfields, G. (2015). Quantitative comparison of 21 protocols for labeling hippocampal subfields and parahippocampal subregions in in vivo MRI: towards a harmonized segmentation protocol. *NeuroImage, 111*, 526-541. doi:10.1016/j.neuroimage.2015.01.004

Yushkevich, P. A., Avants, B. B., Pluta, J., Das, S., Minkoff, D., Mechanic-Hamilton, D., . . . Gee, J. C. (2009). A high-resolution computational atlas of the human hippocampus from postmortem magnetic resonance imaging at 9.4 T. *NeuroImage, 44*(2), 385-398.

Yushkevich, P. A., Pluta, J. B., Wang, H., Xie, L., Ding, S. L., Gertje, E. C., . . . Wolk, D. A. (2015). Automated volumetry and regional thickness analysis of hippocampal subfields and medial temporal cortical structures in mild cognitive impairment. *Hum Brain Mapp, 36*(1), 258-287.

Zarei, M., Patenaude, B., Damoiseaux, J., Morgese, C., Smith, S., Matthews, P. M., . . . Jenkinson, M. (2010). Combining shape and connectivity analysis: an MRI study of thalamic degeneration in Alzheimer's disease. *NeuroImage, 49*(1), 1-8. doi:10.1016/j.neuroimage.2009.09.001

Zhuang, J., Tyler, L. K., Randall, B., Stamatakis, E. A., & Marslen-Wilson, W. D. (2014). Optimally Efficient Neural Systems for Processing Spoken Language. *Cerebral Cortex, 24*(4), 908-918. doi:DOI 10.1093/cercor/bhs366

Zijdenbos, A., Forghani, R., & Evans, A. (1998). Automatic quantification of MS lesions in 3D MRI brain data sets: validation of INSECT. *Medical*

Image Computing and Computer-Assisted Intervention—MICCAI'98, 439-448.

7 Curriculum Vitae

CLEMENS SCHROEDER

Favreweg 2

8304 Wallisellen

078/951 90 06

clemens.schroeder@uzh.ch

* 22. Mai 1988

Education

01/2015 - today	University of Zurich PhD student, Department of Psychology
09/2012 - 06/2014	Master of Science in Psychology Grade 5.7, Master's thesis 6.0 Title master's thesis: Self-control exertion, amygdala activation, and emotional memory
09/2008 - 06/2012	Bachelor of Science in Psychology Grade 5.2, Bachelor's thesis 5.5 Title bachelor's thesis: Long-term potentiation of motor cortex through motor learning

Personal experience

01/2015 - today	University of Zurich PhD student, Department of Psychology - Neuropsychological assessments - Data acquisition, processing and analysis - Writing of ethics proposals and manuscripts
03/2014 - 12/2014	Gerontopsychiatric Center Hegibach, Zurich Research assistant - Data analysis - Literature research - Support in writing of manuscripts
05/2012 - 05/2014	University of Zurich, SNF project "neural correlates of

	self-control" Research assistant - Execution of fMRI measurements - Organisation and planning of study appointments
12/2013 - 02/2014	University of Zurich SNF project "Agendasetting" Student employee - Analysis and coding of media content
08/2011 - 07/2013	University of Zurich, Chair of General Psychology, Motivation Semester assistance - Literature research - Experiment conduct - Manuscript review - Data processing and analysis
02/2012 - 06/2012 02/2011 - 06/2011	University of Zurich, IPMZ - Institut für Publizistikwissenschaft und Medienforschung Zürich Tutor for lecture "Statistik und Datenanalyse" (statistics and data analysis) - conduct tutorial lessons accompanying the lecture - Discussion of tutorial contents - Contact for students - Proctor, test correction
02/2011 - 08/2012	Flughafen Zürich AG Employee surveys - Conduct personal interviews with passengers for quality management
09/2008 - 11/2008	Apple Retail Switzerland GmbH Concierge - Welcome and redirect customers - Help with simple requests

Other

Languages

German	mother tongue
English	fluent
French	good knowledge

IT skills

Good skills: MS Office

Basic skills: MATLAB, C++, shell scripting, HTML5, AMP (MySQL 5, PHP 5), R, SPSS

Publications

Kälin, A. M., Park, M. T., Chakravarty, M. M., Lerch, J. P., Michels, L., Schroeder, C., ... & Leh, S. E. (2017). Subcortical Shape Changes, Hippocampal Atrophy and Cortical Thinning in Future Alzheimer's Disease Patients. *Frontiers in Aging Neuroscience*, *9*. doi: 10.3389/fnagi.2017.00038

Leh, S. E., Kälin, A. M., Schroeder, C., Park, M. T. M., Chakravarty, M. M., Freund, P., Gietl, A. F., Riese, F., Kollias, S., Hock, C., & Michels, L. (2015). Volumetric and shape analysis of the thalamus and striatum in amnestic mild cognitive impairment. *Journal of Alzheimer's Disease*, *49*(1), 237-249.

Schroeder, C.*, Leh-Seal, S. E.*, Kälin, A. M., Hock, C., Michels, L**, & . Kollias, S.**. Informing participants about the study purpose: A hidden peril in studies of resting state fMRI connectivity?. Major revision. *Neuroimage*.

Leh, S. E.*, Schroeder, C.*, Chen, J. K., Mallar Chakravarty, M., Park, M. T. M., Cheung, B., ... & Petrides, M. (2017). Microstructural integrity of hippocampal subregions is impaired after mild traumatic brain injury. *Journal of Neurotrauma*, *34*(7), 1402-1411.

Schroeder, C., Park, M. T. M., Germann, J., Chakravarty, M. M., Michels, L., Kollias, S., ... & Leh, S. E. (2017). Hippocampal shape alterations are associated with regional Aβ load in cognitively normal elderly individuals. *European Journal of Neuroscience*, *45*(10), 1241-1251.

* Shared first authorship

Selected presentations

03.2017 Winter Brain Symposium 2017 (Presentation)

- Subcortical shape measures in cognitively healthy individuals aged 85 years and above

06.2016 OHBM 2016 (Posters)

- Hippocampal shape is associated with regional Aβ load in cognitively normal elderly individuals
- Informing participants about the study purpose affects resting state fMRI connectivity
- Microstructural integrity of hippocampal subregions is impaired after mild traumatic brain injury

11.2015 Tag der Forschung 2015 (Poster, **1st Poster Prize**)

- Local shape differences are associated with SUVR and neuropsychological performance in healthy elderly individuals

02.2015 Winter Brain Symposium 2015 (Presentation)

- Impaired white and gray matter integrity without cognitive impairment in mild traumatic brain injury after a motor vehicle accident

Zurich, November, 2017